

# Dendritic Polyglycerol-Based Microgels and Bulk Hydrogels for Cell Encapsulation Therapies

Inaugural-Dissertation  
to obtain the academic degree  
Doctor rerum Naturalium (Dr. rer. Nat.)

submitted to the Department of Biology, Chemistry, and Pharmacy  
of Freie Universität Berlin

by

Era Kapourani

from Tirana, Albania

August 2017

The following work was carried out within the research group of Prof. Dr. Rainer Haag from March 2013 until August 2017 at the Institute of Chemistry and Biochemistry of the Freie Universität Berlin.

1. Reviewer: Prof. Dr. Rainer Haag, Freie Universität Berlin

2. Reviewer: Priv. Doz. Dr. Kai Licha, Freie Universität Berlin

Day of defense: 25.10.2017

*To our Kristian, who left us all so early.*

## Acknowledgements

This thesis is the result of many experiences I have encountered from dozens of remarkable individuals, who I also wish to acknowledge.

First and foremost, I wish to thank my supervisor Prof. Dr. Rainer Haag for the opportunity to pursue a PhD in a very interesting field in his research group. I would also like to express my gratitude to PD Dr. Kai Licha for undertaking the co-referee of my dissertation. My special acknowledgements are addressed to Dr. Jens Dervedde and Dr. Katharina Achazi for all the help and the long discussions on the biologic facets of my topics. For the numerous NMR spectra, the thorough interpretation of lots of them and for the eagerness to help whenever it was needed I would like to thank Dr Schäfer, head of the NMR Spectroscopy Department.

I could not forget the contribution of many very important members of our group without whom a lot would not be possible. For the help with all the administrative issues and especially for the ease with which such matters were managed I wish to thank Jutta Haas. For assuming plenty of these tasks and for being a very good friend the last three years I would like to thank Dr. Wiebke Fischer. For all the help with management issues the past year, I would like to thank Dipl.-SpOec. Eike Ziegler. I would also like to thank Dr. Monika Wyszogrodzka for lending me an ear the past two years. Our lab assistants Andrea Schulz, Katharina Goltsche, Marleen Selent, Paul Hillmann, Elisa Quaas and Cathleen Schlesener are especially acknowledged for their kind help and support with everything from laboratory consumables, orders, organization, safety issues to conduction of numerous analyses. Especially for all the help the last three years, the eagerness the friendly cooperation and many fun moments I would like to thank Anja Stöshel.

For the intensive proof reading of this thesis I wish to thank Dr. Pamela Winchester, my father Dr. Anastasis Kapouranis, my very good friends M.Sc. Alex Oehrl, M.Sc. Magda Ferraro, M.Sc. Falko Neumann and my partner Dr. Johann Moschner.

All the lab members of 33.04, former and current are gratefully acknowledged for the help, support, and the very nice working atmosphere. I would like to specially thank Dipl.-NanoSc. Michael Unbehauen for his helpfulness, motivation, the many funny moments in the lab and of course for the free of charge German lessons. M.Sc. Felix Reisbeck is thanked for being the good mood and the music guru of our lab, whereas Anja Stöshel for being the ‘soul’ of lab organization. At this point I would like to express my gratitude to all the former and current Post-Docs, PhD, Master, and Bachelor students of our group from whom I have learnt a lot and who have in any way helped me, supported my work, and become good friends of mine.

This work would not have been possible without the financial support of the Dahlem Research School (DRS), the SFB 765, the Helmholtz Zentrum Geesthacht and the Nanoscale Cluster. They are all sincerely appreciated for their contribution throughout the duration of my PhD work.

Besides my colleagues and the funding organizations I would like to acknowledge my family and dearest friends. First and foremost, I wish to thank my mother, father and brother in Athens for standing by me the whole way through all its bumps and its little and big successes. I owe you three a big part of my advances so far. I could not skip at this point my daja Nasho and Kela for their care, interest, and for always looking up on me during this whole endeavor. Katrin and Sven are thanked for reminding me that there is always a way and everyone should individually define its merits. I would like to thank these two also for offering me a peaceful office and home that made the writing process smooth and in fact fun.

My friends have too brought me a bit further either from far abroad or by going along the same or similar paths with me. Prof. Dr. Athanasios Giannis, who by now is a dear friend to me, I would like to especially express my gratitude for being my very first mentor and showing me the beauty and joy behind nature's carbons. I would like to thank him also for pointing the direction to the Haag-group and its research, now my own as well. For all the fun, peaceful, intense, everyday moments I would like to thank the 'Lunch group' and the 'Kuchenkolloquium' with all their former and current members. Katharina Huth, Alex and Magda are acknowledged for all the deep or dorky discussions in our office. It is my wish to thank Magda and Alex for the past two very nice years of our friendship. It has been a blast! My special gratitude is expressed to my oldest friend Βαγγέλης for the long, funny, and meaningful discussions even overseas. I would like to thank him for reminding me that having fun is maybe the most important prerequisite in scientific work.

I could not conclude this section without especially distinguishing one person that has been my 'partner in crime' the past five and half years. So, I would like to especially thank my best friend and partner Johann for his understanding and the many helpful discussions on my topics specifically on the synthetic part of this work. Also, I would like to thank Johann for his patience, kindness, and loving care through every day and for encouraging me to go on and never give up. I am looking forward to what is to come next!

## List of abbreviations

2D	two-dimensional
3D	three-dimensional
AC	Adenyl Cyclase
ADP	Adenosine Diphosphate
Ar	Argon
ATP	Adenosine Triphosphate
BCN	bicyclo[6.1.0]non-4-yn-9ylmethyl(4-nitrophenyl)carbonate
CA	Cellulose Acetate
cAMP 2	cyclic Adenosine Monophosphate 2
CCK-8	Cell Counting Kit 8
cLSM	confocal Laser Scanning Microscopy
CNS	Central Nervous System
d	Day(s)
D <sub>2</sub> O	deuterated water
DAG	Diacylglycerol
DCM	Dichloromethane
DMEM	Dulbecco's Modified Eagle's Medium
DMF	Dimethylformamide
DMSO	Dimethyl Sulfoxide
DPBS	Dulbecco's Phosphate Buffered-Saline
dPG	dendritic Polyglycerol
dPGS	sulfated dendritic Polyglycerol
DPN	Diabetic Peripheral Neuropathy
ECM	Extracellular Matrix
EDTA	Ethylenediaminetetraacetic Acid
EEGE	Ethoxyethyl Glycidyl Ether
EGDMA	Ethylene Glycol Dimethacrylate
ELISA	Enzyme-Linked Immunosorbent Assay
EO	Ethylene Oxide
Epac2A	exchange protein directly activated by cAMP 2
equiv.	Equivalents
Et	Ethyl
EtOH	Ethanol
Et <sub>3</sub> N	Triethylamine

Ex/Em	Excitation/Emission
EWG	Electron Withdrawing Group
FCS	Fetal Calf Serum
G	$\alpha$ -L-Guluronic Acid
G-6P	Glucose-6-Phosphate
GAD	Glutamic Acid Decarboxylase
GDP	Gross Domestic Product
GLP-1	Glucagon-Like Peptide-1
GLUT1	Glucose Transporter 1
GPC	Gel Permeation Chromatography
GSIS	Glucose-Stimulated Insulin Secretion
hG	high Glucose
hrs	Hours
Hz	Hertz
IA-2	Insulinoma Antigen-2
IAA	Insulin Autoantibodies
ICA	Islet Cell Cytoplasmic Autoantibodies
IgG	Immunoglobulin G
IKVAV	Isoleucine-Lysine-Valine-Alanine-Valine-containing peptide
IR	Infrared
<i>J</i>	coupling constant
$K_{ATP}$	ATP-sensitive $K^+$ channels
kDa	kilodalton
IPG	linear Polyglycerol
lG	low Glucose
LEA	Lower Extremity Amputation
M	$\beta$ -D-Mannuronic Acid
MeOH	Methanol
MeOH-d4	deuterated Methanol
$M_n$	number average molecular weight
Ms	Mesyl
MSC	Mesenchymal Stem Cell
MWCO	Molecular Weight Cut-Off
NMR	Nuclear Magnetic Resonance
NC	Negative Control

PA	Polyamide
PAH	Polyallylamine Hydrochloride
PAMPs	Pathogen Associated Molecular Patterns
PDADMAC	Poly(diallyldimethylammonium chloride)
PDI	Polydispersity Index
PDMS	Polydimethylsiloxane
PEEGE	Poly(ethoxyethyl glycidyl ether)
PEG	Polyethylene Glycol
PES	Polyethersulfone
PHEMA	Poly(hydroxyethyl methacrylate)
PI	Propidium Iodide
PKA	Protein Kinase A
PKC	Protein Kinase C
PLGA	Poly-L-Glycolic Acid
PLC	Phospholipase C
PMAA	Polymethacrylic Acid
PMMA	Polymethyl Methacrylate
PP	Pancreatic Polypeptide
ppm	parts per million
P/S	Penicillin/Streptomycin
PSS	Sodium Polystyrene Sulfonate
PTFE	Polytetrafluoroethylene
<i>p</i> -TsOH	<i>para</i> -Toluenesulfonic acid
PU	Polyurethane
PVA	Polyvinyl Alcohol
PVP	Polyvinylpyrrolidone
RGD	Arginylglycylaspartic Acid
ROP	Ring Opening Polymerization
r.t.	Room Temperature
SPAAC	Strain-Promoted Alkyne-Azide Cycloaddition
T1D	Type 1 Diabetes
T1DM	Type 1 Diabetes Mellitus
T2D	Type 2 Diabetes
THF	Tetrahydrofuran
Tol.	Toluene

UNOS	United Network of Organ Sharing
UV	Ultraviolet
vol %	volume %
VDCC	Voltage Dependent Calcium Channels
wt %	weight %
WHO	World Health Organization
ZnT8	Zinc Transporter-8



# Table of Contents

1	Introduction.....	1
1.1	Cell encapsulation technologies .....	1
1.2	Cell encapsulation therapeutic approaches .....	3
1.3	Polymeric materials for cell encapsulation .....	5
1.4	Geometry of the capsules .....	16
1.5	Encapsulation chemistries .....	17
1.6	Cell encapsulation procedures.....	19
1.7	Anatomy and histology of pancreas .....	22
1.8	Pancreatic $\beta$ -cells: insulin release and type 1 diabetes .....	24
1.9	Type 1 diabetes: available treatments.....	32
1.9.1	Insulin therapy .....	32
1.9.2	Pancreas transplantation.....	33
1.9.3	Islet cell transplantation .....	34
2	Research goals.....	42
2.1	Dendritic Polyglycerol-Based Microgels for Cell Encapsulation Therapies .....	42
2.1.1	Objective .....	42
2.1.2	Results and discussion .....	44
2.1.3	Conclusions .....	64
2.2	Dendritic Polyglycerol-Based Microgels and Bulk Hydrogels for Transplantation of Pancreatic Islet Cells .....	67
2.2.1	Objective .....	67
2.2.2	Results and discussion .....	69
2.2.3	Conclusions .....	82
2.3	Summary .....	85
3	Experimental.....	88
3.1	Materials and methods.....	88
3.1.1	Reagents.....	88
3.1.2	Measurements.....	88
3.2	Synthesis .....	90
3.2.1	Synthesis of ethoxyethyl glycidyl ether EEGE 5 .....	90
3.2.2	Synthesis of six-arm-star-shaped polyglycidol S-PG 4 .....	91
3.2.3	Synthesis of six-arm-star-shaped polyglycidol-hexavinyl sulfonate S-PGV3 3....	92
3.2.4	Synthesis of six-arm-star-shaped polyglycidol hexaazide S-PG-hexaazide 2. ....	92
3.2.5	Synthesis of six-arm-star-shaped polyglycidol hexaazide S-PG-hexaazide P1 ....	93
3.2.6	Synthesis of linear monobromo-poly(ethoxyethyl glycidyl ether) (monobromo-PEEGE 4) .....	94
3.2.7	Synthesis of linear $\alpha$ -bromo- $\omega$ -mesyloxy-poly(ethoxyethyl glycidyl ether) ( $\alpha$ -bromo- $\omega$ -mesyloxy-PEEGE 3) .....	94

3.2.8	Synthesis of linear $\alpha$ , $\omega$ -bisazido-poly(ethoxyethyl glycidyl ether) ( $\alpha$ , $\omega$ -bisazido-PEEGE 2) .....	95
3.2.9	Synthesis of linear $\alpha,\omega$ -bis-azido-PG ( $\alpha,\omega$ -bis-azido-IPG P2).....	96
3.2.10	Synthesis of linear $\alpha,\omega$ -bis-azido-PEG P3 .....	96
3.2.11	Synthesis of dPG-polymesylate 4.....	97
3.2.12	Synthesis of dPG-polyazide 3 .....	97
3.2.13	Synthesis of dPG-polyamine 2 .....	98
3.2.14	Synthesis of dPG-poly(bicyclooctyne) (dPG-polyC P4) .....	98
3.2.15	Synthesis of surfactant KBT .....	99
3.2.16	Synthesis of dPGS-polyazide P5 .....	100
3.2.17	Synthesis of $\alpha$ , $\omega$ -bis(bicyclooctyne)-PEG P6 .....	100
3.3	<i>In Vitro</i> studies .....	101
3.3.1	Cytotoxicity assay of NIH/3T3 cells by use of Cell Counting Kit-8 (CCK-8)....	101
3.3.2	Treatment of mammalian NIH/3T3 cells prior to microfluidic encapsulation ...	101
3.3.3	Treatment of mouse insulinoma $\beta$ -TC-6 cells prior to microfluidic encapsulation .....	101
3.3.4	Treatment of mouse insulinoma $\beta$ -TC-6 cells prior to encapsulation in bulk hydrogels .....	102
3.4	Microfluidic templating .....	102
3.4.1	Microfluidic devices .....	102
3.4.2	Microfluidic encapsulation of mouse fibroblast NIH/3T3 cells.....	102
3.4.3	Microfluidic encapsulation of mouse insulinoma $\beta$ -TC-6 cells .....	104
3.5	Encapsulation of mouse insulinoma $\beta$ -TC-6 cells in dPGS-based bulk hydrogels	105
3.6	Cytocompatibility of dPG-based hydrogels with NIH/3T3 <i>via</i> live-dead staining	106
3.7	Cytocompatibility of dPGS-based hydrogels with $\beta$ -TC-6 cells <i>via</i> live-dead staining .....	106
3.8	Quantification of the released insulin from $\beta$ -TC-6 cell-laden dPGS bulk hydrogels <i>via</i> ELISA .....	107
4	Appendix.....	108
4.1	NMR spectra .....	108
4.2	GPC traces.....	120
4.3	IR spectra .....	121
4.4	<i>Curriculum Vitae</i> .....	123
5	References.....	124

# 1 Introduction

## 1.1 Cell encapsulation technologies

Cell encapsulation is a technology with which artificial three-dimensional (3D) scaffolds are developed that can carry and protect living cells from their external environment.<sup>[1-3]</sup> The initial historical evidence of this technology places its introduction at the beginning of the 20<sup>th</sup> century, when the seminal reports of Bisceglie showed that tumor cells enveloped in immunoprotective membranes could survive long after their transplantation in the abdominal cavity of guinea pigs.<sup>[4]</sup> It is based on the immobilization of cells within a polymeric semipermeable membrane that allows both an influx of oxygen and nutrients to nourish the enclosed cells and an outflux of therapeutic molecules and metabolic waste (Figure 1). At the same time, the permselective nature of the membranes eliminates the entry of damaging elements of the immune system with high molecular weights up to 150 kDa to their cell-containing microenvironments.<sup>[5-7]</sup>

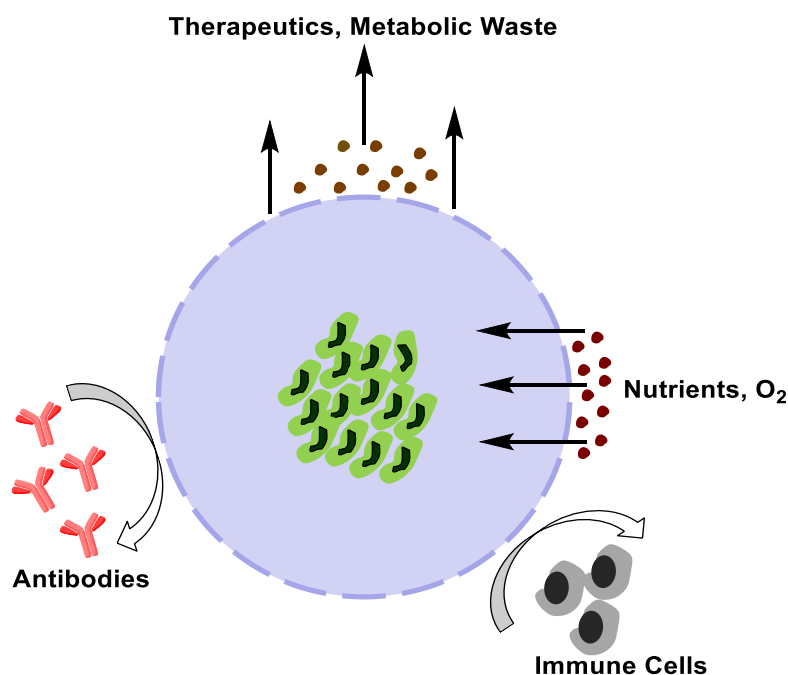


**Figure 1.** Principle of cell encapsulation. Cells are immobilized in a semipermeable membrane scaffold that protects them from immune responses and allows a bidirectional diffusion of nutrients and oxygen as well as secreted therapeutics and metabolic waste.

Apart from the immune isolation, encapsulation also allows the protection of the cell content from mechanical stress. The potential to promote and control the viability and proliferation of the encased cells as well as the release of therapeutic products fuelled the

development of several cell-based therapies. With a focus on drug and cell delivery, these therapies are currently being used for organ replacement, tissue engineering and regenerative medicine purposes.<sup>[8]</sup>

To ensure long-term functional survival of the enclosed cells and thereby, the long-term delivery of therapeutics for the treatment of chronic diseases, a suitable relation between the stability, biocompatibility, durability, and diffusional properties of the immunoisolation device is highly desired.<sup>[8]</sup> Thus, the capsules are generally engineered to consist of hydrogels due to their favorable properties. Hydrogel-based particles are water-swallowable but non-soluble and can be prepared as well as scaled-up under mild conditions inducing no harm to the targeted cells. Their high water content is paramount for the enclosed cells, providing the hydrated environment necessary to facilitate the physical, and biochemical stimuli that guide cellular processes such as differentiation, proliferation, and migration. The soft and pliable features of the hydrogels prevent, or at least reduce, the frictional or mechanical irritation with surrounding tissues, a crucial aspect when cell delivery or stem cell therapeutic approaches are envisioned. Due to their polar surface, there is virtually no interfacial tension with surrounding tissues and fluids, leading to a minimization of cell adhesion and protein adsorption. Hydrogels offer a high degree of permeability especially for low molecular weight nutrients and metabolites. On the whole, they constitute reliable biocompatible materials that have attracted considerable attention in biomedical applications.<sup>[9]</sup>

Cell encapsulation as a therapeutic approach aims to tackle present difficulties related to organ transplantation, scarcity of functional organs, side-effects of immunomodulatory protocols or immunosuppressants, and whole graft rejection.<sup>[6-11]</sup> The presence of an immune-isolating membrane holds promise for the reduction or even elimination of life-long immunosuppressive regimes that have been associated with severe side-effects in transplant recipients. The following approach allows engraftment of non-human, xenogeneic tissue, or of genetically modified cells to express a specific protein or factor without the need to intervene in the host's genome.<sup>[12]</sup> Immune-privileged cellular grafts are ideal for treatments that require a long-term, controlled, and continuous release of therapeutics. This targeted, sustained source of *de novo* synthesized molecules results in more physiological concentrations locally and in the systemic circulation.<sup>[13]</sup> High toxicities through the burst release of large amounts of the required drug due to damage of the capsules can also be avoided.<sup>[12]</sup> Cell-based therapies combine the safety of implantable, retrievable medical devices with the delivery of the therapeutic agents for prolonged periods of time without needing to repeat the treatment.<sup>[14]</sup>

## 1.2 Cell encapsulation therapeutic approaches

Cell encapsulation today attracts considerable attention and constitutes a largely researched field due to its ample therapeutic potential, which extends beyond organ transplantation. Apart from presenting medium and long-term drug-delivery platforms, the field has evolved towards the design and fabrication of intelligent 3D scaffolds that can be used either to monitor enclosed cells and provide real-time release of biotherapeutics or to develop biomimetic matrices bearing peptides to direct cellular fate.<sup>[15-17]</sup> Interestingly, the applications of the field have recently largely increased in stem cell research. It is a highly versatile strategy that provides a cost-efficient way to study and promote stem cell growth and differentiation in a synthetic 3D scaffold while, simultaneously being a dynamic platform for cell retention and delivery in different anatomical locations.<sup>[18,19]</sup>

The progress of the field has gone hand-in-hand with significant biological, technological, and pharmaceutical challenges. A few of the emerging advances in the field include the development of both non- and biodegradable 3D capsules, magnetocapsules for non-invasive cell-monitoring, as well as the general improvement of its biosafety. Additionally, the enhanced access to the Central Nervous System (CNS) and the eye with reduced-size particles, and the substantial complementation of stem cell research with novel biomimetic particles constitute significant achievements of cell encapsulation therapies.<sup>[8]</sup> Two opposing processes define the therapeutic versatility of this strategy: the robustness of carriers for drug delivery versus the slow/fast degradation of scaffolds for cell delivery and tissue engineering. The principal applicability of encapsulation technologies has been repeatedly demonstrated with its most profound achievement being the presence of various encapsulation strategies in clinical experimental settings as different clinical trials have been performed or are currently ongoing. This has paved the way for numerous therapeutic approaches for chronic diseases including diabetes mellitus, anemia, bone and cartilage defects, myocardial defects, CNS deficiencies, and cancer among others.<sup>[15-17,20-23]</sup>

Apart from the aforementioned applications of therapeutic cell encapsulation, stem cell-based therapies are advancing considerably with an increasing demand for novel, sophisticated scaffolds that enable a controlled delivery of the respective cells. In this case the constructed capsules are not designed to act as immune barriers, which therefore excludes the need for external coatings. On the contrary, they are envisioned to act more as supportive matrices to facilitate the correct grafting of the implanted cells. The most typically

implemented scaffolds for these purposes are produced *in situ* upon gelling of injectable hydrogels. However, capsules especially in the micrometer scale are generally more favored due to their large surface area, the capacity to enclose a higher number of cells per volume unit, [24,25] as well as their potential to be incorporated in more complex cell delivery systems and organ printing. [24,26]

Among the design demands of capsules in cell delivery applications, the degradation rate serves a critical function and should be adjusted to meet the time requirements of both the grafted and host cells for the subsequent scaffold replacement. During degradation, the enveloped cells remodel their microenvironment by depositing their own extracellular matrix (ECM). Apart from cell migration the degradation process can direct cellular behavior by regulating the release of matrix tethered biomolecules, which promote different cellular functions. [27,28] It should be particularly stressed that the appropriate degradation profiles established *in vitro* do not necessarily apply *in vivo* where the biological pathways are governed by the physiology of the targeted implantation site. [29]

A fundamental consideration of this technology is to employ processes and materials that do not harmfully interfere either with the embedded cells or the adjacent host tissues. [29,30] Therefore, the polymers constructing the capsules are functionalized with adhesion moieties which serve as recognition and anchoring sites for the cells resembling their natural ECMs. Consequently, the crucial cell-matrix and cell-cell signaling pathways are facilitated preventing cellular apoptosis, whereas various cellular functions including migration, release, and subsequent proliferation and spreading are enhanced. [24,31,32]

To fine-tune the degradation profiles of the polymeric scaffolds, two strategies have been applied that involve either chemically or cellularly induced membrane disruption. The former, which is also the most commonly utilized, consists of incorporation of functional groups susceptible to hydrolysis by partial oxidation of the polymer chains. Thus, varying the oxidation degrees of the obtained capsules triggers controlled release of the enveloped cells. [33,34] The alternative approach, relies on the modification of the polymeric building blocks with specific sequences recognized and cleaved by metalloproteases secreted from the cells. This allows interactions of the encapsulated cells with the surrounding hydrogel matrix and the neighboring cells in a dynamic fashion that more realistically resembles the physiological processes activated during wound healing or regeneration. [35,36]

Cell delivery holds great promise for applications in tissue engineering and regenerative medicine. Biologically relevant implanted cells that are released in damaged areas can either directly adhere to the afflicted site or elicit secretion of multiple cytokines and growth factors,

which guide the remodeling of the affected tissue.<sup>[37,38]</sup> The majority of study cases in this field involve bone regeneration mostly actuated by the release of mesenchymal stem cells (MSCs).<sup>[24]</sup> MSCs have also been reported to play a pivotal role in angio- and arteriogenesis.<sup>[39,40]</sup> The potential of MSCs to induce vascularization is highly significant in expanding the scope of regenerative therapies and promoting the adaptation and functional survival of cellular transplants, the death of which due to hypoxia only days after engraftment represents one of the main hurdles for clinical translation of various cell-based therapies.<sup>[8]</sup>

Although cell-based therapeutic approaches are highly promising, ideal, and with no question clinically applicable capsules as vehicles for cells or drugs are so far not available. This could be partially attributed to the inadequacy, to specifically distinguish the factors that contribute to success or failure of the transplanted device. Several successful cases are already known but to date a finalized set of recommendations with general validity is not accessible, due to an incomplete understanding of the fundamental aspects of the respective successes or failures. A first indication would be to thoroughly study the numerous variations in the way encapsulation scaffolds can be produced as well as the utilized materials.<sup>[41]</sup>

### **1.3 Polymeric materials for cell encapsulation**

The field of cell encapsulation has made use of both naturally occurring and synthetic polymers. Generally, three main classes of natural polymers have been described: polysaccharides, polypeptides, and polynucleotides. Polysaccharides are the most commonly used natural polymers in cell encapsulation. This is probably because polysaccharides allow encapsulation of cells under relatively mild conditions and generally do not impair the functional survival of the cells.<sup>[1-3]</sup> Also, most polysaccharides form hydrogels which as previously discussed confer very favourable properties to the respective encapsulation systems.<sup>[9]</sup>

#### **Alginates**

The most commonly applied biopolymers in encapsulation research are alginates. Originally introduced for the encapsulation of pancreatic islet cells for their transplantation as a potential treatment of type 1 diabetes,<sup>[1-3]</sup> alginate has also been utilized for various applications including endocrine and recombinant cells for the delivery of therapeutic gene products,<sup>[42,43]</sup>

in bioartificial kidneys, [44] for the protection of hepatocytes, [45] and for bioartificial parathyroids.[46]

Alginates are anionic polysaccharides primarily derived from the brown algae *Laminaria hyperborean*, *Macrocystis pyrifera*, and *Ascophyllum nodosum*. They are linear copolymers composed of two types of repeating units: 1–4 linked  $\alpha$ -L-guluronic acid (G) and  $\beta$ -D-mannuronic acid (M), which are dispersed through alginates in different concentrations and in different lengths (Figure 2).[47] The alternating G M units favor rapid binding of divalent cations such as calcium, barium, and strontium with binding affinities increasing with content and length of the G blocks, whereas the cross-linking density of the obtained ionic gel is highly based on the cation concentration. High-G content alginates produce capsules with great mechanical strength, while high-M alginates exhibit elastic properties. The mechanical integrity of alginate capsules is, however, sensitive to the presence of chelating agents such as EDTA, citrate, phosphate, and lactate, as well as monovalent cations such as  $\text{Na}^+$ . [48] The latter as well as the high porosity of alginate gels impeding immunoprotection, are addressed by coating the alginate gels with cationic polymers of a synthetic origin. The most intensively studied and characterized cationic polymers for alginate coating are poly-L-lysine and poly-L-ornithine. However, polyethylene glycol (PEG), glutaraldehyde, chitosan, agarose, cellulose sulfate with the polycation poly(methylene-co-guanidine), diblock polymers of poly-L-lysine and PEG, and polyallylamine have also been applied.[49]

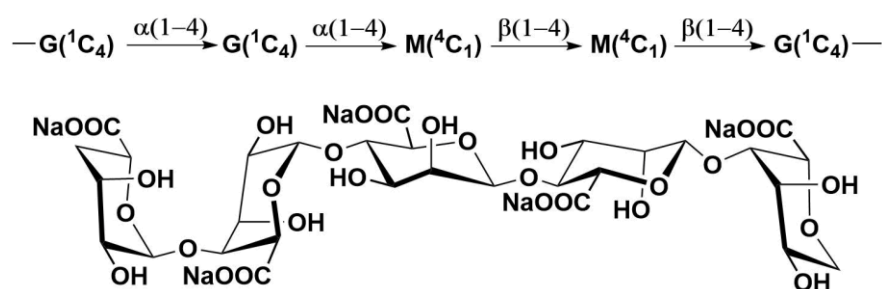


**Figure 2.** Simplified structure of alginate composed of  $\alpha$ -L-guluronic acid (G) and  $\beta$ -D-mannuronic acid (M) repeating units.

Alginate-based capsules are probably the most studied in cell encapsulation in terms of their biotolerability. To ensure full immune protection of their cellular payloads, alginates should undergo multiple purification steps to prevent host responses related to immunogenic substances, such as proteins, endotoxins, and polyphenols.[50] These compounds that are also present in other natural polymers can elicit severe toxic responses upon diffusion on the

surface of the capsules.<sup>[50]</sup> According to recent reports alginates may contain so-called pathogen-associated molecular patterns (PAMPs), which are highly conserved molecular motifs found in pathogens but also throughout nature.<sup>[51]</sup> The latter most likely present in various other natural polymers too, are responsible for the initiation of inflammatory responses. Although these facts are well known, they have received minor attention in similar studies of other natural polymers.

### Agarose

Agarose is a polysaccharide isolated from agar. It is composed of  $\beta$ -D-galactopyranosyl and 3,6-anhydro-L-galactopyranosyl monomeric units, coupled through 1  $\rightarrow$  3 bonds (Figure 3). Agarose allows the encapsulation of cells under mild conditions and reportedly does not interfere with the functional survival of cells.<sup>[49]</sup> Its capsules have been used to immune protect islet xenografts and insulinoma cells for the treatment of diabetes, genetically modified fibroblasts to treat brain disorders, hybridoma cells for immunological disorders, and kidney cells.<sup>[49]</sup> By varying the polymer's concentration different properties are conferred to the resulting gels with only 5 % usually being enough for the proper immune isolation of encapsulated cells.

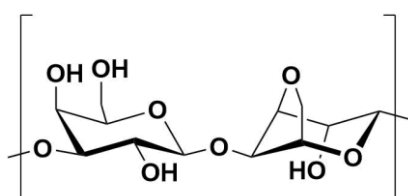


**Figure 3.** Simplified structure of agarose composed of  $\beta$ -D-galactopyranosyl and 3,6-anhydro-L-galactopyranosyl monomeric units coupled through 1  $\rightarrow$  3 bonds.

Agarose gels can only support limited survival of encapsulated xenogeneic tissue, which is likely attributed to the inadequacy of these hydrogels to prevent the diffusion of cytotoxic immunoglobulin G (IgG).<sup>[52]</sup> To tackle this problem, the gelation procedures are complemented either with the increase of agarose concentration up to 7.5 - 10 % or with a coating layer of the surface with another polymer.<sup>[53]</sup> Coatings like polyacrylamide or polystyrene sulfate were shown to be impermeable to antibodies but did not significantly improve the longevity of the grafts as they elicit major host responses.<sup>[54]</sup> In general, the widespread applicability of agarose is also hampered by other issues including the presence of toxic molecules before, during, and after encapsulation,<sup>[55]</sup> the absence of a definitive

process for the optimization of permeability<sup>[55]</sup> and the lack of pure, reproducible sources of agarose.<sup>[56]</sup>

### **Chitosan**

Chitosan is a poly  $\beta(1 \rightarrow 4)$ -2-amino-2-deoxy- $\beta$ -D-glucan, deacetylated chitin, with reactive amino and hydroxyl groups, and thus a strong affinity to polyanions. With the exception of low molecular weight samples, it is only soluble in acidic aqueous solutions and has versatile mechanical properties<sup>[49]</sup> (Figure 4). Due to its poor dissolution at physiologic pH, chitosan has not been as intensively tested as alginate or agarose for immunoprotection. It is mostly used to produce micrometer-sized hydrogels for cells that benefit from cationic environments or for the fabrication of degradable capsules. As such, chitosan has been used to construct scaffolds for the encapsulation of PC12 cells for the treatment of Parkinson's disease, hepatocytes, fibroblasts, human bone marrow stromal cells, and cardiomyocytes.<sup>[49]</sup>

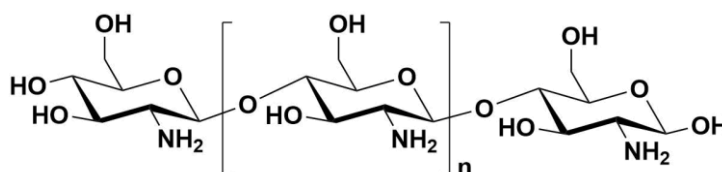


**Figure 4.** Simplified structure of chitosan, a poly  $\beta(1 \rightarrow 4)$ -2-amino-2-deoxy- $\beta$ -D-glucan.

Chitosan is an overall cationic biopolymer with mucoadhesive properties, which render it cytotoxic and thus unsuitable as a cellular vehicle.<sup>[57]</sup> However, it has been suggested that it can form stronger bonds with alginate than poly-L-lysine and as such it could serve as a coating material for alginate capsules.<sup>[58]</sup>

### **Cellulose**

Cellulose consists of a linear chain of  $\beta(1 \rightarrow 4)$ -linked D-glucose units (Figure 5) and constitutes the structural component of the primary cell wall of green plants, many forms of algae, and oomycetes.<sup>[49]</sup> The biodegradable nature of cellulose has been the subject of debates concerning its uses in tissue repair. In animals and humans, it is argued that its degradation either does not happen at all or is very slow due to the absence of a hydrolase needed to cleave its  $\beta(1 \rightarrow 4)$  bonds. Cellulose has been applied for the encapsulation of cytotoxic epithelial cells for the treatment of pancreatic cancer, insulin-producing cell lines (HIT-T15), embryonic kidney cells, and hybridoma cells. It has been suggested that physical

transformations of specific structures of cellulose could achieve significant modulations of its degradation and thus render it a versatile biopolymer with extended applications.<sup>[49]</sup>

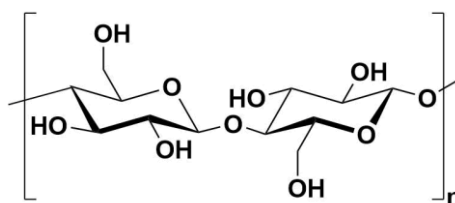


**Figure 5.** Simplified structure of cellulose consisting of a linear chain of  $\beta(1 \rightarrow 4)$ -linked D-glucose units.

The biotolerability of cellulose remains a subject of debate.<sup>[59]</sup> Although, cellulose capsules are compatible with the functional survival of enveloped cells they were found to induce minor inhibition of cell proliferation of their cell content.<sup>[60]</sup> Some reports suggest that an inflammatory response can occur against cellulose, while others claim the initiation of no harmful effects on the encapsulated cells.<sup>[61]</sup> This highlights the need for an in-depth study of the physicochemical properties of cellulose capsules.

### **Collagen**

Collagen is a family of biopolymers with a high content of glycerin residues (33 %) counting to date 29 identified and described members (Figure 6).<sup>[49]</sup> It is present in humans in five dominant types, of which over 90 % is type I. Because of its abundance, the latter is the most commonly used in cell encapsulation. It is one of the most versatile polymers as an immune isolation barrier especially for anchorage-dependent cell types, such as stem cells, hepatocytes, and fibroblasts. Collagen hydrogels can be prepared in a number of different geometries, including strips, sheets, sponges, and beads.<sup>[49]</sup>

Collagen undergoes very rapid enzymatic degradation<sup>[62]</sup> and has been reported to elicit minor humoral responses. Its application as the fundamental constituent of capsules is limited because of its weak mechanical properties and its short-term stability, whereas, it is difficult to control its permeability.<sup>[62]</sup> To introduce non-degradability, collagen-based capsules are coated with an outer shell of polyhydroxyethylmethacrylate (PHEMA), polymethacrylic acid (PMAA), and polymethyl methacrylate (PMMA) which is supposed to enhance cell survival and function.<sup>[63]</sup>

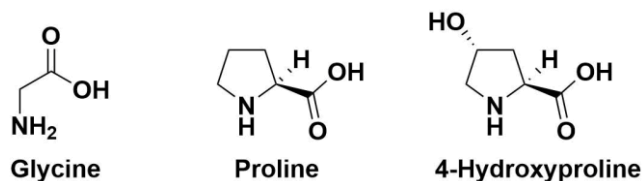


**Figure 6.** Collagen is a family of molecules that is available in at least 29 types. A basic feature of collagen is the high content in glycine, proline, and hydroxyproline.

### Xanthan

Xanthan is a natural polysaccharide, the main chain of which is composed of (1 → 4)- $\beta$ -D-glucose units with a terminal  $\beta$ -D-mannose,  $\beta$ -D-glucuronic acid, and  $\beta$ -D-mannose side chain that has  $\beta$ -D-(1 → 2) and D-(1 → 4) linkages (Figure 7).<sup>[49]</sup> Xanthan is derived from the bacterial coating of *Xanthomonas campestris* and has been mostly applied in drug delivery. However, it has recently also been introduced for the encapsulation of chondrocytes. Xanthan's robustness towards a broad range of temperatures, pH, and electrolytes render it highly favorable as a biomaterial for *in vivo* studies. It is crucial for the survival of the transplanted cells that their hydrogel carrier withstands changes of the microenvironment at the implantation site.<sup>[49]</sup> The latter may however, induce undesirable modifications in the surface properties of xanthan capsules leading to biointolerability.<sup>[64]</sup> Further studies are required to determine whether xanthan qualifies as a biopolymer for the cell encapsulation and immunoprotection.

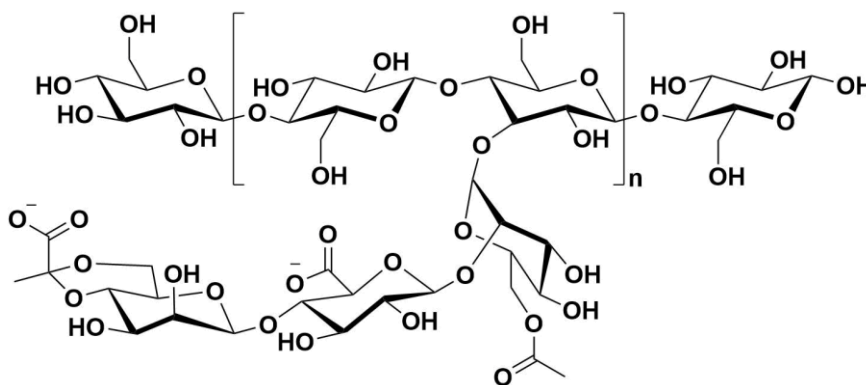


**Figure 7.** Simplified structure of xanthan, consisting of (1 → 4)- $\beta$ -D-glucose units with a terminal  $\beta$ -D-mannose,  $\beta$ -D-glucuronic acid, and  $\beta$ -D-mannose side chain that has  $\beta$ -D-(1 → 2) and D-(1 → 4) linkages.

In general, natural polymers suffer from batch-to-batch variations and are mostly isolated in moderate scales or engineered for desired properties only through tedious processes.<sup>[49]</sup> To address these shortcomings, synthetic polymers have been employed in the

encapsulation of cells. Furthermore, there are various available elegant and straightforward procedures to improve the biotolerability or reinforce the mechanical properties of synthetic polymers. Nevertheless, for the application of most synthetic polymers encapsulation procedures are required that make use of toxic solvents,<sup>[49]</sup> which could lead to viability and cell function losses. This poses a significant limitation in cases where scarce cadaveric tissues are available such as the transplantation of pancreatic islets, hepatocytes, or kidney cells for the treatment of various diseases. Consequently, only a few synthetic polymers fulfill the criteria of optimal compatibility with enveloped cells. Furthermore, bioorthogonal encapsulation procedures are employed to minimize the associated risks that do not interfere with the functional viability of the targeted cells.

### **Polyethylene glycol (PEG)**

PEG is an aliphatic polyether generated by the ring-opening polymerization (ROP) of ethylene oxide (EO) (Figure 8). Its favorable properties ranging from high flexibility, hydrophilicity, and high water-solubility in practically all concentrations to its very low immunogenicity, antigenicity, and toxicity have established the commercial use of this polymer for an immense variety of applications, especially in pharmaceutical, cosmetic, and medical areas.<sup>[65]</sup>

PEG has also been used for the encapsulation of a broad range of cell types, including pancreatic islets, chondrocytes, osteoblasts, and mesenchymal stem cells.<sup>[49]</sup> PEG macromeres functionalized with methacrylate or acrylate groups undergo rapid crosslinking upon exposure to ultraviolet or visible light in the presence of the appropriate photoinitiators. Various gelation procedures have been developed in the past two decades with the majority of cell encapsulation applications being performed *via* photopolymerization of PEG diacrylate prepolymers. Besides the above-mentioned advantages, PEG chains can be readily coupled with functional peptides to mimic physiological extracellular matrices for the support of the functional survival of encapsulated cells.<sup>[49]</sup> Furthermore, PEG-hydrogels present a short diffusion time scale, with low protein adsorption on their surfaces.

Although, cell encapsulation *via* photopolymerization has been considerably successful, it proceeds *via* generation of free radicals that can induce cell damage and loss of function as outlined in various reports on other polymers.<sup>[66]</sup> This has been the subject of only a few PEG studies and it remains to be further elucidated if the free radical formation impacts the longevity and function of only specific encapsulated cells.<sup>[67]</sup>

### **Polyvinyl alcohol (PVA)**

Polyvinyl alcohol is derived from polyvinyl acetate through hydrolysis of its vinyl acetate groups to vinyl alcohols (Figure 8). It is slightly soluble in ethanol but insoluble in other organic solvents and as a thermoplastic polymer, it can be converted to different structures by freeze-thawing processes. It has been applied for the encapsulation of genetically engineered cells that secrete neurotransmitters and neurotrophic factors for the treatment of neurodegenerative disorders such as Alzheimer's, Huntington's, and Parkinson's disease. It has also been applied for the encapsulation of pancreatic islets for the treatment of diabetes and pituitary disorders.<sup>[49]</sup>

The gelation of PVA is performed through iterative freeze/thaw cycles.<sup>[68]</sup> To employ this procedure in the presence of cells, cryoprotectants such as glycerol are necessary. Despite their use, significant losses of the functional survival of the cells has been observed.<sup>[69]</sup> An additional obstacle in the application of PVA is its low hydrophilicity which accounts for poor adhesion of the enveloped cells on the inner surface of its capsules.<sup>[70]</sup> This leads to an inadequate nutrition of the immunoprotected cells, which has been proposed to be circumvented by the generation of chitosan-based composite systems.<sup>[71]</sup> This strategy served to increase the hydrophilicity of the surface, but the produced composites and gels suffered from poor stability.<sup>[69]</sup> Thus, it has been suggested that additional cross-linking steps, such as the implementation of a natural polysaccharide (e.g., alginate or chitosan) as a supportive matrix for the enclosed cells, may be required to prolong stability.<sup>[69,72]</sup> Although this poses an important improvement, it is an approach that has not yet achieved general success in cell encapsulation.

### **Polyurethane (PU)**

Polyurethane (PU) is an elastomer (Figure 8) which is mainly produced by the catalytic reaction of a polyol, typically a polypropylene glycol or polyester polyol, with diisocyanate. PU has widespread biomedical applications including vascular grafts and artificial hearts, and has been utilized for the generation of hollow fibers that served as carriers for pancreatic islets, pituitary tissue, and PC12 cells.<sup>[49]</sup>

After transplantation, PU-cellular carriers can undergo biodegradation leading to graft failure.<sup>[73]</sup> To increase the durability of its gels, PU has been mixed with hydrophilic or hydrophobic polymers such as polydimethylsiloxane (PDMS).<sup>[74]</sup> The biocompatibility or biotolerability of PU as an immunoisolation barrier is still a subject of debate. PU capsules are hydrophobic and can trigger host immune responses. Therefore, a treatment with

hydrophilic reagents such as Tween 80 has been applied. Although this approach improves the performance of PU-capsules through increasing their hydrophilicity, decreasing their surface energy, and reducing the severity of immune responses, it has been associated with failure of the enveloped tissues.<sup>[75,76]</sup>

### **Polyethersulfone (PES)**

Polyethersulfone (Figure 8) is a thermoplastic polymer that is predominately applied to encapsulate cells in hollow fibers. The fibers are formed by the polymerization of dichlorodiphenyl sulfone with dihydroxydiphenyl sulfone in the presence of sodium carbonate.<sup>[49]</sup> The targeted cells are mixed with a matrix of collagen or alginate to facilitate functional survival, and then injected in PES fibers. Both ends of the fibers are usually sealed by photopolymerized acrylic glue. The outer surface of polyethersulfone capillaries is rough and consists of open pores. These structures have been shown to provide a suitable area for vascular tissue formation, which may be beneficial for the function of cells after transplantation.<sup>[49]</sup> To promote vascular ingrowth and enhance the secretory functions of the encapsulated cells, the hydroxy methylation ( $\text{CH}_2\text{OH}$ ) of polyethersulfone capillaries has been suggested. PES-hollow-fibers have been used for pancreatic islets, myoblasts, and fibroblasts.<sup>[49]</sup>

The main disadvantage of PES-hollow-fibers is the limited viability of the encapsulated cells because of an insufficient nutrient supply, especially in the center of the capsules. Polyethersulfone as a membrane in dialysis therapy shows acceptable biotolerability with blood, which however, does not meet the requirements for immunoprotection devices.<sup>[77]</sup> PES is highly hydrophobic and as such associated with a high risk of protein adsorption after prolonged periods of implantation.<sup>[78]</sup> Coating with silane or blending hydrophilizing additives, such as polyvinylpyrrolidone (PVP), have been recommended to increase the biotolerability of PES membranes.<sup>[79]</sup> Nevertheless, these methods have not yet been used for cell encapsulation.

### **Sodium polystyrene sulfonate (PSS)**

Sodium polystyrene sulfonate (PSS) is the sodium salt of polystyrene sulfonic acid. This polymer is thermoplastic. Sodium polystyrene sulfate has the advantage that it is readily soluble in water (Figure 8). It has been used for the encapsulation of pancreatic islets and red blood cells.<sup>[49]</sup>

To improve its biocompatibility, sodium polystyrene sulfonate has been used in combination with agarose as well as with other neutralizing cationic polymers including polyallylamine hydrochloride (PAH) or poly(diallyldimethylammonium chloride) (PDADMAC).<sup>[79]</sup> However, this optimization technology suffers from stability limitations, because sodium polystyrene sulfonate / PAH layers cannot withstand the shear forces during and after transplantation, which, therefore, impedes their use in biomedical applications.<sup>[80]</sup> Apart from poor mechanical stability, PSS evokes undesired complement-activating effects, rendering it unsuitable for broad application in cell encapsulation.<sup>[81]</sup>

### **Polyacrylates**

The most commonly applied polyacrylates for cell encapsulation are polyhydroxyethylmethacrylate (PHEMA) and hydroxyethyl methacrylate–methyl methacrylate (HEMA–MMA) (Figure 8). Water-insoluble polyacrylates have been applied for the microencapsulation of hepatocytes, fibroblasts, PC12 cells, human hepatoma cells, hybridoma cells, and pancreatic islets.<sup>[49]</sup>

Although a wide variety of mammalian cells can be encapsulated in HEMA–MMA or other polyacrylates, there are considerable differences of their performance *in vitro* and *in vivo*. This could probably be attributed to biotolerability issues. According to findings of various reports materials, such as fibrinogen, IgG, fibronectin, and other components of the complement system, deposit on the surface of implanted HEMA–MMA capsules.<sup>[82]</sup> Additionally, severe host immune responses with an eventual graft rejection shortly after transplantation have been documented for HEMA–MMA capsules implanted in animal models.<sup>[83]</sup> Ethylene glycol dimethacrylate (EGDMA) has been suggested to replace HEMA because contamination in the monomer solutions of the latter can be the cause of poor biotolerability. However, there are no available data on potential solutions for this problem.<sup>[83]</sup>

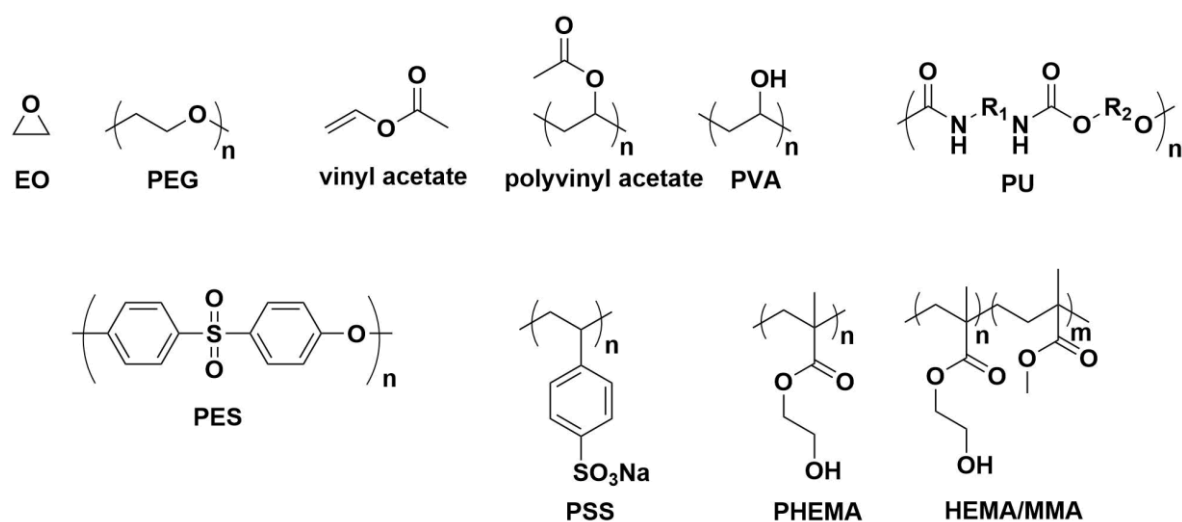


**Figure 8.** Structures of synthetic polymers: PEG, polyvinyl acetate, PVA, PU, PES, PSS, PHEMA, HEMA/MMA and of monomers EO and vinyl acetate.

Many new polymers have been applied in cell encapsulation in the past decades. They have been mainly introduced to overcome the limitations of other polymers, such as insufficient biotolerability in the host,<sup>[84]</sup> undesired graft loss, poor mechanical stability *in vivo*, and low permeability that impairs cell survival.<sup>[7]</sup> Apart from alginate, none of these new polymers have been properly characterized, which severely limits the clinical translation of their scaffolds in cell transplantation.

The composition and sequential characteristics of alginate have been thoroughly studied and shown to have a direct effect on the properties of capsules.<sup>[85]</sup> The relationship between chemical structure of the polymer and its functional importance in capsule formation has not yet been addressed for other polymers. A fundamental property of the polymers applied in cell encapsulation is their molecular weight that has been used to determine the viscosity and rheological properties of the polymer solution, which, in turn, give a measure of the quality and mechanical strength of the final capsule.<sup>[86]</sup> Another issue in natural polymers is the presence of endotoxins in their solutions with devastating consequences for the biotolerability of the resulting capsules.<sup>[5]</sup> Moreover, the permeability of the devices is only rarely reported.<sup>[7]</sup> This is rather surprising because the devices are being applied as a barrier for the immune system and should at least not allow the entry of cytotoxic molecules above 100 kDa.<sup>[7]</sup> These parameters are not documented in the vast majority of papers on cell encapsulation.

To date, the best documented and studied polymer is alginate and thus, presently has the highest chance of success in clinical applications.<sup>[7]</sup> Nonetheless, this does not indicate that alginate is the most adequate polymer. Cell encapsulation requires a more systematic

approach for the characterization of the properties of the applied polymers. This would enable proper interpretations of the obtained results and pave the way for further innovations.<sup>[49]</sup>

#### **1.4 Geometry of the capsules**

The encapsulation of living cells generates mainly two types of geometries: macro- and microcapsules. Living cells in macrocapsules are enveloped in relatively large diffusion chambers with semipermeable properties. Diffusion chambers have been produced in the form of flat sheets, hollow fibers, and disks.<sup>[87]</sup> Macrocapsules can be constructed either as intra- or extravascular devices.<sup>[52]</sup> The former contain cells within hollow capillaries attached directly to the recipient's vascular system. Thus, they provide better access to nutrients and oxygen as well as immediate recognition of changes in the concentration of various factors in the bloodstream and they facilitate higher diffusion of the secreted substances from the encapsulated cells. However, a major disadvantage of these devices is the high risk of causing thrombosis, which requires life-long systemic anticoagulation therapies with potential adverse effects. Hence, overall, they are poor candidates for widespread use in clinical transplantation.

Thus, the most ongoing research in the field currently focuses on extravascular devices, in which cells are embedded within semipermeable diffusion chambers and implanted under the skin or in the peritoneal cavity without direct vascular access. The required procedure is minimally invasive, and the implants can be easily retrieved or replaced in case of graft failure or for substitution purposes. This technology has proved highly successful in experimental settings in both animal models and humans and is highly promising for various applications.<sup>[88,89]</sup> Nevertheless, macrocapsules are characterized by a relatively low surface-to-volume ratio and can only support a quite low density of enveloped cells, which does not exceed 5 - 10 % of the volume fraction. Additionally, high amounts of nutrients are necessary to generate an adequate diffusion gradient to reach the cells, which usually impairs their survival. In cases of demand of large cell masses, the low cell density respectively implies the transplantation of a high number of such devices. The latter poses a significant barrier to their engraftment in the human body, considering the space limitations of the implant sites. Therefore, currently the research on macroencapsulation focuses on the development of techniques that increase nutrition for tissues.<sup>[49]</sup>

On the other hand, microcapsulation is not associated with surface-to-volume ratio issues. It consists of immobilizing cells in capsules; the size of one dimension of which is in

the region between 100 - 500  $\mu\text{m}$ . This implies high cell density, which allows a fast exchange of therapeutic molecules and has been shown to closely mimic the release of insulin and glucose. These favorable properties have encouraged several studies with a focus on the development of microcapsules that elicit low or no inflammatory responses for the cure of endocrine diseases.<sup>[49,90,91]</sup>

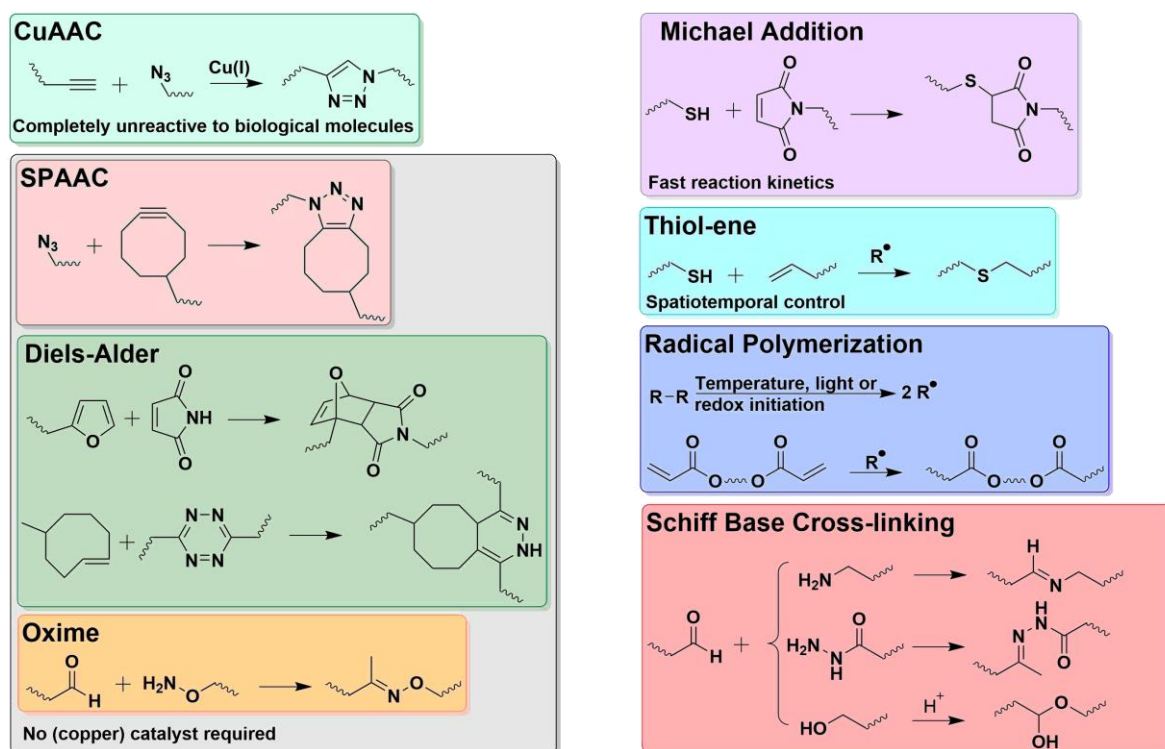
## 1.5 Encapsulation chemistries

The applied chemistry for the cross-linking of the polymers to generate the macro- or microcapsules constitutes one more factor that highly influences the longevity of the encapsulated cells. It is thus crucial that neither the natural or synthetic polymers nor the chemistry interfere with the enclosed cells during or after the encapsulation procedure. In the case of alginates, the cross-linking is based on the electrostatic binding of the anionic repeating units of the polymer with divalent cations:  $\text{Ca}^{2+}$ ,  $\text{Ba}^{2+}$  and  $\text{Sr}^{2+}$ . A barium mediated gelation is highly favored because the cation has a high affinity not only to G but also to M monomeric units thus it affords capsules of higher mechanical stability and better permselectivity.<sup>[47,92]</sup>

In spite of these advantages, there are reports that highlight the toxicity of barium and raise concerns about the safety of transplants originated from  $\text{Ba}^{2+}$ -mediated cross-linking. In fact, it has been shown that  $\text{Ba}^{2+}$  inhibits potassium channels in cell membranes at concentrations greater than 5 - 10 mM and at gelation times longer than 15 minutes.<sup>[93]</sup> As a result,  $\text{Ca}^{2+}$  has been the main cation for the gelation of alginates to microcapsules for cell therapies.

To promote a long lifetime of the engrafted cells, bioorthogonal chemistries have proven to be very powerful, elegant strategies, since their first applications.<sup>[94]</sup> Besides being fast and efficient at physiological temperatures, these approaches ideally make use of no toxic catalysts or harmful substances and solvents for the cells (Figure 9). One such bioorthogonal strategy that has been heavily studied<sup>[95]</sup> and recently applied to encapsulate living cells in bulk hydrogels involves the strain-promoted alkyne-azide cycloaddition (SPAAC).<sup>[96]</sup> Although this approach is promising, there is still need for new versatile SPAAC routes that expand ways to further manipulate the still unexploited cellular potential.<sup>[97]</sup>

## Click reactions - Chemical Cross-linking



Well characterized reaction kinetics, facile *in situ* polymerization, mild and cell-compatible reaction conditions

**Figure 9.** Types of bioorthogonal chemistries applied in cell encapsulation.<sup>[94]</sup>

Furthermore, the most widely used synthetic material for the immunoisolation of cells in numerous investigations is polyethylene glycol. The majority of these studies employed acrylate-derivatives of PEG which were gelled *via* UV-light catalysis in the presence of a photoinitiator.<sup>[98–100]</sup> Although these studies have generated promising results of a long survival of encapsulated islets with insulin release, the exposure to UV light regardless of its duration can entail a significant toxicity to various sensitive cell types and represents a barrier for the clinical translation of these strategies. Thus, further research in this regard is necessary to improve the current manufacture procedures and develop new approaches that could augment cell transplantation as a life-long, definitive treatment of chronic endocrine diseases.

## 1.6 Cell encapsulation procedures

Based on the reasons detailed in Sections 1.2 and 1.3, this thesis will be limited to the discussion of data on microencapsulation procedures that utilize the most documented natural polymer: alginate as a constituent of the microscale-sized matrices.

The two most widely used devices for microencapsulation are the air-syringe pump droplet generator and the electrostatic bead generator.<sup>[101]</sup> The first employs simple dropwise extrusion of alginate from a needle into a bath of divalent ions ( $\text{Ca}^{2+}$  or  $\text{Ba}^{2+}$ ) and relies on gravity to overcome the surface tension of the droplet at the tip of the needle, to produce particles with diameters approaching 2000  $\mu\text{m}$ . However, as detailed above, smaller capsules would be more suitable implants to meet the space limitations of the human body. Implementing a shorter distance from the needle to the calcium bath was envisioned to overcome the size problem of this process. This modification was insufficient because the distance, however short, remains still long enough for gravity to act on the much denser cells in the alginate droplet pulling it to the bottom edge during bead formation. Consequently, some cells are located on the edge of the capsule after alginate cross-linking and can be exposed to the host immune system. However, in physiological solutions or once they are implanted, beads made of  $\text{Ca}^{2+}$ -alginate undergo osmotic swelling causing an increase of permeability, destabilization, and, finally, the disruption of the capsule. This is a result of the constant interchange between  $\text{Ca}^{2+}$  and other non-gelling ions ( $\text{Na}^+$ ,  $\text{Mg}^{2+}$ ) and because of the higher affinity of  $\text{Ca}^{2+}$  to chelating agents such as phosphate and citrate than to alginate. To overcome these limitations, resulting beads are usually coated with an additional polycation layer, usually a poly-L-ornithine or poly-L-lysine that strengthens the matrix and adjusts its permeability. Nevertheless, owing to the immunoreactivity of the polycation layer a second coating layer of alginate is necessary to avoid implant rejection. The additional coatings, produce spheres of large diameters thus conferring substantial difficulties to this approach in effectively reducing the sizes of the produced capsules. (Figure 10).<sup>[48,93]</sup>

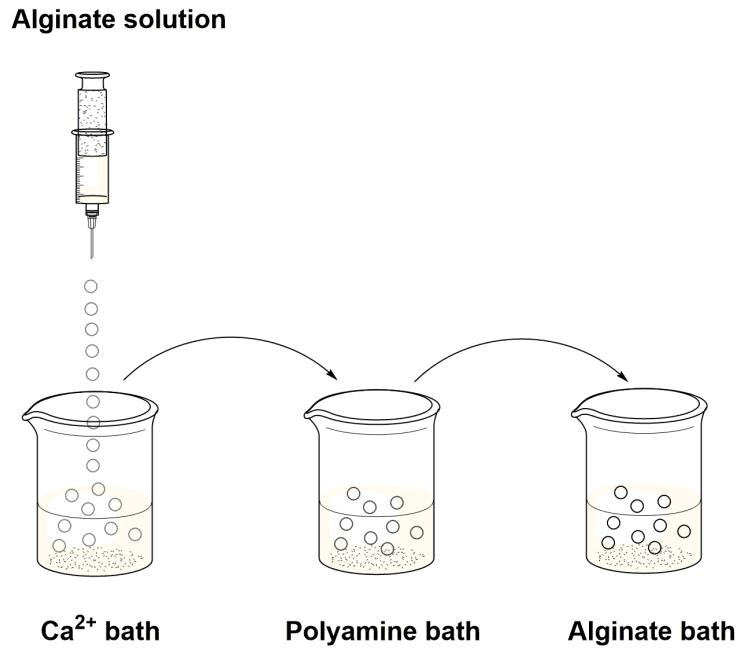


**Figure 10.** Air syringe-pump microcapsule manufacture. An alginate suspension of cells is cross-linked in a calcium bath. The formed droplets are then coated with a polyamine and subsequently with an additional alginate layer.<sup>[48]</sup> Copyright 2014, Elsevier.

The second approach relies on differences in potential which cause an accumulation of charge on the surface of the droplet subsequently reducing surface tension to produce a jet of solution. Pulsing the voltage potential at specific frequencies breaks the flow into discrete droplets of uniform size, smaller than those achieved without electrostatic assistance (Figure 11). The electrostatic-mediated droplet production is nowadays the most widely used technique for the generation of alginate encapsulated cells as it combines efficiency with cytocompatibility and introduces no additional sources of contamination.<sup>[48]</sup>

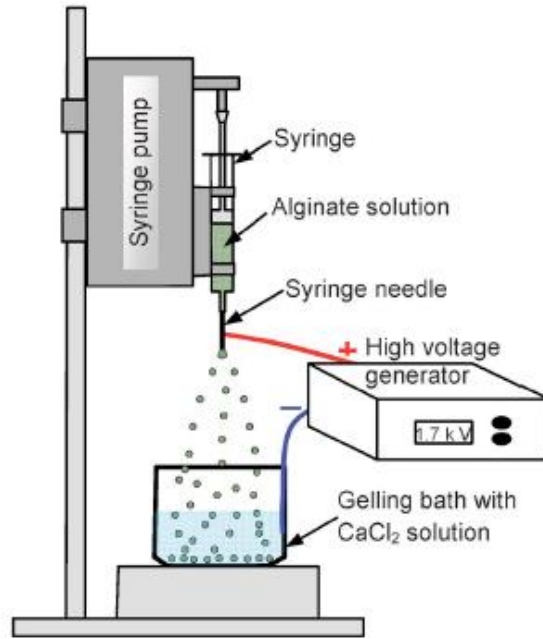


**Figure 11.** Electrostatic bead generator. An alginate suspension of cells produces a liquid jet upon potential gradient. Specific frequency pulses break the jet into discrete, small alginate microcapsules.<sup>[102]</sup> Copyright 2009, The American Society of Mechanical Engineers.

A promising approach to improve the production rates of encapsulated cells is the vibrating nozzle encapsulation. This technology can increase the liquid extrusion rate forming a liquid jet at the tip of the needle. Upon vibration, the formed liquid jet breaks into discrete droplets generating a large number of small diameter alginate spheres in a short time (Figure 12). To circumvent vibration damping resulting from highly viscous liquids, the instruments are equipped with a jet-cutting tool. The latter could damage large cells and cell clusters through high shear forces and introduce difficulties in maintaining aseptic conditions.<sup>[48]</sup>

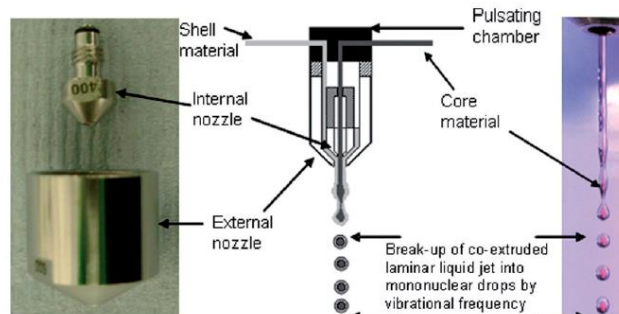


**Figure 12.** Two-flow nozzle system for the fabrication of alginate microspheres bearing cells.<sup>[103]</sup> Copyright, 2011 Taylor & Francis Online.

As largely reviewed recently, a variety of techniques including electrospraying or the most recent microfluidic fabrication<sup>[104]</sup> is the objective of ongoing optimization studies. However,

there is currently no commercially available microencapsulation device that satisfactorily meets the optimum requirements for cell microencapsulation. An acceptable speed to microencapsulate large masses of cells as well as reproducibility in the generation of highly homogeneous spherical shapes and sizes to promote proper function of the enclosed cell populations are highly demanded.

## **1.7 Anatomy and histology of pancreas**

The pancreas is a composite glandular organ that contains both an exocrine and an endocrine component. With its two types of parenchymal tissue, it is part of the gastrointestinal system and simultaneously an endocrine organ. In adult humans, most of the pancreatic tissue (almost 95 %) is devoted to exocrine function, consisting of acinar and duct cells with associated connective tissue, vessels, and nerves.<sup>[141]</sup> Formed in bundles that resemble grape clusters (Figure 13), the acinar cells produce digestive enzymes which they secrete *via* the ducts into the duodenum, to assist the digestion and absorption of nutrients in the small intestine. Located between the clusters of acinar cells are scattered patches of another type of secretory tissue, collectively known as islets of Langerhans, named after the German pathologist Paul Langerhans (19<sup>th</sup> century) who discovered them. The islets accounting for only 1 - 2 % of the organ carry out the endocrine functions of the pancreas, and release hormones in the bloodstream to control energy metabolism and storage throughout the body.<sup>[142]</sup>

The normal human pancreas weighs approximately 80 grams and it is shaped like a fish. It contains about a million islets, the size of which varies greatly, with the majority (almost 70 %) measuring 50 - 200  $\mu\text{m}$  in diameter and consisting of several thousand individual cells.<sup>[145]</sup> There are at least five different types of secretory endocrine cells typically interspersed in the islets:  $\alpha$ -,  $\beta$ -,  $\gamma$ -,  $\delta$ -, and  $\epsilon$ -cells. The most common, making up 50 - 80 % of the total islet cells are the  $\beta$ -cells, which secrete insulin and amylin. The  $\alpha$ -cells produce glucagon and amount to 30 - 35 % of the total islet population. The  $\delta$ -cells, accounting to 3 - 10 % of the islets of Langerhans produce somatostatin<sup>[146]</sup> whereas the  $\gamma$ -cells with a similar overall proportion (3 - 5 %) secrete pancreatic polypeptide and are also known as PP-cells. Lastly, minority populations of ghrelin cells, the  $\epsilon$ -cells comprising less than 1 % of the total islet cells, produce the hormone ghrelin.<sup>[145]</sup>

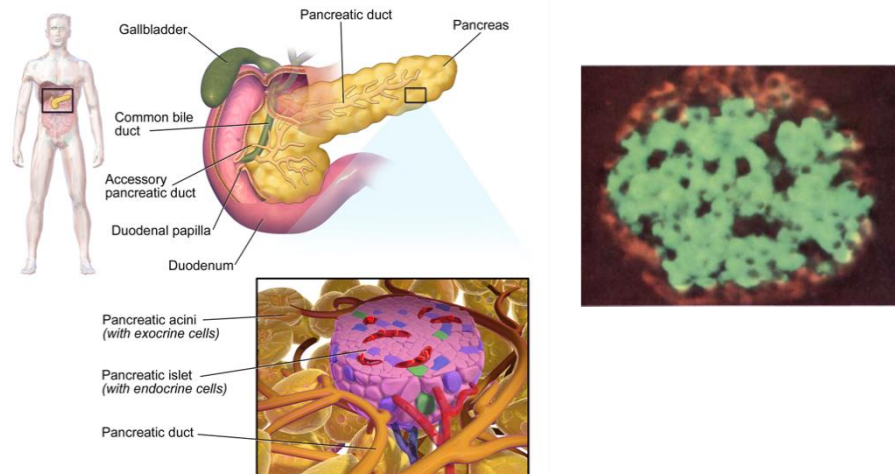


**Figure 13.** Simplified depiction of the adult human pancreas, its exocrine cells, and endocrine islets.<sup>[143]</sup> Copyright 2016, Boundless. To the right: enlarged photomicrograph of pancreatic islet. Fluorescent insulin antibodies (green) show that insulin-containing  $\beta$ -cells characteristically occupy the center of the islet. Glucagon antibodies (red) stain the  $\alpha$ -cells located at the periphery of the islet that also hosts the  $\delta$ - and  $\epsilon$ -cells.<sup>[144]</sup> Copyright 1988, Scientific American.

The anatomic proximity of the  $\alpha$ -,  $\beta$ -, and  $\delta$ -cells in the islets of Langerhans is very important and renders the feedback system in the pancreatic islets paracrine.<sup>[147]</sup> This type of cell-cell communication is based on the activation and inhibition of the islet cells by endocrine hormones produced in the islets. Insulin activates the  $\beta$ -cells and inhibits the  $\alpha$ -cells,<sup>[143]</sup> whereas somatostatin and glucagon appear to have a paracrine relationship as they each affect the secretion of the other and both affect the rate of insulin release.<sup>[147]</sup> Furthermore, somatostatin and glucose decrease the secretion of pancreatic polypeptide, which, in turn is known to self-regulate the pancreatic secretion activities, both endocrine and exocrine.<sup>[148]</sup> Ghrelin inhibits glucose-stimulated insulin secretion from beta cells in the pancreatic islets. Ghrelin does this indirectly by promoting local negative feedback mediated by somatostatin from pancreatic delta cells, which selectively express the ghrelin receptor.<sup>[149]</sup>

## 1.8 Pancreatic $\beta$ -cells: insulin release and type 1 diabetes

The pancreatic  $\beta$ -cells constitute an autonomous system that responds in ambient blood glucose concentration changes in order to maintain glucose homeostasis. In humans, blood glucose levels normally range from 80 - 120 mg/dL (4.4 - 6.7 mM). Even in cases of starvation, these levels should be maintained above 40 mg/dL (2.2 mM). Upon increase of the blood glucose, there is a resultant flux of the latter across the GLUT1, 2, and 3 transporters in the  $\beta$ -cell. Subsequently, within the  $\beta$ -cell, glucose is phosphorylated from ATP to glucose-6-phosphate (G-6P) in a step catalyzed by glucokinase (Figure 15).

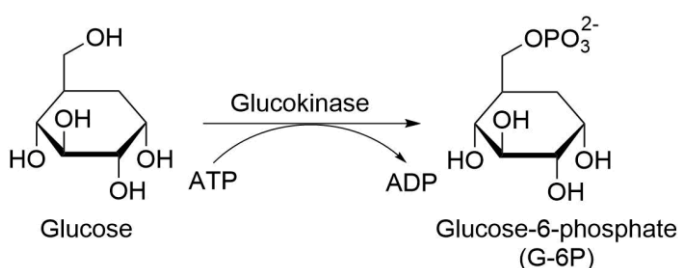


**Figure 15.** Glucokinase-catalyzed phosphorylation of glucose by ATP in the pancreatic  $\beta$ -cells.

This is the rate-limiting step of insulin secretion and as such glucokinase is considered the “glucose sensor” for the  $\beta$ -cell. Once in the mitochondria, G-6P is metabolized *via* the Krebs cycle to produce ATP, which triggers a cascade of signals within the  $\beta$ -cell necessary for the glucose-stimulated insulin secretion (GSIS). In detail, the resultant ATP binds and closes the ATP-dependent potassium channel, which disables the passive flow of  $\text{K}^+$  ions outside the cell, leading to depolarization of the cell membrane. Once the cell is depolarized, the L-type voltage-gated calcium channels are triggered to increase the influx of calcium and thus the cellular calcium concentrations. In response to the increased cytoplasmic  $\text{Ca}^{2+}$  concentration, the prohormone precursor proinsulin is enzymatically cleaved to produce equimolar amounts of insulin and peptide C. Both insulin as well as C-peptide are stored in mature, non-coated secretory granules and consequently exocytosed in the bloodstream, which stimulates the migration of additional insulin-loaded vesicles to the cell membrane (Figure 16).<sup>[150]</sup> C-peptide presents only negligible extraction by the liver but a constant peripheral clearance. As a result, it has a longer half-life than insulin measuring 20 - 30 minutes as opposed to 3 - 5 minutes for insulin. Thus, it is present in the systemic circulation in concentrations almost five times higher than insulin.<sup>[151]</sup>

This simplified description of glucose-induced insulin secretion is only a part of the more complex process that is considered the primary secretory pathway of the hormone (Figure 17). The complete route includes amplifying cascades that augment GSIS and are either metabolic, actuated by amino acids, free fatty acids, and glucose itself or neurohormonal involving the parasympathetic innervation and molecular amplifiers such as GLP-1. This activation of  $\beta$ -cells' endocrinal response to increased blood glucose levels occurs postprandially and is known as 'bolus' insulin release, whereas the body's demands are covered overnight or between meals by lower insulin amounts secreted, which is referred to as 'basal' insulin.<sup>[150]</sup>

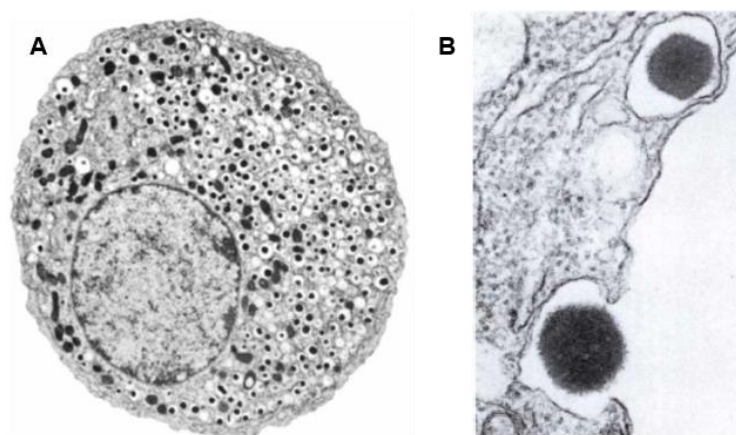


**Figure 16.** Electron microscopy images of pancreatic  $\beta$ -cells. (A)  $\beta$ -cell loaded with insulin. The numerous circular vesicles containing dark blobs are the uncoated secretory granules in which insulin is stored ready to be released from the cell if the concentration of glucose in the bloodstream increases. (B) Exocytosis of insulin from a pancreatic  $\beta$ -cell. One secretory granule is about to fuse with the cell's membrane and release insulin into the extracellular milieu, whereas the other granule has opened and insulin is being secreted.<sup>[144]</sup> Copyright 1988, Scientific American.

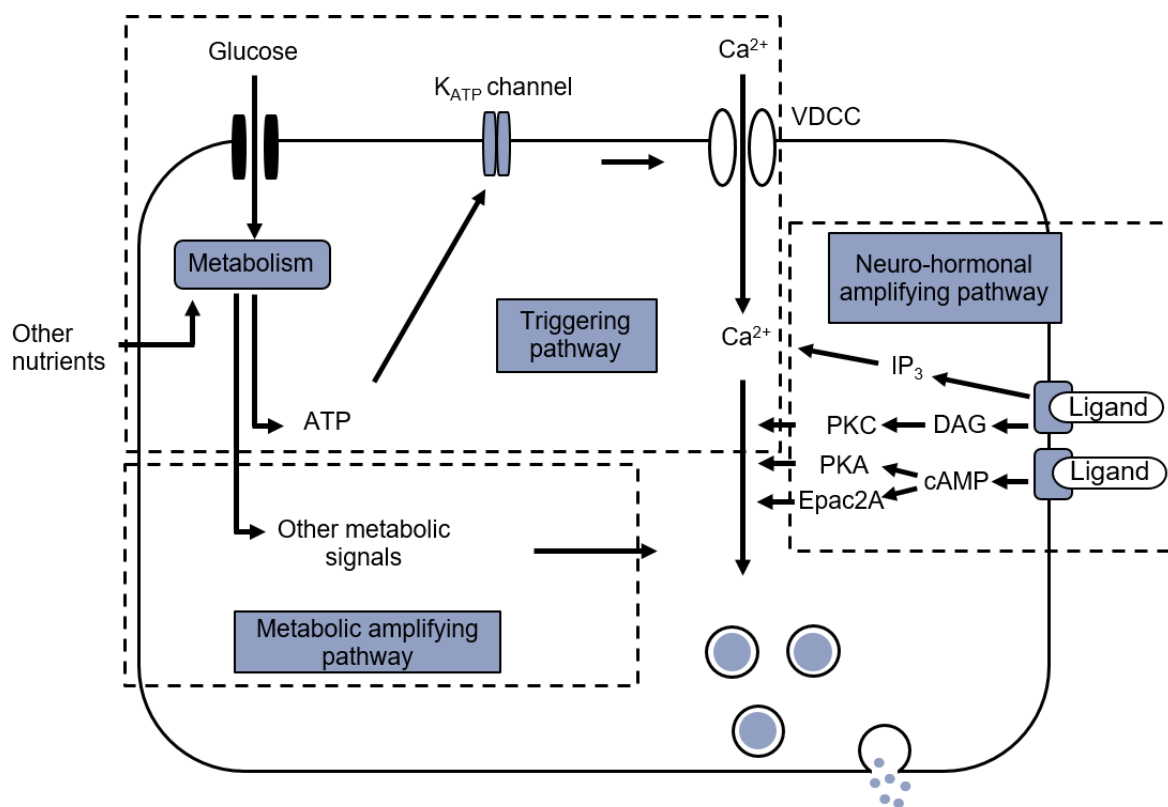


**Figure 17.** Glucose-stimulated insulin secretion (GSIS). Glucose metabolism results in an enhanced cytoplasmic ATP/ADP ratio, which prompts closure of ATP-sensitive  $K^+$  ( $K_{ATP}$ ) channels in the plasma membrane evoking membrane depolarization and subsequent opening of voltage-gated  $Ca^{2+}$  channels (VDCC). This culminates in an increase in cellular  $Ca^{2+}$  influx, a primary driver of the GSIS mechanism.  $Ca^{2+}$ , vesicle docking, and fusion events can also be modulated by agents acting through the phospholipase C (PLC)/protein kinase C (PKC) or adenylyl cyclase (AC)/protein kinase A (PKA) pathways. DAG and Epac2A stand for diacylglycerol and the exchange protein directly activated by cAMP 2, respectively.<sup>[150]</sup> Copyright 2016, American Pancreatic Association.

In type 1 diabetes mellitus (T1D or T1DM), a misregulation of the immune system results in immunological intolerance towards insulin-producing  $\beta$ -cells. T1D is characterized by the inflammation of islets of Langerhans and, subsequently, the selective destruction of the  $\beta$ -cells.<sup>[152]</sup> As a result, there is no or scarcely any insulin available to ensure the basal-bolus insulin dynamic and thus maintain glucose homeostasis. Adapting to insulin deficiency, all metabolic processes culminate in a state of biochemical starvation. The latter is characterized by high amounts of glucose in the bloodstream, which due to inadequate insulin, cannot be taken up by muscle or organ tissue. To circumvent the lack of glucose, the liver shifts to the metabolism of fatty acids and thus produces large amounts of ketone bodies and glucose that are released in the bloodstream. Being moderately strong acids, ketone bodies serve to reduce the pH value of the blood, a condition known as diabetic ketoacidosis. As a result, tissue functions are severely impaired especially in the CNS, which could

ultimately lead to coma. With almost no glucose being metabolized and new glucose being diffused in the blood from the liver, the reabsorptive capacity of the renal tubules is exceeded, which leads to excretion of glucose. Along with glucose, water is also removed through the renal circulation, rendering an untreated diabetic in the acute phase of the disease both hungry and thirsty. Because of the sugar in the urine, the disease received the name ‘mellitus’ which is the Latin word for honey.<sup>[153]</sup>

T1D is a chronic, progressive life-long disease and one of the most common endocrinal metabolic conditions diagnosed mainly in young children and adolescents.<sup>[154]</sup> Initially reported to affect only the youth and therefore long called ‘juvenile diabetes’, it is nowadays known to occur at any age.<sup>[155]</sup> Over the last decades, its prevalence has been increasing worldwide with profound implications, not only on an individual but also on a social level. The diabetic complications posing a major cause of morbidity and mortality in persons with T1D, as well as the imperfections of the available therapies, impede the long-term health and the overall quality of life of the affected.<sup>[156]</sup> Furthermore, T1D imposes a large financial burden on the global health-care system and wider global economy. Its costs involve direct medical as well as indirect expenses associated with loss of productivity, premature mortality, and the negative impact of the disease on nations’ gross domestic product (GDP).<sup>[157]</sup>

As of 2014, an estimated 422 million people have diabetes mellitus of which T1D accounts for 5 - 10 % between 21 and 42 million affected individuals (Figure 34).<sup>[156,158]</sup> Moreover, the latest findings estimate the global cost of diabetes for 2015 US \$1.31 trillion or 1.8 % of GDP, rendering the respective costs of T1D alone US \$131 billion. North America was the most affected region relative to GDP and also the largest contributor to global absolute costs. However, on average, the financial burden as percentage of GDP was larger in middle-income countries than in high-income countries.<sup>[159]</sup>

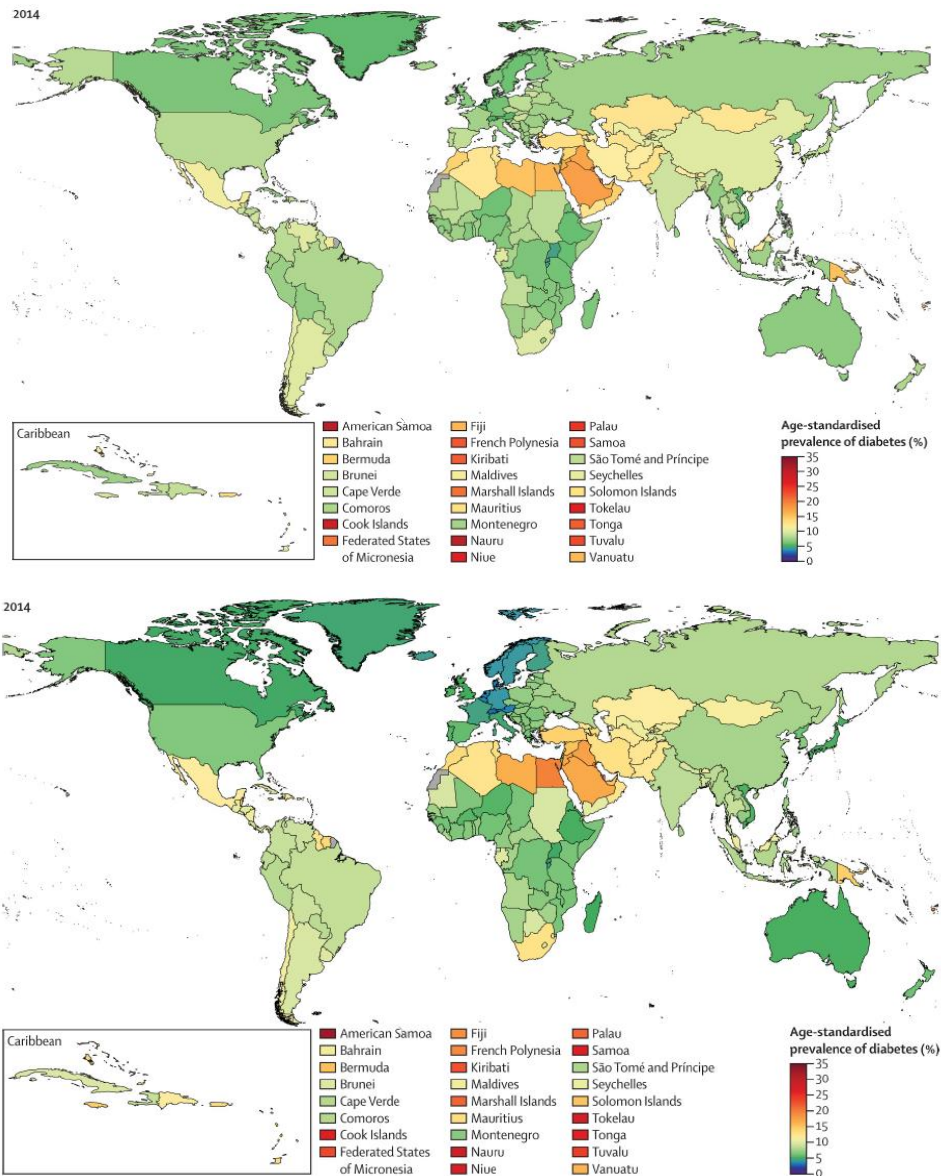


**Figure 18.** Age standardized prevalence of diabetes in adult men (top) and women (bottom) in 2014. 5 - 10 % of the cases account for T1D incidence worldwide.<sup>[159]</sup> Copyright 2017, Elsevier.

The increasing incidence of T1D in children and adolescents is likely to result in increasing numbers of individuals with diabetes-related complications in their early adulthood. These complications are not only limited in diabetic ketoacidosis and all its risks but extend further to neurologic, micro-, and macrovascular conditions as well as hypoglycemia. Although cardiovascular disease is not specific to diabetes, T1D is associated with at least a 10-fold increase in cardiovascular disease as compared with an age-matched non-diabetic population.<sup>[160]</sup> Additionally, childhood-onset T1D presents a 4-fold higher probability of premature mortality due to diabetic nephropathy and its excessive risk of end-stage renal failure.<sup>[161]</sup> With a relatively low prevalence among persons with T1D worldwide,

diabetic retinopathy, is another microvascular complication of the disease. It is manifested as diabetic macular edema affecting almost 3 % of the T1D individuals worldwide, of which approximately one third is threatened with vision loss.<sup>[162]</sup> It is common that diabetic complications are correlated and giving rise to additional symptoms. As such, lower extremity amputation (LEA) has met in the past decades with a declining incidence in Europe and the USA. LEA however, remains higher in patients with T1D and is especially associated with higher cardiovascular mortality compared to healthy individuals. A further debilitating complication of T1D is diabetic peripheral neuropathy (DPN) that has been well characterized in adults, with prevalence rates ranging from 10 - 26 % in newly diagnosed adults with diabetes. Growing attention is drawn to the younger T1D-population exhibiting DPN which has been only poorly characterized.<sup>[163]</sup>

The most serious diabetic complication is hypoglycemia which occurs particularly to persons with T1D with an incidence rate of 30 % annually.<sup>[164]</sup> It constitutes a true medical emergency which requires prompt recognition and treatment to prevent organ and brain damage. The spectrum of symptoms depends on duration and severity of hypoglycemia and varies from autonomic activation to behavioral changes to altered cognitive function to seizures or coma. The short- and long-term complications include neurologic damage, trauma, cardiovascular events, and death.<sup>[165]</sup>

The exact etiology and pathogenesis of T1D is still unknown. Due to its highly heterogenous geographic and ethnic epidemiology, it is difficult to reach conclusive results from the related epidemiologic studies. Although a genetic proclivity to T1D has been found 8 to 15-fold higher in first-degree relatives, the majority of newly detected cases (>85 %) has been sporadic.<sup>[166]</sup> Thus, a genetic predisposition to the disease is only alleged to explain some of the geographic variability of its occurrence, but it cannot account for its rapidly increasing frequency.<sup>[156]</sup> Through multiple observations, the primary ones being the 500-fold variance in disease incidence based on geographic locale, seasonal variance in disease onset, and the major increases in the prevalence of this disease, particularly over the last half-century, a potential influence of environmental factors on T1D has been postulated. However, environmental factors that influence T1D's development have not been specifically isolated, only circumstantial ones. On the contrary, epidemiological studies have associated infant diet, viruses, and perhaps increased hygiene as contributing factors to this disease.<sup>[167]</sup>

One of the most important aspects of T1D is its diagnosis, especially regarding its detection at an early stage before its onset in children or adults. The poor understanding of its histopathology hampered initially proper disease diagnosis and often led to false

classification of T1D and T2D and thus inadequate therapies for the affected. The seminal discovery of islet cell cytoplasmic autoantibodies (ICA) in 1974 did not only offer clues to the autoimmune basis of the disease but also aided in providing some degree of clarity to the difficulties associated with disease classification and its diagnosis.<sup>[167]</sup> The sought antibodies include glutamic acid decarboxylase (GAD), insulin autoantibodies (IAA), insulinoma antigen-2 (IA-2), and zinc transporter-8 (ZnT8). While the presence of high titers of one or more of these autoantibodies makes the diagnosis of T1D likely, a few points must be kept in mind. (1) A significant proportion of patients with T1D are autoantibody-negative, particularly in Asia and Africa. (2) Autoantibody titers tend to diminish with time since the onset of diabetes. (3) Rarely autoantibodies may be positive in T2D.<sup>[166]</sup>

In daily practice, it is often still difficult to discern between type 1 and type 2 diabetes as their substantial overlap has become evident. There are specific laboratory criteria at onset of diabetes, which, however, have no definite thresholds that would allow a precise disease classification, or they are not exclusively correlated with either type. Moreover, various theories such as the “accelerator hypothesis” have been proposed that, despite the genetic differences, type 1 and type 2 diabetes constitute basically the same disorder distinguished only by the rate of  $\beta$ -cell destruction and the causal factors (the so-called accelerators) leading to  $\beta$ -cell loss. The latter include high intrinsic rate of apoptosis, insulin resistance and autoimmunity, which act in different individuals to varying degrees. Insulin resistance is central for the development of T2D, although in some cases T1D may also manifest a certain degree of insulin resistance.<sup>[168]</sup>

Apart from the identified autoantibodies, signifying the disease, C-peptide has been long considered an important marker that could assist diabetes classification and choice of the appropriate treatment. Due to the nature of its production, C-peptide is directly associated with functional residual  $\beta$ -cell mass in diabetic persons, whereas because of its long half-time low-cost, ultrasensitive assays have been developed that enable its detection at levels as low as 1.5 - 2.5 pmol/L. These monoclonal antibody assays give a measure of the potency of the affected person to secrete insulin at the time point of the assay. C-peptide levels are profoundly low or absent in patients with T1D and are characterized by a declining tendency that could continue even decades after diagnosis.<sup>[166]</sup> Thus, a confirmation of T1D years after its onset could be possible with a C-peptide test, provided that the obtained values of its concentrations are low.<sup>[151]</sup> In addition, several studies have investigated the association of autoantibodies, mainly of ICA, with the temporal changes in C-peptide levels. Their findings, of high ICA concentrations at a young age of diagnosis identify T1D with an increased risk

of rapid loss of residual  $\beta$ -cell function.<sup>[169]</sup> A rising incidence of type 2 diabetes among younger individuals accounts for a further hurdle in the clinical classification and therapy of the disease.<sup>[151]</sup> Moreover, it has been frequently observed that the C-peptide levels between type 1 and type 2 diabetes overlap substantially upon diagnosis, which renders the utility of C-peptide assays in differentiating the types significant only in long-standing diabetes. The right diagnosis and subsequent treatment are also hampered by conditions such as glucotoxicity, in which hyperglycemia of any etiology manifests suppressed C-peptide levels.<sup>[166]</sup>

The search for additional markers for T1D, as well as autoantibodies or C-peptide continues. Such efforts are warranted to refine our ability to predict T1D and to improve monitoring (e.g., therapeutic efficacy, mechanism, safety) interventions aimed at the prevention or reversal of the disorder.<sup>[167]</sup> It is also worthwhile to consider interventions at diagnoses that attempt to avoid the losses in  $\beta$ -cells after clinical onset, which might ultimately lead to better long-term metabolic control and thus a reduced risk of chronic diabetic complications.<sup>[169]</sup> The growing prevalence of diabetes with a higher rate in low- and middle-income countries than in high-income countries is an important indicator of the lack of a well-resourced health system. The establishment of the latter in Europe and other affluent countries might identify people at high risk of diabetes at an earlier stage and use lifestyle and dietary modification or drugs to prevent or delay its onset.<sup>[158]</sup> Nevertheless, low awareness of the disease's symptoms in the community and among health care providers is nowadays often evident even in high-income countries. Consequently, specific diabetic complications such as diabetic ketoacidosis often resulting from delayed care could be largely preventable.<sup>[170]</sup>

## 1.9 Type 1 diabetes: available treatments

### 1.9.1 Insulin therapy

Since its first application in the therapy of diabetes in 1921, exogenous insulin continues to be the mainstay for the treatment of T1D, constituting virtually the only highly non-invasive treatment that allows survival of the affected persons.<sup>[47]</sup> In fact, if appropriately modulated, exogenous insulin therapy regimens may substantially reduce the risk of developing secondary, chronic complications from T1D, especially micro- and macro-angiopathy, a combination that leads invariably to retinopathy, disabling neuropathy, cardiovascular disease, and terminal renal failure.<sup>[171]</sup> These regimens are based on intensive insulin treatment to achieve optimum glycemic control and ensure normal blood glucose levels. This can be accomplished using multiple daily injections or continuous subcutaneous insulin infusion delivered *via* a pump, which often incorporates an automated bolus calculator for appropriate insulin dosage.<sup>[172]</sup> Insulin pumps today are frequently equipped with a glucose sensor which was shown to improve glycemic control compared to daily insulin injections.<sup>[173]</sup> Additionally, important requirements for the success of these regimens in regulating the blood glucose concentrations are the repetitive blood sugar monitoring as well as a carefully controlled diet and exercise.<sup>[48]</sup>

However, apart from its crucial advantages, insulin therapy is associated with several pitfalls that derive from the fundamental lack of exogenous insulin administration to reproduce the stimulus-induced insulin secretory kinetics of normal  $\beta$ -cells under physiological conditions. Compared to the superior physiologic endogenous glucose homeostasis, intensive insulin therapy regimens mostly allow only brittle regulation of the blood glucose levels regardless of the delivery system.<sup>[171]</sup> These therapeutic schemes with their non-continuous monitoring of the circulating blood glucose and the subsequent adjustment of insulin dosage increase the risk of life-threatening hypoglycemic episodes. None of the current insulin therapies, either conventional or optimized *via* augmented insulin pumps, has prevented the occurrence of hypoglycemia.<sup>[48,172,173]</sup> Also from a diabetic's point of view, the treatment remains expensive, is highly complex and requires strictly actuated blood glucose monitoring, insulin dosing, and overall dietary lifestyle. A proper, personalized glycemic control is not universally possible for every affected person, whereas the treatment is not always completely effective even in the case of established normoglycemia.<sup>[174]</sup>

### 1.9.2 Pancreas transplantation

An alternative to tackle the insufficiencies of the pharmacological treatment of T1D and also the most direct approach to the replacement of diseased endocrine tissue is whole pancreas transplantation. The first applications of this strategy, as early as 1894, almost 30 years before the discovery of insulin, involved transplantation of grafts of non-human origin (xenografts) either in parts or as minced injectables. Envisioned to cure diabetes mellitus, the method could only achieve a temporary relief of the symptoms of the disease and was at the time inevitably fatal. As a solution to the imminent mortality of xenogeneic implants, a graft derived from a human cadaver (allograft) was first transplanted in whole in a type 1 diabetic in 1966. The technique met with significant challenges did not become commonplace until the early 1990s. In 2014 there were more than 35.000 transplant reports worldwide according to data of the International Pancreas Transplant Registry.<sup>[48,175]</sup> Unlike, heart, lung, and liver transplants, whole pancreas transplantation is not a life-saving operation, but one to improve quality of life. In addition, the number of donors with transplant-quality pancreases is very low. Thus, the procedure is restricted only to the T1D afflicted who suffer from end-stage renal failure and is usually performed in conjunction with kidney transplantation. As such, it remains a non-viable option for the majority of the population affected by T1D calling for new optimized approaches for the improvement of glycemic control.<sup>[48,92]</sup>

A successful whole pancreas transplantation provides a closed-loop system to achieve tight blood glucose normalization, insulin independence, and restoration of hypoglycemia unawareness with improvement in both quality and quantity of life.<sup>[92,175]</sup> The success of the procedure is determined by several factors that are primarily improved immunosuppression as well as donor and recipient selection protocols. More recent improvements in graft surveillance techniques including the introduction of pancreatic biopsy have significantly increased the half-life of implants. One- and five-year patient and graft survival rates are now similar to those of kidney, liver, and cardiac transplantations, with UNOS data reporting a 71 % five-year pancreas graft survival and a 80 % five-year patient survival.<sup>[175]</sup> However, although clinically successful, whole pancreas transplantation has its disadvantages. It is a major surgical intervention, with a high morbidity risk associated with the drainage of the exocrine fluids or early thrombosis of the graft, which even nowadays contributes notably to its rejection.<sup>[175]</sup> To ensure longevity of the implants and no immune responses of any kind, the recipients must adhere to a life-long immunosuppressive regime. Although undeniably necessary, many anti-rejection drugs can elicit serious side effects, such as increased susceptibility to infection, renal dysfunction, hyperlipidemia, anemia, mouth ulcers, and a

theoretically increased risk of cancer. In limited cases, the severity of the side-effects has led to discontinuation of the applied immunosuppression.<sup>[92]</sup> Furthermore, a number of studies in pancreas transplant recipients with T1D have noted that many of them, although insulin-independent, display impaired or even diabetic glucose tolerance based on standard WHO criteria. This may be related to injuries caused during the transplantation process.<sup>[176]</sup> The ultimate drawback of this treatment is the recurrence of autoimmune T1D leading to graft failure despite effective immunosuppression. To date this has been observed only in a few cases and is associated with typical histological features of insulinitis, one of the first stages of immune activation against the pancreatic  $\beta$ -cells.<sup>[175]</sup>

### **1.9.3 Islet cell transplantation**

The severe limitations of insulin therapy and whole pancreas transplantation directed the design of new therapeutic approaches for T1D towards cell encapsulation for the transplantation of islet cells. In brief, this technology consists of encasing insulin-producing  $\beta$ -cells in bioinert semi-permeable polymeric membranes that serve to protect the cells from both mechanic stress and immune responses of the host.<sup>[13]</sup> The surrounding capsules allow diffusion of nutrients and oxygen that are necessary for the functional survival of the cells while simultaneously ensuring outflux of metabolic waste and insulin upon demand. The semi-permeable nature of the cellular carriers characterized by pore sizes of a few nanometers prevents the entrance of larger immune cells or antibodies.<sup>[8]</sup> Therefore, such cell-bearing artificial matrices are highly promising as transplants for long-term vitality of the immobilized cells and for fine regulation of the blood glucose levels with an aim at normoglycemia (Figure 19). Moreover, the transplantation of islet cells is a minimally invasive procedure. It can deliver insulin in a minute-to-minute manner as dictated by the host's time-specific needs without requiring repeated transplantations. Thus, this approach would not rely on immunomodulatory protocols to avoid implant rejection or recurrence of autoimmune diabetes and therefore could also circumvent the potential side-effects of immunosuppressants.<sup>[13]</sup>

The first successful islet transplantation in man was reported in 1980 and was performed on patients with chronic pancreatitis, who underwent total or near total pancreatectomy, followed by transplantation of their own isolated islets (autologous implants), which prevented diabetes pathogenesis.<sup>[177]</sup> With the further development of islet isolation technologies pure human islets were accessible, which considerably advanced the

field of islet transplantation and encouraged new attempts of clinical islet transplantation for diabetes in the late 1980s and 1990s.<sup>[101]</sup> It was in 1989, when the first person with diabetes successfully received purified human islets implanted into the portal vein resulting in the elimination of insulin requirements for 37 days. Several additional islet implants for many months of partial function were demonstrated in follow-up studies.<sup>[47]</sup>

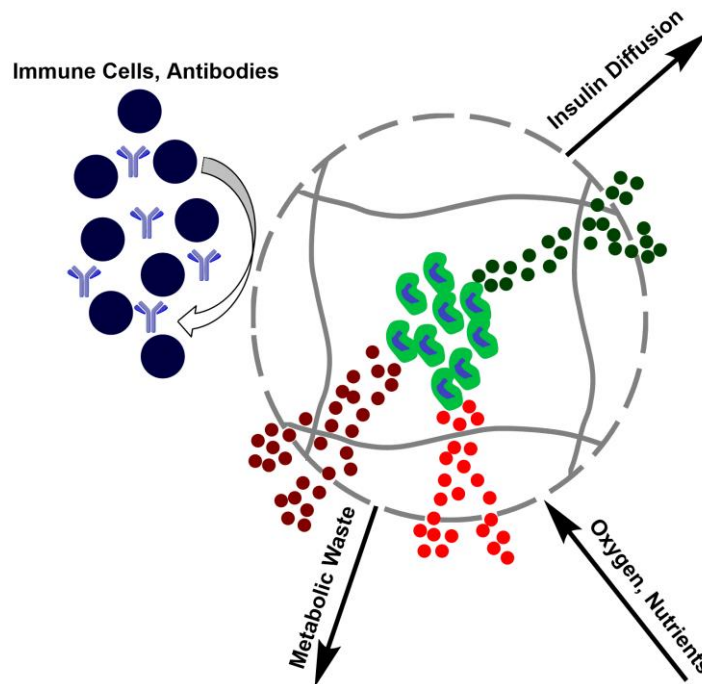


**Figure 19.** Principle of islet cell encapsulation. A semi-permeable membrane allows bidirectional diffusion of insulin, metabolic waste, oxygen, and nutrients, while simultaneously preventing entrance of immune cells and antibodies.

To determine the potential of the approach to circumvent immunosuppression, various studies were conducted on small and larger animal models showing in the first case that immunoisolation or use of immunoprivileged sites alone was enough for successful islet transplantation, but none of the employed strategies worked consistently in large animals.<sup>[101]</sup> It is critical to note that immunosuppressive protocols were widely accepted for islet transplantation in humans and therefore all successful clinical islet implants that have followed to date have required immunosuppression for graft acceptance.<sup>[47]</sup> Unfortunately, most immunosuppression strategies applied in solid organ transplantation were found to be highly diabetogenic because they made use of glucocorticoids. As a result, alloislet transplantation attempted in selected patients with T1D had only limited success, whereas insulin-independence post transplantation was inconsistent and transitory with less than 10 % of recipients being insulin-free at one year.<sup>[177]</sup>

This situation drastically changed in 2000 when a steroid-free immunosuppressive protocol for human islet transplantation known as the “Edmonton protocol” was established. Thus, renewed efforts involving experienced islet transplant programs were possible, which further promoted the development of new islet transplant centers. The generated data repeatedly confirmed the Edmonton protocol and signified a considerable progress for the field without, however, surmounting the existing barriers of human islet transplantation.<sup>[101]</sup> It was fast concluded that infusion of a larger than expected islet mass was required for insulin independence, which was not always achieved, while the function of the implants declined or was lost in the longer term in most recipients. Nevertheless, since its beginning and over the past 30 years, islet transplantation has evolved into a conceptually valid replacement therapy for some patients with severely labile T1D. Recently, a phase 3 multicenter study of islet transplantation for prevention of hypoglycemia in severe labile individuals with T1D completed enrollment. According to few of its preliminary results in 2014 approximately 55 % of patients were insulin independent one year after transplantation, but a large majority had only improved blood glucose control with fewer episodes of hypoglycemia.<sup>[101]</sup> The broader application of human islet transplantation as a  $\beta$ -cell replacement therapy to encompass a significantly large part if not the whole of the T1D population will require improvement in metabolic function, avoidance of the immune system, and a means to address the shortage of organs for donation.<sup>[171]</sup> Generating large numbers of functional human  $\beta$ -cells from pluripotent stem cells has recently raised the interest in the application of this approach to meet the need for an inexhaustible source of donor tissue. This promising outcome has yet to prove its potential and success as a widespread clinical strategy, especially regarding the challenges presented by the host’s immune barriers.<sup>[101]</sup>

### **1.9.3.1 Sizes and shapes of capsules for islet cell transplantation**

The immunoisolation of pancreatic islets has been performed either as macro- or microencapsulation. In the first case, multiple islets are enclosed in large capsules with diameters in the range of 0.5 - 1.5 mm. Having a relatively low surface-to-volume ratio, the macrocapsules can only support a quite low density of embedded cells, not exceeding 10 % in volume, to ensure adequate supply of oxygen and nutrients. Consequently, macrocapsules have long been considered rather impractical, as more large devices would be necessary to provide sufficient masses of islets. This presents a significant barrier to their transplantation in the human body, regarding the space limitations of the conventional implantation sites.

Additionally, low surface-to-volume ratio results in slow glucose-insulin exchange which also interferes with glucose regulation.<sup>[101]</sup> Furthermore, objects too large for macrophage phagocytosis initiate processes that result in the fusion of macrophages into foreign-body giant cells. These multinucleated bodies act as amplifiers of the immune response by secreting cytokines and chemokines that eventually recruit fibroblasts, which actively deposit matrix to isolate the foreign material.<sup>[178]</sup> Nevertheless, islet cells in macrocapsules of 1.5 mm diameters that were transplanted in immune-competent diabetic mouse models were able to restore blood-glucose control for up to 180 days, a period more than five times longer than for implants within microcapsules.<sup>[179]</sup>

On the other hand, microencapsulation of pancreatic islets has attracted more attention and has been the widely preferred approach for their transplantation. It entails immobilization of one or two islets in capsules of diameters typically between 100 to 500  $\mu\text{m}$ . With a high surface-to-volume ratio and subsequently a high cellular density, microcapsules were envisioned to perform better as barriers to the immune responses of the host.<sup>[101]</sup> Unfortunately, even small, bioinert implants can activate the immune recognition, which thereafter initiates a cascade of cellular processes leading to foreign body reactions. Persistent inflammation, formation of foreign body giant cells (fused macrophages), fibrosis (walling-off), and damage to the surrounding tissue lead to a 100- $\mu\text{m}$  layer of thick fibrotic tissue that usually envelops the implanted device within less than a month. These undesirable effects can be both deleterious to the function of the cells and a cause of significant pain and discomfort for the recipient.<sup>[179]</sup>

To improve the performance of the microcapsules against foreign body responses, only limited studies have concentrated on the geometry of the microsized vehicles apart from their sizes. Various shapes were examined, of which circular rods presented the best option with minimal foreign body responses followed by pentagonal and then triangular. Further research has described that the implant shape can profoundly influence macrophage behavior at the interface of percutaneous implants and has shown that smooth, well-contoured implants with no acute angles are of higher biocompatibility. Thus, microcapsules for the transplantation of pancreatic islets can vary in sizes, not exceeding 500  $\mu\text{m}$ , but are conventionally and predominantly spherical biomedical devices.<sup>[179]</sup>

### 1.9.3.2 Transplantation sites of encapsulated islet cells

Normally, pancreatic islets have a dense glomerular-like capillary network in which the capillaries course through the islet in a tortuous fashion that is ideal for the delivery of oxygen and nutrients to the islet cells and for the dispersal of the secreted hormones to the target organs. This pancreatic islet angioarchitecture is unfortunately lost during the process of isolation and *in vitro* culture of pancreatic islets preceding transplantation. The islet vasculature dedifferentiates or degenerates and consequently the pancreatic islets are supplied immediately after transplantation with oxygen and nutrients solely by diffusion from the surrounding tissues. The revascularization process is initiated within a few days, and the islets are generally thought to be fully revascularized by one month after transplantation. The loss of vasculature and the slow revascularization of the implanted islet grafts contribute significantly to losses of transplanted cells shortly after transplantation.<sup>[180]</sup>

A large body of data is available on the choice of the appropriate transplantation site to promote revascularization and eventually functional performance and longevity of the grafts. Islet implantation sites are typically located so that the secreted insulin can enter portal venous circulation either through the hepatic portal vein or through venous drainage of the peritoneal cavity to allow normalization of blood glucose levels.<sup>[48]</sup> While a close contact with the blood stream is critical, it is difficult to find such a site, because it should combine the capacity to bear a large graft volume in the immediate vicinity of blood vessels.<sup>[181]</sup> Additionally, it should provide the islets with an increased oxygen tension and overall a microenvironment that prevents early islet loss thereby enhancing islet engraftment.

To promote a successful clinical translation, it is important that the engraftment site can be attained through a minimally invasive procedure and remain easily accessible for functional and morphological follow-up of the islets post transplantation.<sup>[182]</sup> Unfortunately, no site in the human body combines all the desired properties for the transplantation of encapsulated pancreatic islets. Initially, the liver was chosen especially because the intraportal infusion provides ready access to systemic circulation due to its highly vascularized tissues. However, the islet cells are also exposed at this site to high concentrations of toxic immunosuppressive drugs and to a high risk of rejection *via* blood-mediated inflammatory responses initiated by the liver. It is also not possible to retrieve the infused islets from the liver after their engraftment.

Thus, other sites including the spleen, the renal capsule, the peritoneal cavity, and the subcutaneous tissue were investigated. The subcutaneous space would allow a much easier monitoring or retrieval of the grafts but it is also poorly vascularized.<sup>[48]</sup> To overcome this

limitation, which is also present in the peritoneum, biocompatible prevascularization devices were constructed and implanted in diabetic mouse models prior to islets. As a result, although normoglycemia was achieved in all mice, a lower degree of vascularization was observed than in the liver.<sup>[181]</sup>

More recently, the greater omentum was investigated as a suitable transplantation site in a non-human primate diabetes model. The omental pouch, fits almost all desired requirements particularly if the islet graft is immobilized to a subcutaneous or intramuscular portion of the abdominal wall. Higher C-peptide values and gradually a decreasing exogenous insulin demand suggest that this extrahepatic transplantation site has high potential as an alternative site for clinical islet cell transplantation.<sup>[182]</sup>

### **1.9.3.3 Materials of capsules for islet cell transplantation**

Various naturally occurring or synthetic polymers have been used for the encapsulation of pancreatic islets. Of the natural polymers, alginate has dominated the vast majority of studies for treatments of T1D due to its biocompatibility, easy manipulation, gel forming capacity, and *in vivo* performance.<sup>[93]</sup> Specifically, alginate microspheres have been extensively evaluated as immunoisolating carriers for donor pancreatic islets.<sup>[179]</sup> A simplified illustration of an alginate structure is shown in Section 1.3 of this work, whereas the gelation procedure as well as the employed processes for the encapsulation of islet cells in this biopolymer are detailed in Section 1.6.

Besides their natural abundance and highly biocompatible profile, alginates have been extensively used in islet cell encapsulation studies due to the fast and straightforward microsphere gel formation already upon dripping an alginate solution in a solution of one of the divalent cations ( $\text{Ca}^{2+}$ ,  $\text{Ba}^{2+}$ ,  $\text{Sr}^{2+}$ ). Apart from a variety of studies on the optimization of the permselectivity and stability of alginate gels,<sup>[47]</sup> strenuous efforts have recently identified triazole-containing alginate analogs that substantially reduce foreign body reactions in both rodents and, for at least six months, in non-human primates. The distribution of the triazole modification creates a unique gel surface that inhibits recognition by macrophages and eventual fibrous deposition.<sup>[178]</sup> Furthermore, such triazole-alginate macrocapsules were transplanted in an immune-competent diabetic mouse model achieving long-term glycemic correction and glucose responsiveness without immunosuppressive therapy.<sup>[183]</sup>

As detailed in Section 1.3, despite their significant advantages, alginates suffer as natural polymers from substantial limitations that have highlighted the need to explore the

utility of synthetic polymers as biomaterials for the immune encapsulation of pancreatic islets. Synthetic polymers can also be tailor-made to improve biotolerability or reinforce mechanical properties of the generated capsules.<sup>[49]</sup> Due to the thorough description of the variety of synthetic polymers used for the cell and especially islet encapsulation, this part will only focus on the most commonly employed materials from this category.

The most highly investigated synthetic polymer as a building block of macro- or microencapsulation cell systems is PEG.<sup>[49,171,184]</sup> Consequently, the evaluation of the performance of immunoisolated allogenic pancreatic islet cells in PEG capsules, *in vitro* and *in vivo* has been the objective of numerous studies. As it has repeatedly been the case, encapsulated islets release insulin when subjected to glucose challenges and are able to restore normoglycemia in diabetic immunocompromised mice for several days to months. In fact, PEG-implants of xenogeneic tissue are also highly successful, remain viable, and further produce insulin 30 days post transplantation in rat diabetic models.<sup>[104,184,185]</sup>

Other synthetic polymers that have been examined in the islet cell encapsulation as a potential treatment for T1D include poly-L-glycolic acid (PLGA), various polyacrylates, polyepoxides such as SU-8, and PVA, which has been mainly utilized to produce immune-privileged pancreatic islets in macrocapsules.<sup>[49,184,186,187]</sup>

#### **1.9.3.4 Microencapsulation processes**

Various technologies have been applied and optimized in the field of pancreatic islet encapsulation in alginates for the treatment of T1D. One of the biggest challenges remains the scaling up of the manufacturing process. The two most widely used devices for microencapsulation are the air-syringe pump droplet generator and the electrostatic bead generator.<sup>[178]</sup> The operation principles of these kinds of apparatus have been described in Section 1.6 and will be omitted in this part.

A major drawback in the design of these instruments is that they are incapable of producing sufficient numbers of microcapsules in a short-time period to permit mass production of encapsulated and viable cells for transplantation in large animals and humans. A prolonged encapsulation process adversely affects the viability of the cells. To address this problem, a multi-needle approach has been described which makes use of four needles to generate more than one encapsulated cell at a time. Although this scale-up poses a significant progress, it fails to meet the high production rates required to meaningfully produce sufficient

quantities of encapsulated and viable cells to serve millions of T1D patients in need of cell transplantation.<sup>[101]</sup>

A promising approach to improve the production rates of encapsulated islets is the vibrating nozzle encapsulation, which, however, could damage large cells and cell clusters through high shear forces and introduce difficulties in maintaining aseptic conditions.<sup>[48]</sup>

As exhaustively reviewed recently, a variety of techniques including electrospraying or the most recent microfluidic<sup>[104]</sup> fabrication is the objective of ongoing optimization studies. However, there is currently no commercially available microencapsulation device that satisfactorily meets the optimum requirements for islet microencapsulation. There is a great need for a relatively fast way to microencapsulate large masses of islets as well as reproducibly generate highly homogeneous spherical shapes and sizes to promote proper function of the encased cells. Extensive and routine clinical use of microencapsulated islets and a successful development and availability of a reliable mass production device for manufacturing microencapsulated islets for transplantation are paramount for treatment of diabetic patients.<sup>[101]</sup>

### **1.9.3.5 Chemistry for the encapsulation of islet cells**

The employed chemistry cross-linking the polymers to generate the macro- or microcapsules surrounding the pancreatic islets constitutes one more factor that highly influences the longevity of the enclosed cells. In this regard, the outlined points in Section 1.5 apply also for the immune isolation of pancreatic islets and will not be discussed in this section.

As a concluding remark, the need for further research in this subfield of islet cell encapsulation should be highlighted. It is crucial to improve the current manufacture procedures and develop new approaches that could augment islet transplantation as a life-long, definitive treatment of type 1 diabetes.

## **2 Research goals**

### **2.1 Dendritic Polyglycerol-Based Microgels for Cell Encapsulation Therapies**

#### **2.1.1 Objective**

The aim of this work is to develop new types of polyglycerol-based microgel scaffolds for the encapsulation of cells. Fueled by the current limitations of microscale cell carriers conferred by the available biomaterials, three macromonomers and a crosslinker were prepared for the fabrication of three different 3D artificial extracellular matrices (ECMs). A star-shaped polyglycerol-hexaazide, an  $\alpha, \omega$ -bisazido-linear polyglycerol, an  $\alpha, \omega$ -bisazido-linear polyethylene glycol and dendritic polyglycerol-poly(bicyclooctyne) would be used as building blocks in this approach. They would be functionalized accordingly to facilitate a bioorthogonal SPAAC gelation. This protocol has been established in our group and has proven to be a very efficient, elegant approach for various studies in the presence of living cells.<sup>[105-108]</sup> Thus, to extend its spectrum of applications, it is implemented in this strategy to eliminate risks of cytotoxicity and eventual impairment of the functional viability of the cells. As a proof of concept, mouse fibroblast cells of the NIH/3T3 cell line would be enveloped in the synthetic ECMs. To develop the designed microgel scaffolds with fine-tuned geometries in a highly reproducible fashion microfluidic templating would be applied.<sup>[109,110]</sup> The performance of cell-bearing microgels would then be determined by confocal microscopy imaging which also allows the comparison of the behavior of the enclosed cells in each synthetic extracellular matrix.

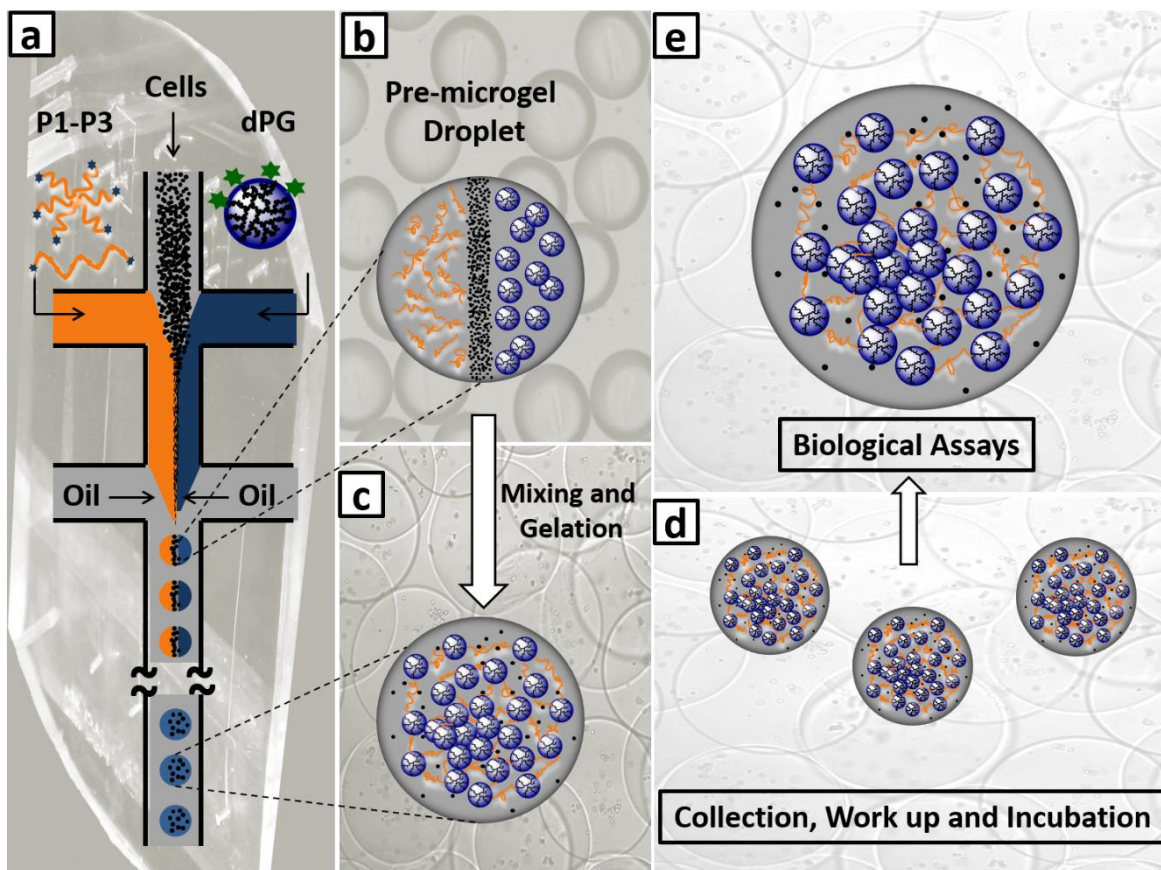


**Figure 20.** Simplified illustration of microfluidic templating of cell-laden 3D artificial dPG-based scaffolds.

## 2.1.2 Results and discussion

### 2.1.2.1 Synthesis of polymer precursors P1-P4

The first step of the employed strategy involved the synthesis of the macromonomers **P1-P3** and the cross-linker **P4**, as shown in Figure 21. The applied synthetic processes were implemented in this approach because they allowed the generation of the desired products in an elegant, and efficient manner. The commercial availability of the starting materials along with the high yielding reactions, afforded the designed compounds on a multigram scale.

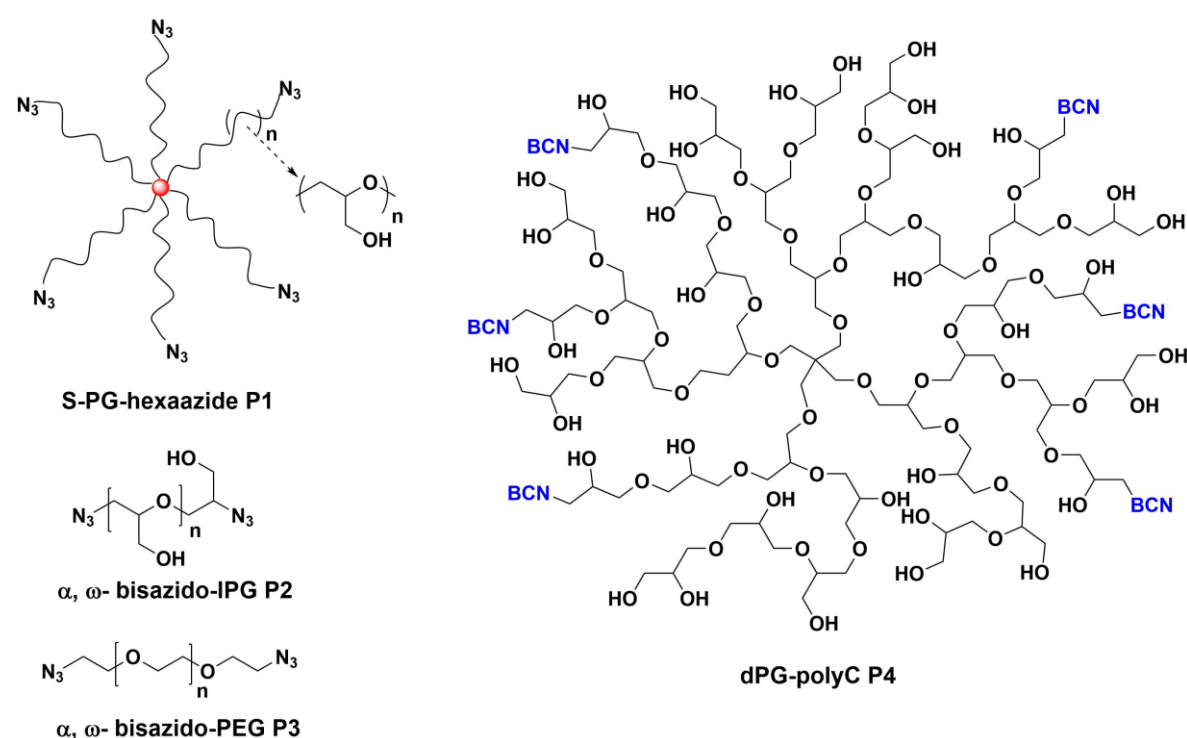


**Figure 21.** Schematic representation of the macromonomers **P1-P3** and cross-linker **P4**.

### 2.1.2.2 Synthesis of star-shaped polyglycerol-hexaazide (S-PG-hexaazide P1)

The use of star-shaped polyglycerols as materials for biological applications has been only sparsely reported. Most of these cases investigate the potential of mesoporous silica nanoparticles coated with star-shaped polyglycerol methacrylates or hyperbranched polyglycerol star-shaped particles as vehicles for drug delivery.<sup>[111,112]</sup> Our group has contributed a substantial body of data to the uses of dendritic polyglycerol as a biomaterial for several biomedical applications.<sup>[113]</sup> Nevertheless, the applicability of our polyglycerols as building blocks for cellular carriers on terms of the functional survival of the enclosed

cells has not yet been fully explored. The lack of representative data on star-shaped polyglycerols in the field of cell encapsulation as well as our expertise on dendritic polyglycerol fueled the use of both architectures in the microfluidic fabrication of cell-laden microparticles.

The first macromonomer synthesized was S-PG-hexaazide. For its preparation, a four step-protocol was established that included polymerization, introduction of vinyl sulfonate moieties, nucleophilic substitution with  $\text{NaN}_3$ , and subsequent acidic deprotection.

To prepare well-defined star-shaped polyglycerols a protected glycidol monomer was utilized. Generally, glycidyl derivatives are liquids, which renders the respective experimental procedures very facile. Although there are various commercially available glycidyl monomers, ethoxyethyl glycidyl ether (EEGE), the most frequently used, was chosen for this work. Bearing an acetal group, this monomer is stable during the applied polymerization and can be fully deprotected under mild acidic conditions.<sup>[114]</sup> EEGE was synthesized through the reaction of glycidol and ethyl vinyl ether catalyzed by *p*-TsOH, as described by Fitton *et al.*<sup>[115]</sup>

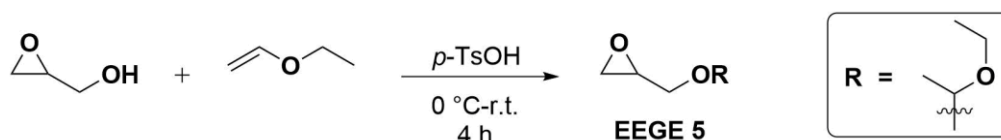


**Figure 22.** Synthesis of EEGE monomer.

S-PG was synthesized *via* anionic ring opening polymerization of EEGE (Figure 22). The initiator of this polymerization was dipentaerythritol, the hydroxy groups of which were activated by 0.1 equiv. of potassium *tert*-butoxide. To achieve a controlled polymerization, only roughly 10 % of the hydroxy groups of dipentaerythritol should be deprotonated with the remaining 90 % being latent. Upon complete removal of the formed *tert*-butanol, the monomer was added, and the polymerization started by heating at 60 °C. The known protocol established by Möller *et al.* was slightly modified to generate even milder conditions in the reaction mixture. Therefore, the desired S-PG was obtained in a high yield after 5 days of reaction.<sup>[116]</sup> Quantitative  $^{13}\text{C}$  NMR analysis of the star-shaped PEEGE confirmed the presence of six end-groups per molecule and thus the successful formation of a six-armed star polymer with an  $M_n$  of almost 11695  $\text{g mol}^{-1}$ . Analysis by gel permeation chromatography (GPC) showed a very narrow molecular weight distribution of the produced

polymer (PDI = 1.03) but with a significant discrepancy in the molecular weight ( $M_n$ , 7767 g mol<sup>-1</sup>) as opposed to the determination *via* quantitative NMR spectroscopy.

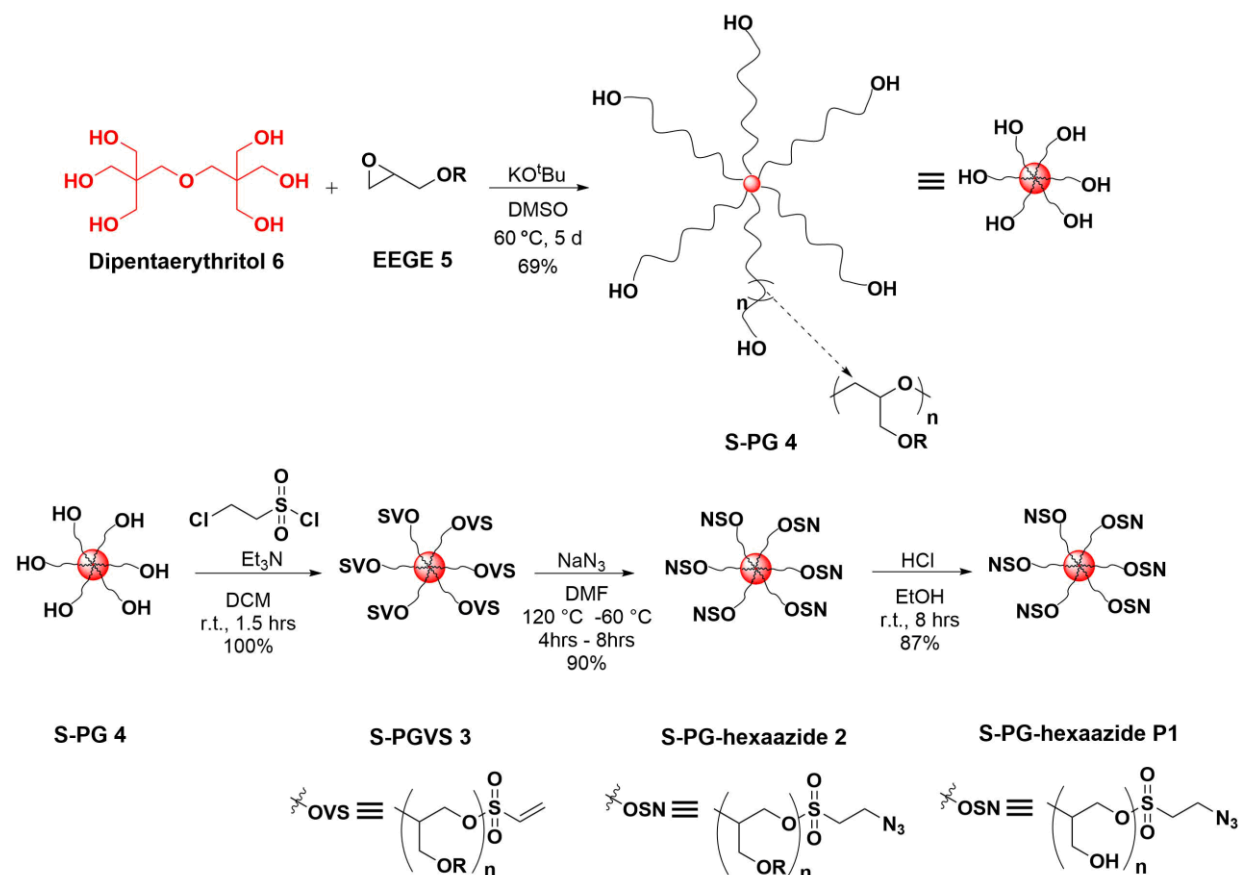


**Figure 23.** Synthesis of S-PG, **4** and further functionalization to S-PG-hexaazide, **P1**.

The next modification involved the insertion of vinyl sulfonate groups at the six hydroxy end-groups of polyglycerol **4**. To this end, the latter was treated with triethylamine and 2-chloroethylsulfonate in dichloromethane at room temperature to form the vinyl sulfonate-functionalized S-PGVS **3** (Figure 23). To determine the degree of conversion of this step, end-group <sup>1</sup>H NMR analysis was performed, which verified the successful addition of six vinyl sulfonate groups to the polymer chains. The integrals corresponding to the sp<sup>2</sup>-hybridized carbons of the vinyl sulfonates were compared with the respective of the methyl groups of the acetal protected repeating units, resulting in a functionalization degree around 100 %. Apart from their highly selective introduction, vinyl sulfonate moieties are very reactive towards addition or nucleophilic substitution reactions and can be readily removed *via* hydrolysis of the resulting sulfonate esters. Additionally, their high reactivity towards various amines renders them very advantageous in ligation chemistry as was also recently shown.<sup>[116]</sup>

Facilitating a wide range of transformations, organic azides have assumed an important position in a broad variety of disciplines such as bioorganic chemistry and material science.<sup>[117]</sup> Due to its highly versatile chemistry, this moiety was incorporated to all three macromonomers of this study (**P1-P3**) through a relatively straightforward approach, that not only enables bioorthogonal cycloaddition but is also a pathway to complex structures. Therefore, the obtained analogue **3** was treated with sodium azide initially at 120 °C for 4 hours and subsequently at 60 °C overnight to yield S-PG-hexaazide **2**. The complete Michael addition of the azides to the vinyl sulfonates was confirmed *via* <sup>1</sup>H NMR through the missing peaks of sp<sup>2</sup>-hybridized carbons. Additionally, the presence of a vibration band at 2105 cm<sup>-1</sup> in the obtained IR spectrum typical for azide-moieties further confirmed the desired modification.

The final step in the preparation of S-PG-hexaazide **P1** consisted of the acidic cleavage of the acetal protecting groups. The previously generated **2** was treated with 3 wt % aqueous hydrochloric acid at room temperature. After 24 hours, the deprotected, fully hydrophilic S-PG-hexaazide, **P1** was obtained in 87 % yield. The structural validation of **P1** was performed *via* NMR spectroscopy and GPC. The disappearance of the peaks typical for the aliphatic protons of the acetal groups was evidenced in both <sup>1</sup>H and <sup>13</sup>C NMR spectra. The measured GPC trace showed a very narrow molecular weight distribution (PDI = 1.10) of the synthesized polymer with a number average molecular weight ( $M_n$ ) of 4919 g mol<sup>-1</sup>. This newly developed reactive polymer is being used for the first time as a building block in the microfluidic encapsulation of cells.

### 2.1.2.3 Synthesis of $\alpha$ , $\omega$ -bisazido-linear-polyglycerol ( $\alpha$ , $\omega$ -bisazido-IPG **P2**)

Linear polyglycerol (IPG) was implemented in this strategy due to its biocompatibility profile, which is slightly superior to the gold standard PEG its high structural resemblance to PEG, and its multifunctionality.<sup>[118]</sup> Additionally, both PEG and dPG have been well used in the microfluidic templating of microgels.<sup>[119]</sup> We recently demonstrated that linear PEG chains with an  $M_n$  of 6000 g mol<sup>-1</sup> are crucial to increasing microgel elasticity thus, favoring cell viability.<sup>[119]</sup> To this end, an S-PG and an IPG of a similar  $M_n$  were synthesized, that would eventually allow overall comparison of the behavior of the different developed microgels in this study.

Heterobifunctional linear poly(EEGE) with -OH and -Br ends and a  $M_n$  of 10000 g mol<sup>-1</sup> was prepared *via* monomer activated anionic polymerization, following the procedure from Carlotti *et al.*<sup>[120]</sup> As for the star-shaped polymer, the synthesis of well-defined linear

polyglycerol requires the protection of the hydroxyl function of the monomer prior to polymerization. Thus, the most frequently used monomer, EEGE was also applied in this case, due to the efficiency and ease of the protection step and the eventual polymer deprotection *via* mild, acidic treatment.<sup>[120]</sup>

A binary initiating system composed of Oct<sub>4</sub>NBr as initiator and *i*-Bu<sub>3</sub>Al as catalyst / activator was utilized for the controlled anionic polymerization of EEGE, as a protected form of glycidol. The use of [*i*-Bu<sub>3</sub>Al]/[Oct<sub>4</sub>NBr] ratios higher than 3 is required to achieve quantitative polymerization and generation of medium molecular weight PEEGEs. An increased monomer concentration favors fast reactions, but can result in broadening of the molar mass distribution, suggesting the contribution of side reactions in these conditions, probably to some extent through transfer to *i*-Bu<sub>3</sub>Al.<sup>[120]</sup> Therefore, for the purposes of the presented strategy, 4 equiv. of *i*-Bu<sub>3</sub>Al were added to a mixture of Oct<sub>4</sub>NBr and EEGE in a ratio of 1:83, at 0 °C, yielding PEEGE of 11192 g mol<sup>-1</sup> with a polydispersity index of 1.06. In this case, the obtained molar masses of PEEGE increase linearly with the monomer conversion up to the final yield, exhibiting an overall narrow distribution. As reported by Carlotti *et al.*, such a narrow distribution of the molar masses indicates the formation of a 1:1 initiating and propagating complex of low basicity. This strongly minimizes transfer reactions to the monomer, and provides high nucleophilicity through the activating excess of Lewis acid, allowing fast reactions at low temperatures (Figure 24).<sup>[120]</sup>

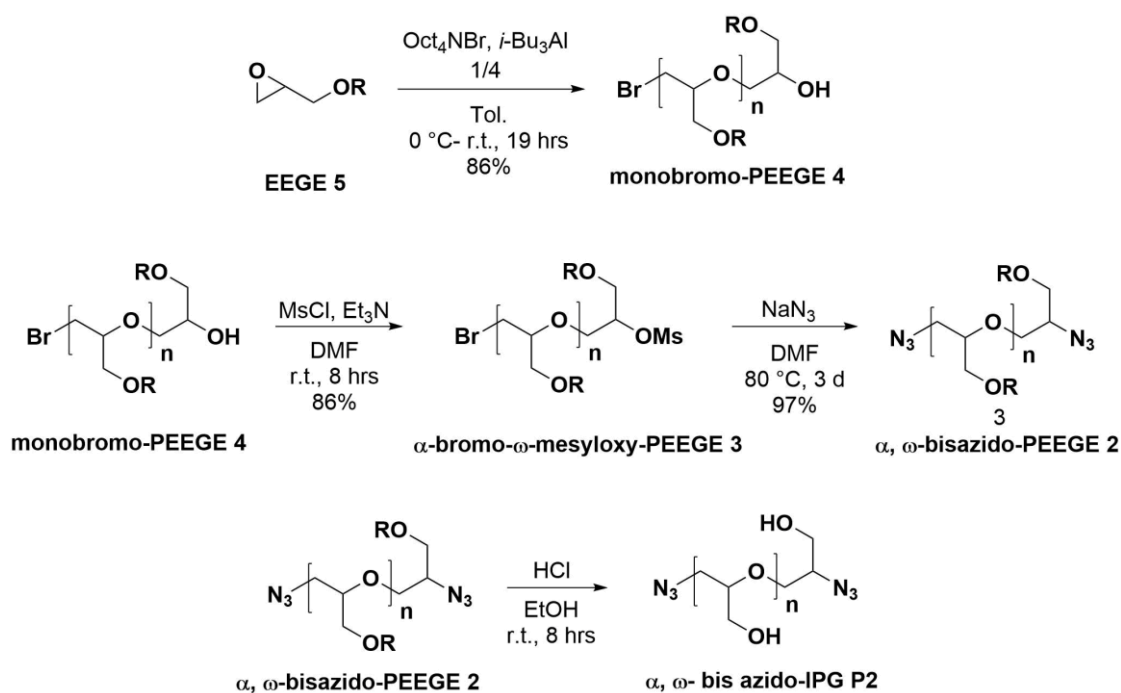


**Figure 24.** Synthesis of PEEGE and further functionalization to  $\alpha, \omega$ -bisazido-IPG **P2**.

The final product, **P2** ( $\alpha$ ,  $\omega$ -bisazido-IPG) was obtained in an overall yield of 59 % after a three step synthetical protocol, established in our group.<sup>[118]</sup> The first modification involved the activation of the end OH-group with triethylamine and subsequent treatment with methanesulfonyl chloride at 0 °C. The  $\alpha$ -bromo- $\omega$ -mesyloxy-PEEGE **3** was obtained after overnight stirring at room temperature in 86 % yield. The desired structure was confirmed *via* <sup>1</sup>H NMR spectroscopy, by the presence of a peak at approximately 3.31 ppm, typical for deshielded methyl protons due to the direct vicinity of sulfur and oxygen heteroatoms. The functionalization of bromide **4** with a mesyl moiety was included in this strategy due to the latter's straightforward and efficient introduction, but also as it constitutes a very good leaving group that can be readily substituted in the following synthetic step.

To introduce the necessary azide functionality for the envisioned SPAAC, **3** was treated with an excess of sodium azide (5.0 equiv. per end-group) at 80 °C for 72 hours. The resulting  $\alpha$ ,  $\omega$ -bisazido-PEEGE **2** was characterized *via* <sup>1</sup>H NMR and IR spectroscopy. The former confirmed the full conversion of the initial end-groups to azides, through the disappearance of the peak at 3.31 ppm corresponding to the methyl protons of the methylsulfonyl moiety. A vibration band at 2100 cm<sup>-1</sup> in the measured IR spectrum, typical for organic azides, also verified the desired structure.

The final transformation of this synthetic protocol, involved the acidic cleavage of the acetal protecting groups in a 3 wt % ethanolic hydrochloric acid at room temperature overnight. These mild reaction conditions afforded  $\alpha$ ,  $\omega$ -bisazido-IPG **P2**, in 83 % yield. As for macromonomer **P1**, the structural characterization of **P2** involved analysis of the respective NMR spectral and chromatographic data. The absence of signals in the aliphatic regions 1.0 - 1.5 and 10.0 - 20.0 ppm corresponding respectively to the protons and carbon atoms of the acetal groups was observed in both <sup>1</sup>H and <sup>13</sup>C NMR. The obtained GPC trace showed very narrow distribution (PDI = 1.09) of the molar masses with an  $M_n$  of 6850 g mol<sup>-1</sup>.

#### 2.1.2.4 Synthesis of $\alpha$ , $\omega$ -bisazido-linear-polyethylene glycol ( $\alpha$ , $\omega$ -bisazido-PEG P3)

One of the purposes of this work was to compare the performance of the newly developed polyglycerol macromonomers and the polyethylene glycol as constituents of microgels for the encapsulation of cells. Linear polyethylene glycol (PEG) was chosen because of its generally favorable properties, including, low intrinsic toxicity and immunogenicity, high hydrophilic character, which is employed to render various hydrophobic drugs water soluble and the introduction of high physical and thermal stability in the various formulations that would otherwise aggregate either *in vivo* or during storage.<sup>[121]</sup> PEG is overall highly biocompatible and can induce changes in the pharmacokinetic administration of drugs through prolonging their blood circulation times. Consequently, there is higher probability that the specific drug would reach its site of action before being recognized as foreign and cleared from the body.

As stated above, we have recently reported that PEG chains with an  $M_n$  of 6.000 g mol<sup>-1</sup> as building blocks for cell carriers increase the elasticity of the formed microgel and therefore favor long-term cell viabilities.<sup>[119]</sup> For an objective comparison of the performance of all macromonomers used in this study, commercially available  $\alpha$ ,  $\omega$ -bisbromo-PEG with an  $M_n$  of 6.111 g mol<sup>-1</sup> (PDI = 1.03) was modified to bear azide moieties at both its ends. The  $\alpha$ ,  $\omega$ -bisbromo-PEG underwent nucleophilic substitution by an excess of sodium azide (5.0 equiv. per Br-group) at 80 °C for 72 hours to give  $\alpha$ ,  $\omega$ -bisazido-PEG P3. The desired transformation was confirmed by the typical vibration band at 2110 cm<sup>-1</sup> in the corresponding IR spectrum.

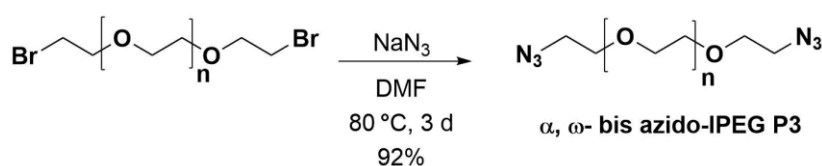


**Figure 25.** Synthesis of  $\alpha$ ,  $\omega$ -bisazido-PEG P3.

### 2.1.2.5 Synthesis of dendritic polyglycerol poly(bicyclooctyne) (dPG-polyC P4)

The necessary dendritic polyglycerol (dPG **5**) for the generation of the cross-linker dPG-poly(bicyclooctyne) (dPG-polyC, **P4**) was kindly contributed by Dr. F. Paulus. It was synthesized *via* ring opening multibranching polymerization of glycidol using a trimethylpropane starter, according to a known procedure.<sup>[122]</sup> Glycidol is a very reactive monomer that can propagate *via* a chain-growth epoxide polymerization and simultaneously initiate polymerization by its free hydroxyl group, leading to uncontrolled oligomer formation through self-condensation steps. However, it was shown that with a slow monomer addition in the reaction mixture and a specific monomer / initiator ratio, a controlled polymerization can be achieved that generates well-defined molecular weights between 1000 - 10000 g mol<sup>-1</sup> and polydispersities below 1.5.<sup>[122]</sup>

Dendritic PGs hold great promise as new polymer scaffolds for life science applications, especially in the treatment of cancer and inflammation, because of their low toxicity, high transport capacity, multivalent charge, and ligand display for targeting biological cells and tissue. Additionally, their anti-inflammatory properties are augmented by excellent protein resistance profiles.<sup>[114]</sup> With several free hydroxy groups on their surface, dPGs can be synthetically tailored to support the construction of various architectures for drug and dye delivery as well as recently demonstrated in our group for cell encapsulation.<sup>[105,119,123,124]</sup>

To enable the bioorthogonal cross-linking *via* SPAAC, cyclooctyne moieties were introduced into polyglycerol **5** through successive modifications of its surface as established in our group. At first, **5** was treated with methanesulfonyl chloride in the presence of pyridine giving dPG-polymesylate **4** with a 10 % degree of functionalization in a 100 % yield, as was confirmed by the quantitative analysis of the corresponding <sup>1</sup>H NMR spectrum. The stoichiometric amount of mesylchloride in this step defines the degree of functionalization of each following step to the final dPG-polyC. As stated previously, mesylates are good leaving groups to facilitate nucleophilic substitution upon treatment with sodium azide at moderate heating (60 °C, 72 hours). Product **3** was obtained in almost quantitative yield as verified in the respective <sup>1</sup>H NMR spectrum and the presence of a sharp vibration band at 2100 cm<sup>-1</sup> in the IR spectrum.

The following transformation involved the reduction of the azide to amine moieties with the addition of triphenyl phosphine in a solution of analogue **3** in equal volumes of tetrahydrofuran and water. This reaction proceeds through formation of an iminophosphorane, accompanied by the evolution of nitrogen gas. The former hydrolyzes in

the presence of water to the corresponding primary amine. The produced dPG-polyamine **2** was obtained in 64 % yield and its structure was validated by the absence of the azide-band in the respective IR spectrum. The last step in this synthetic protocol consisted of the insertion of cyclooctyne functional groups to polyamine **2**. To this end, a carbonate-bearing cyclooctyne was prepared according to a procedure published by van Delft *et al.*<sup>[125]</sup> The cyclooctyne, was then covalently attached to the amine moieties of polyglycerol *via* carbamate formation (Figure 26), giving dPG-polyC **P4** in 93 % yield. The conversion of the polyaminated dPG **2** was deduced from the <sup>1</sup>H NMR spectrum and the degree of functionalization amounted to 9 %, corresponding to ~ 12 cyclooctyne moieties per dPG molecule.

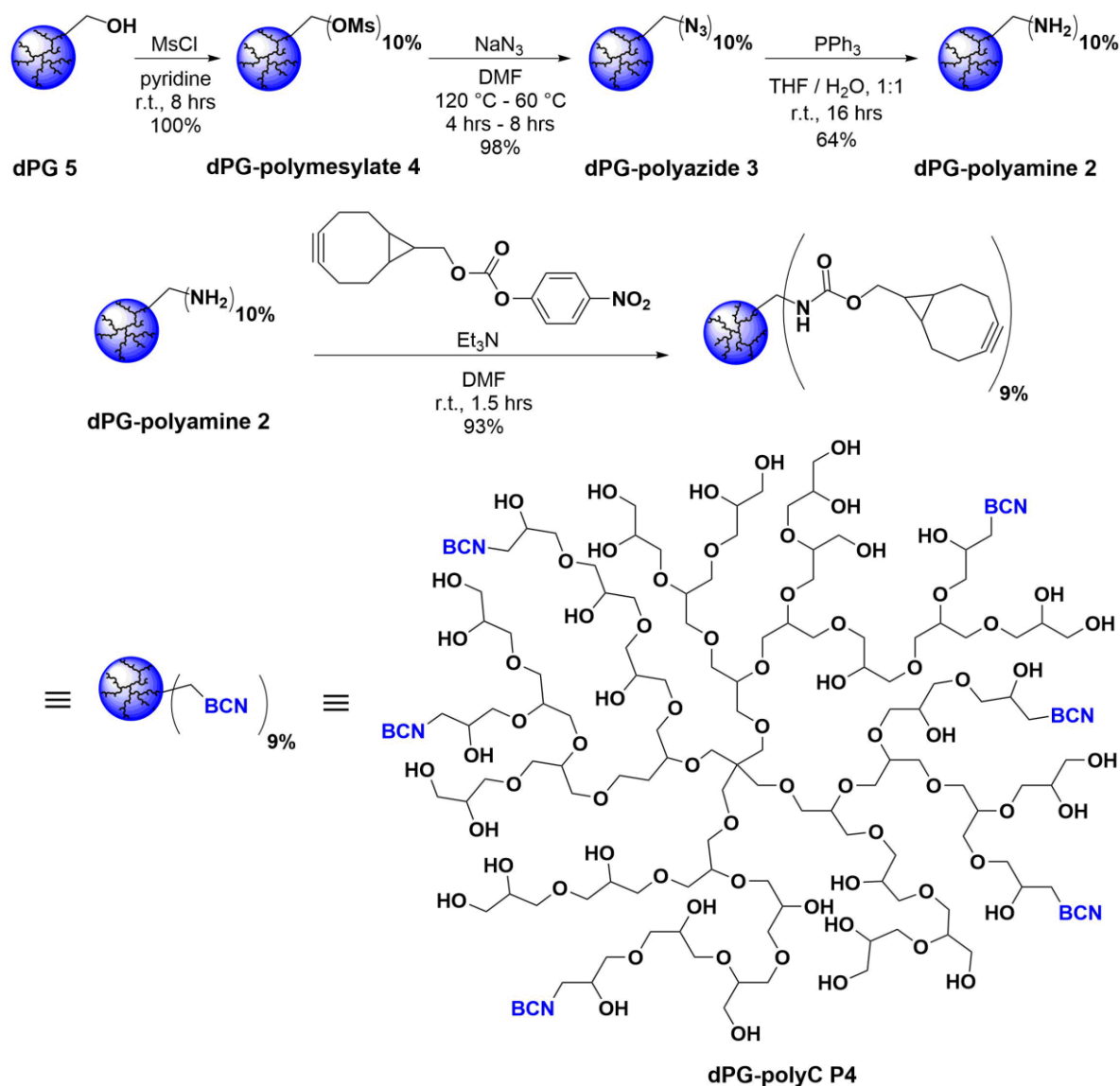


**Figure 26.** Four-step synthetic protocol to dPG-polyC (**P4**).

### 2.1.2.6 Evaluation of the cytotoxicity profile of precursors P1-P4

Prior to microfluidic encapsulation of NIH/3T3 mouse fibroblasts, it was important to assess the cytotoxicity potential of the developed macromonomers **P1-P4** to avoid erroneous results of the viability tests conducted post cell entrapment. To that end, NIH/3T3 cells were cultured in DMEM culture medium containing high glucose (4.5 g/L, hG), 10 % FCS and 1 % PS (penicillin/streptomycin) in a humidified incubator at 37 °C under a 5.0 % CO<sub>2</sub> atmosphere. They were grown in 182.5 cm<sup>2</sup> cell culture flasks and their medium was changed every second day after a rinsing step with DPBS (2 x 10.0 mL). Upon confluency of 70 %, the culture was 1:10 subcultured.

For the evaluation of the toxicity profiles of macromonomers **P1-P4** a series of solutions **S1-S3** with concentrations ranging from as low as 50 g/L up to 200 g/L (Table 1) was prepared and the cell counting kit-8 (CCK-8) was utilized. The assay was designed to include at the highest, the concentration of semi-dilute polymer solutions that was employed for the microfluidic templating of cell-laden microgels. The related amount of polymer was in direct contact with the encapsulated cells during the fabrication process and after in their further culture in the microgel particles.

**Table 1.** Polymers and solutions thereof as used in the cytotoxicity assay with CCK-8.

	Polymer	Solutions (g L <sup>-1</sup> )		
		S1	S2	S3
<b>P1</b>	S-PG-(N <sub>3</sub> ) <sub>6</sub>			
<b>P2</b>	IPG-(N <sub>3</sub> ) <sub>2</sub>	50	100	200
<b>P3</b>	PEG-(N <sub>3</sub> ) <sub>2</sub>			
<b>P4</b>	dPG-polyC			

NIH/3T3 fibroblasts were inoculated in a transparent 96-well-plate and after culture for 24 hours at 37 °C under 5.0 % CO<sub>2</sub>, an aliquot of each solution **S1-S3** of each polymer **P1-P4** were added to the respective wells apart from the well of the control which received pure culture medium. The plate was further incubated for another day. Thereafter, pre-mixed CCK-8 solution, containing the proprietary WST-8 tetrazolium salt, was added to each well. The dehydrogenases present in viable cells reduce this salt to formazan, a yellow dye, the absorbance of which can be measured in the medium (Figure 27).

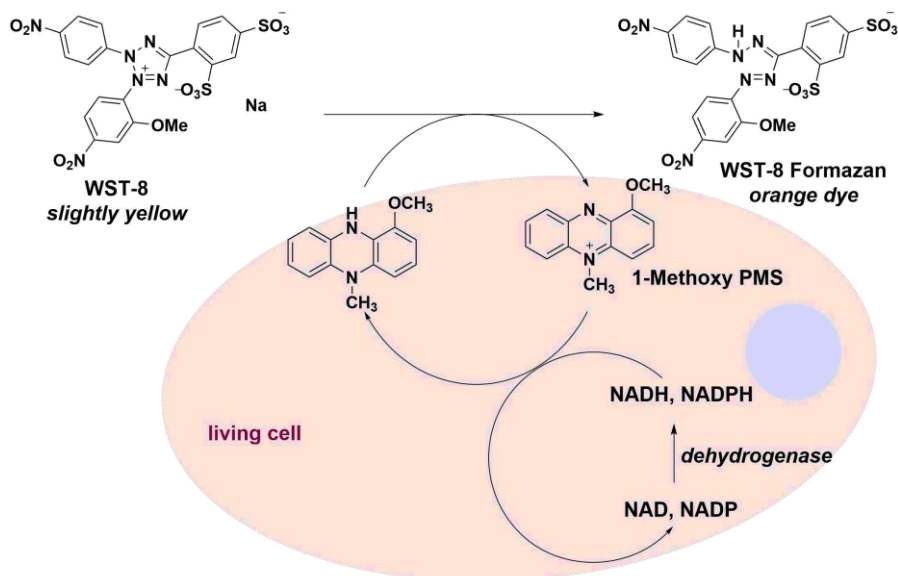


**Figure 27.** Detection mechanism of cell viability with CCK-8. Copyright, 2011 Dojindo EU GmbH, Munich, Germany)

Two hours after addition of the CCK-8 solution, the absorbance was measured at 450 nm using a Tecan Infinite® 200PRO microplate reader. Three independent experimental runs with three triplicates per polymer solution were performed ( $n = 3$ ). The optical density was read at two time points of the study, after 24 and 72 hours, respectively. The collected data are illustrated in Figure 28.

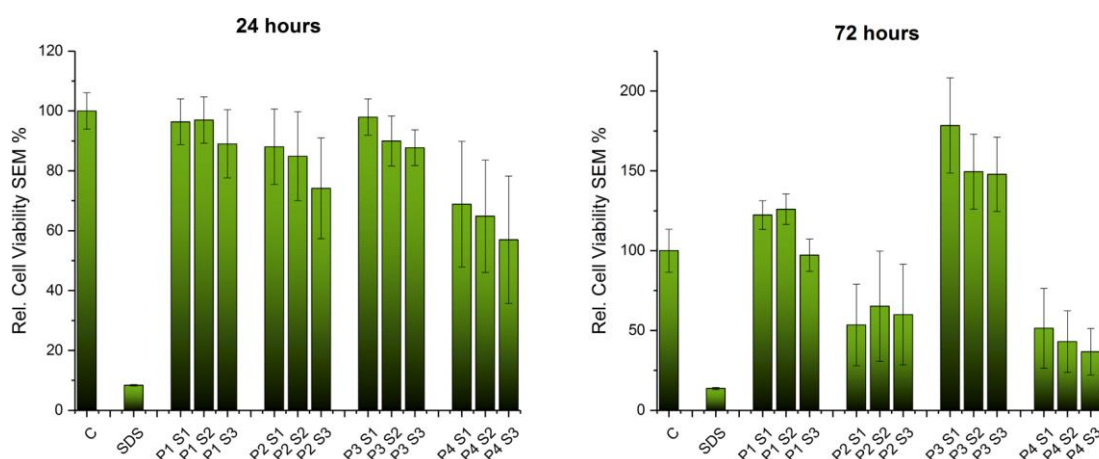


**Figure 28.** Viability profiles of NIH/3T3 cells in solutions **S1-S3** (50, 100, and 200 mg/mL, respectively) of macromonomers **P1-P4** as determined with CCK-8 after 24 and 72 hours. **C** denotes the negative control, which was pure culture medium (DMEM, 10 % FCS, 1 % P/S).

All polymers **P1-P4** conferred very low to moderate toxicity to the NIH/3T3 fibroblasts under the conditions applied in this assay. 24 hours after incubation in the presence of

macromonomer solutions the cells exhibited excellent viabilities in the case of **P1-P3** at concentrations of 50 and 100 g/L, respectively. Lower viabilities were detected for cells in all solutions of polymer **P4** with the poorest performance for **S3**, 200 g/L. Surprisingly, after 72 hours of culture in all solutions of **P1** and **P3**, the cells remained alive with viabilities in the range of those incubated in DMEM (hG, 10 % FCS, 1 % PS) only. The lowest absorption values were recorded for polymers **P2** and **P4**, especially as the macromonomer concentration increased. Overall, the developed polyglycerols (**P1**, **P2** and **P4**) were shown to have extremely cytocompatible profiles with the seeded cell populations remaining either fully or partially viable with no completely dead cells exhibited even after 72 hours of culture. The only polymer that significantly outperformed was polyethylene glycol **P3**, which could be attributed to its established high biocompatibility.<sup>[121]</sup> These results confirmed the advantageous properties of the newly developed polymers **P1** and **P4** and encouraged the application of these as well as of **P2** and **P3** as building blocks for the microfluidic encapsulation of NIH/3T3 cells.

#### **2.1.2.7 Microfluidic templating of cell-laden microgel droplets**

The newly developed macromolecular precursors S-PG-hexaazide, and dPG-polyC as well as bis-azido-IPG and PEG, were utilized in a bioorthogonal SPAAC, which led to three types of NIH/3T3 cell-laden matrices **M1-M3** by applying droplet-based microfluidics. Degradable microgels designed to release their cellular cargo in a pH-regulated manner have been already developed in our group.<sup>[105]</sup> Herein, we sought to extend this approach and gain insight into non-degradable hydrogel biomaterials that could eventually protect their cellular payload from immune responses of potential hosts. The multifunctional nature of the cytocompatible polymeric building blocks,<sup>[123,126]</sup> and the microfluidic patterning allowed tuning the design of the microcapsules in a controlled fashion.

Microfluidics constitutes a powerful, versatile, and elegant technique for the development of micrometer-sized hydrogel particles. The approach, conceptualized to make use of emulsion droplets as templates for the particle synthesis can afford control of the size, shape, and monodispersity of the microparticles by controlling the former parameters of the pre-microgel droplets. This is possible through the generation of a stream of a pre-microgel monomer solution (dispersed phase) in a microchannel, and its periodic break-up by flow focusing with a second, immiscible fluid (continuous phase). Thus, monodisperse,

micrometer-sized droplets are formed that, after solidification, retain their uniform size and shape, yielding polymer particles with precisely controlled morphology.<sup>[118]</sup>

To create monodisperse pre-microgel droplets as templates for the particle synthesis, PDMS microchannels were used that were fabricated by soft lithography and consisted of two sequential cross-junctions, as shown in Figures 20a and 29A (lower part). The two precursor solutions of each azide **P1-P3** and dPG-polyC, as well as the cell-containing medium were injected into three separate inlets of these devices (Figure 29A). Syringe pumps loaded simultaneously all fluids on the microfluidic platform and adjusted their flow rates.

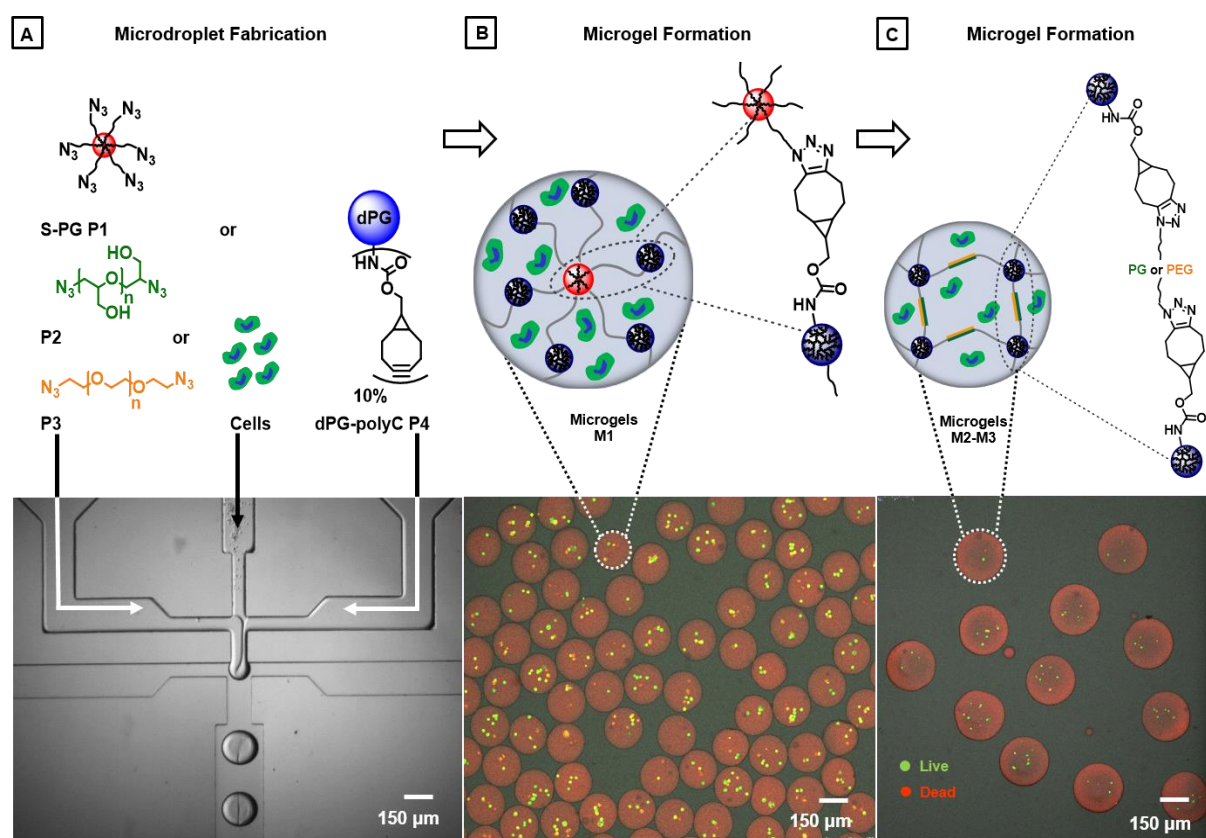


**Figure 29.** Droplet-templated cell encapsulation: (A) A set of azide-functionalized precursors and dPG-polyBCN was prepared. One of the azide-macromonomers, the dPG-crosslinker and NIH/3T3 cells were loaded on a microfluidic device that served to form monodisperse, micrometer-sized precursor capsules. Subsequent mixing of the three components inside the monodisperse droplets led to droplet gelation by SPAAC. (B) Thereby, cell-laden microgel particles **M1** deriving from S-PG-hexaazide and (C) **M2-M3** from  $\alpha, \omega$ -bis-azido-IPG and  $\alpha, \omega$ -bis-azido-PEG, respectively, were formed. The viability of cells encapsulated into the microgel particles was determined by a fluorescence-based live-dead assay, in which living cells were stained green (calcein AM) and dead cells were stained red (ethidium homodimer 1).

After their injection, these three fluids met at the first cross-junction, where they formed a laminar coflowing stream in the microchannel. A second junction, serves for the periodic

break-up of this stream by flow-focusing with a fourth fluid composed of an immiscible hyperfluorinated oil and surfactant mixture. This produced uniform pre-microgel droplets with sizes in the range of 150 - 200  $\mu\text{m}$ , depending on the flow rates and the viscosities of the precursor solutions, as shown in the lower part of Figure 29A. Upon mixing of the three liquids inside the droplets (Figure 29A), the precursors reacted in a SPAAC reaction (Figure 29B and C uppermost part) and formed cell-laden microgels within a few minutes. Typical water swollen product particles bearing encapsulated cells are shown in Figure 29B and C (lower part). To monitor the droplet formation the microtemplate was operated on an inverted optical microscope equipped with a high-speed digital camera. After a sequence of collection, preincubation and work up the preformed microgels were allowed to fully gel overnight at 37 °C under 5.0 %  $\text{CO}_2$ . The concentrations of all macromonomer solutions and the density of the NIH/3T3-cell suspension in cell medium as well as the composition of the used oil are summarized in Table 2.

**Table 2.** Detailed description of microfluidic-templated dPG-based microgels: concentration and composition of all involved components (annotation **P1-P3** as in Table 1, Section 2.1.2.6).

Microgel	Polymer	Concentration of <b>P1-P3</b> in DMEM solution ( $\text{g L}^{-1}$ )	Concentration of dPG-polyC ( <b>P4</b> ) in DMEM solution ( $\text{g L}^{-1}$ )	Macromonomer Concentration in Microgels ( $\text{g L}^{-1}$ )	Density of NIH/3T3-cell-suspension	Consistency of Oil (wt %)
<b>M1</b>	<b>P1</b>	200		200	$1.00 \times 10^7$ in	
<b>M2</b>	<b>P2</b>	350	200	275	1.00 mL DMEM of	Novec 7100
<b>M3</b>	<b>P3</b>	200		200	18 vol % OptiPrep <sup>TM</sup>	1.3 wt % KBT

To ensure similar mechanical properties of the obtained microgels, all azide-bearing macromonomers had the same molecular weights, whereas **P2** and **P3** also had the same degree of functionalization. By extending the delicate control<sup>[118]</sup> of the size, shape, and monodispersity of the emulsion droplets (Figure 30A and B), hydrogels were templated that swelled to uniform sizes of 196  $\mu\text{m}$  (**M1**) or 336  $\mu\text{m}$  (**M2**) and contained homogeneously distributed cells (Figure 30D and E). **M2** pre-microgels could already swell in larger particles shortly after their collection, as observed in Figure 30B. Both microgels **M1** and **M2** exhibited high stability during their microfluidic templating, which was also confirmed in the confocal images recorded 24 hours after their production.

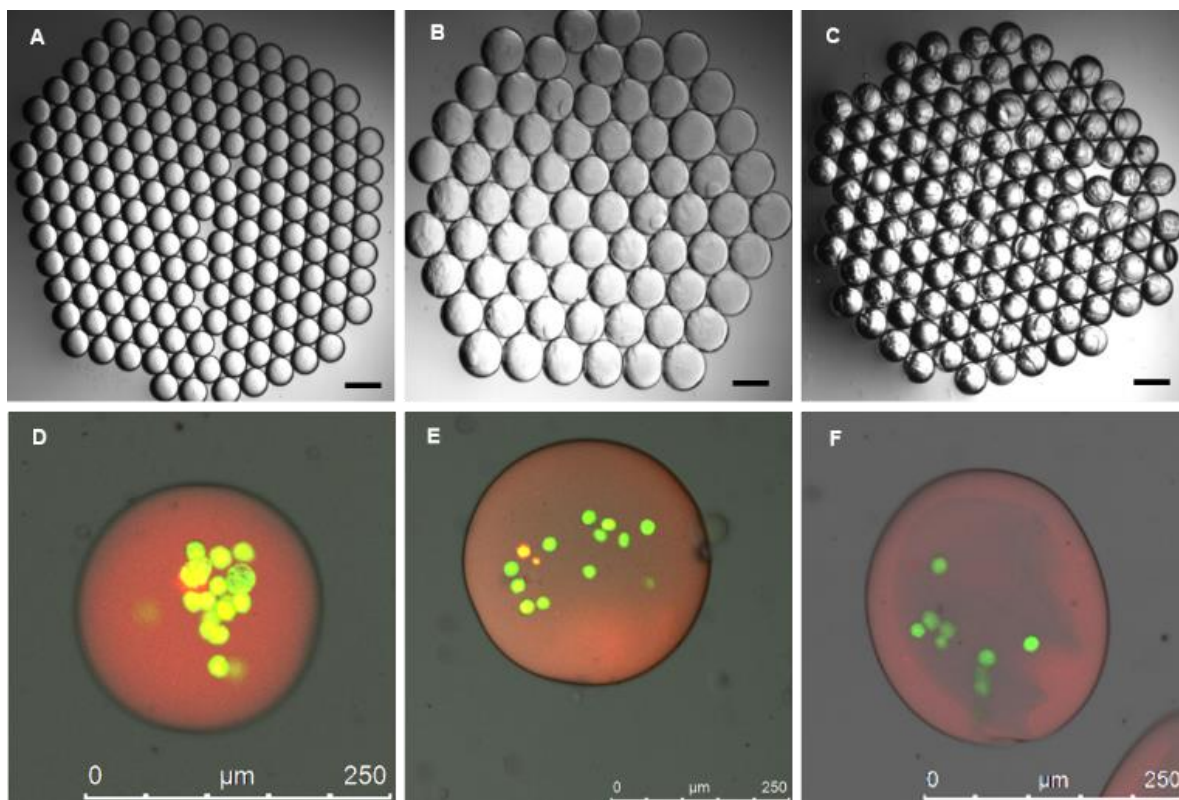


**Figure 30.** Cell-laden, micrometer-sized particles **M1-M3**. NIH/3T3-cell-laden pre-microgel droplets of type (A) **M1**, (B) **M2**, and (C) **M3** visualized under an optical microscope directly after templating (the black scale bars denote 150  $\mu\text{m}$ ). Confocal images of the gelled networks (D) **M1**, (E) **M2** and (F) **M3** and their cellular cargo 24 hours after microfluidic formation. The particles were stained with calcein AM and ethidium homodimer 1.

Although the **M3** pre-microgels appeared to be significantly stable during the microfluidic fabrication and swell at the same degree as pre-microgels **M1** (Figure 30C), no monodisperse distribution of the sizes or shapes of their corresponding hydrogels was observed *via* confocal microscopy 24 hours after their formation. The collected images of these gels are in fact characterized by the presence of scattered small (250  $\mu\text{m}$ ) and relatively large (315  $\mu\text{m}$ ) particles (Figure 31). Such a trend constitutes a hallmark of coalescence which usually proceeds after their collection and especially during their gelation. Consequently, sites of disruption of the poorly stable, semipermeable membrane of the **M3** networks appeared locally and could be observed as lack of distinct borders of the particles (Figure 30F).

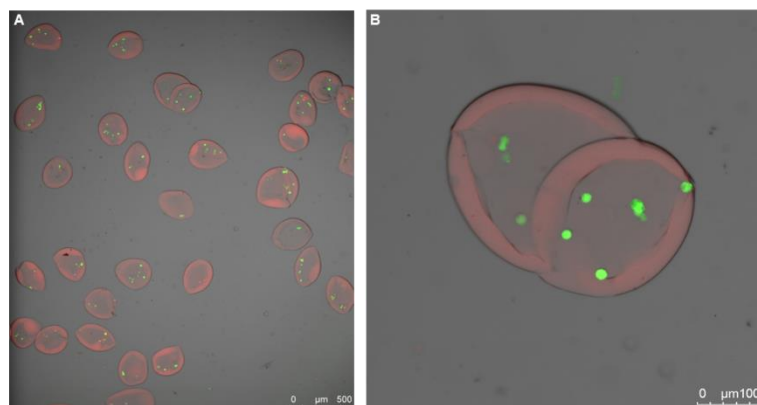


**Figure 31.** Micrometer-sized NIH/3T3 cell-laden particles **M3**. (A) Confocal microscopy images of NIH/3T3-cell-laden microgel droplets of type **M3** visualized 24 hours after microfluidic formation. The droplets appear highly deformed and (B) in the majority coalesced. The particles were stained with calcein AM and ethidium homodimer 1.

### 2.1.2.8 Cytocompatibility profile of cell-laden microgels **M1-M3**

The final step of our strategy consisted of a study of the viability of NIH/3T3 cells encapsulated into dPG-based microgels **M1-M3**. Therefore, the LIVE/DEAD® viability/cytotoxicity kit for mammalian cells was used. A set of calcein AM, which only fluoresces green inside living cells (Ex/Em 495/515 nm) and ethidium homodimer-1, which only penetrates dead cells staining them red (Ex/Em 495/635 nm), allows specimen visualization *via* confocal microscopy. Each of the pretreated aliquots of hydrogels **M1-M3** were observed one day after and at intervals of 7 days after the microfluidic encapsulation. At least three pictures at different positions of each gel were recorded scanning 200 μm on the *z* axis.

After one day of culture, excellent cell viabilities in all polyglycerol-based scaffolds were observed (Figure 32). Hence, neither the chemistry nor the biomaterials employed for the encapsulation impacted the viability or behavior of the cells, which complemented the findings of the cytotoxicity assay (CCK-8) prior to microfluidic templating.

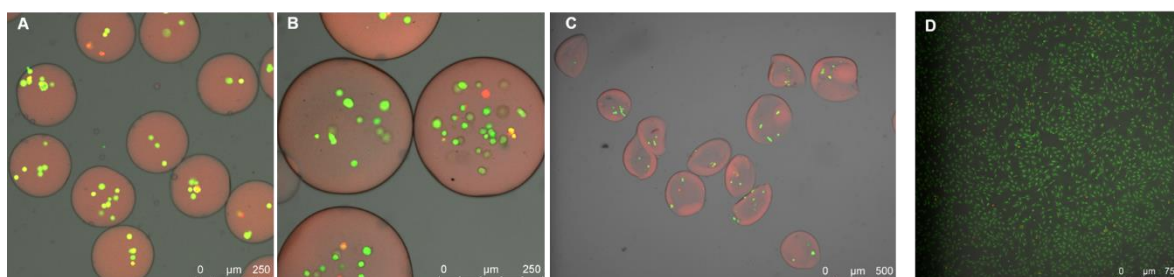


**Figure 32.** Confocal microscopy images of NIH/3T3 cell-laden microgels. (A), (B) and (C) correspond to scaffolds **M1**, **M2** and **M3**, respectively, and were captured 24 hours post microfluidic templating. (D) Naked NIH/3T3 were used as a control. The particles were stained with calcein AM and ethidium homodimer 1.

Cells cultured in **M1** gels remained viable longer than three weeks after entrapment with an eventual significant decrease witnessed on day 31. Additionally, already upon formation but also spanning the whole duration of this study, these gels were stable with highly monodisperse sizes and shapes and exhibited no deformation (Figure 33).

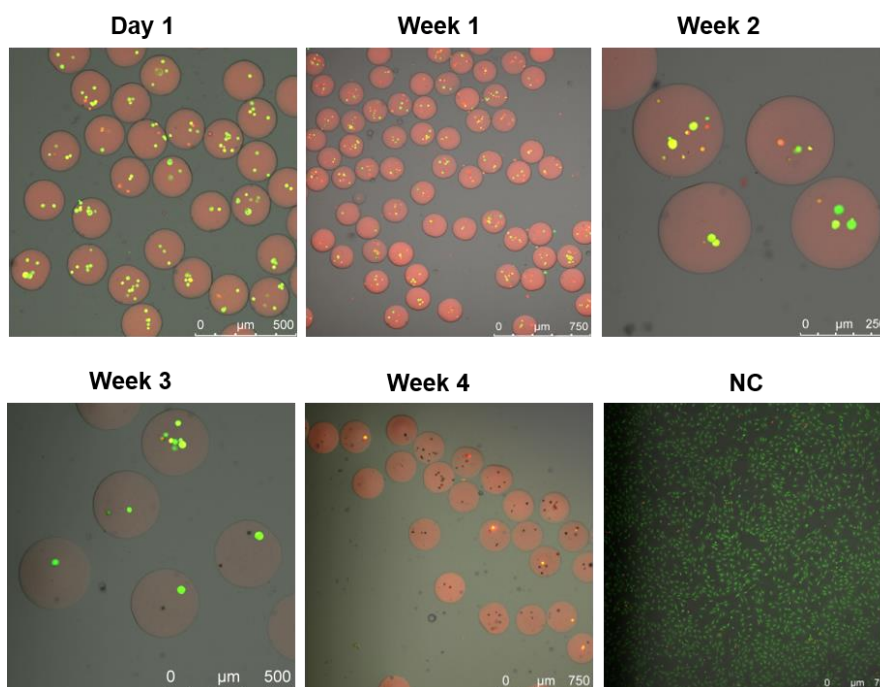


**Figure 33.** Encapsulated NIH/3T3 cells in microgel particles **M1** monitored *via* confocal microscopy in a period of 31 days. The images were taken a day after and subsequently on a weekly basis after the microfluidic entrapment of the cells. Naked NIH/3T3 were used as a negative control. Excellent viabilities were observed for over 21 days with a low number of living cells even four weeks after the encapsulation. The particles were stained with calcein AM and ethidium homodimer 1.

The observation of the cell-laden hydrogel scaffolds **M1**, both on a micro- and macroscopic level, produced no evidence of degradation procedures throughout the time

frame of this study. This behavior could be attributed to the presence of carbamate functionalities on focal points of the microgel networks, which introduced a high durability. Carbamates are known for their chemical stability toward acids, bases, and hydrogenation as well as for their metabolic stability toward enzymes such as aminopeptidases.<sup>[127]</sup> These favorable features explain their intensive use in medicinal chemistry for the generation of prodrugs, which can be readily processed at the biologically relevant target. An extensive study on a large variety of carbamates determined an order for the metabolic lability of the latter depending on the nature of their vicinal groups. It was thus reported that carbamates derived from ammonia or aliphatic amines are sufficiently long-lived,<sup>[128]</sup> whereas the direct vicinity to a strong electron-withdrawing group leads to rapid  $\beta$ -eliminations and degradation.<sup>[129]</sup>

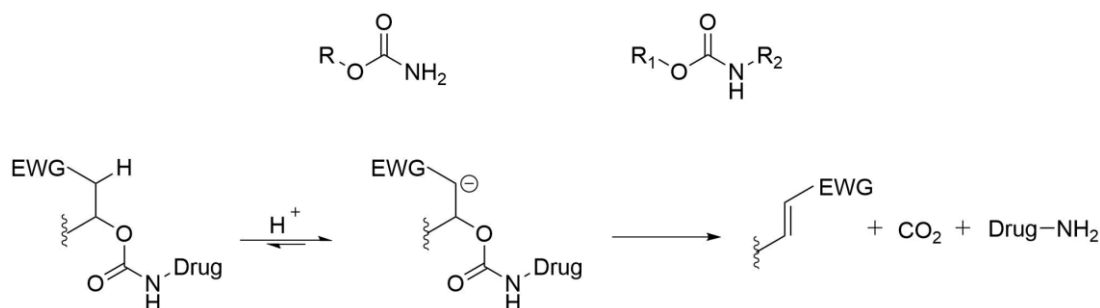


**Figure 34.** Carbamates derived from ammonia and aliphatic amines as well as  $\beta$ -elimination and degradation mechanism of carbamates bearing strong electron withdrawing groups (EWG).<sup>[128,129]</sup>

Since, the carbamate moieties designed in the present study can be classified as alkyl-COO-NH-alkyl, it can be assumed that they contribute a very slow degradation or even non-biodegradable profiles of the developed microgel scaffolds. These features make matrix **M1** an especially fine candidate for encapsulating and transplanting cells to deliver therapeutics. A long-term immunoisolation of the cells would allow production and on-demand release of hormones, factors, or enzymes the absence of which cause various diseases.<sup>[15–17,20–23,130]</sup>

The cells in **M2** carriers, exhibited exceptional viabilities for over 7 days, which then decreased in the second week of culture (Figure 35). **M2** microgels were also stable and had highly monodisperse sizes and shapes throughout the study. Similar to particles **M1**, the high durability of these hydrogels could be associated with the tethered carbamate functionalities in their networks. The short-term survival of the enclosed cells in **M2** matrices could be a result of the mechanical properties of these scaffolds. The elasticity conferred from precursor **P2** promoted the necessary stability of these microparticles but proved unsuitable for the tested cell line. Additionally, due to the higher number of free hydroxy groups of their linear

constituents, **M2** microgels are purely hydrophilic. This attribute could account for insufficient cell adhesion and thus limited cellular lifespan.<sup>[131,132]</sup> These findings suggest that microgels with a composition of type **M2** cannot be used as medical devices yet for cell-based therapies but remain promising, especially after appropriate modifications, for short-term studies of encapsulated cells.<sup>[133-135]</sup>

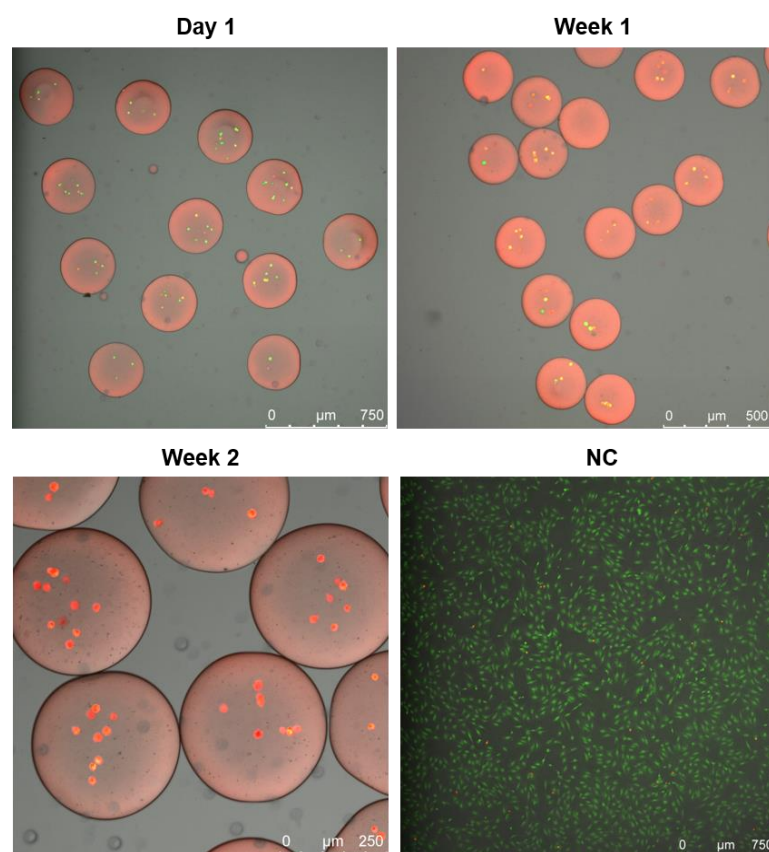


**Figure 35.** Encapsulated NIH/3T3 cells in microgel particles **M2** monitored *via* confocal microscopy in a period of 14 days. The images were taken a day after and subsequently on a weekly basis after the microfluidic entrapment of the cells. Naked NIH/3T3s were used as a negative control. Excellent viabilities were observed for over 10 days with a low number of living cells even two weeks after the encapsulation. The particles were stained with calcein AM and ethidium homodimer 1.

The poorest performance of all three gels was observed for microgels **M3**. Due to the lowest exhibited cytotoxicity of polymer precursor **P3** in CCK-8 assay prior to encapsulation, it was anticipated that the resulting microgels would also outperform. However, the excellent viabilities of their cells recorded one day after the microfluidic fabrication were limited to only seven days in total (Figure 36). Already after one day in culture, insufficient particle stability was noticed, which also led to coalescence and generation of large microgels. This, as well as the inhomogeneity in the sizes and shapes of these hydrogels, can be associated with inadequate or incomplete gelation and highlights the need for a modified microfluidic production of robust networks.

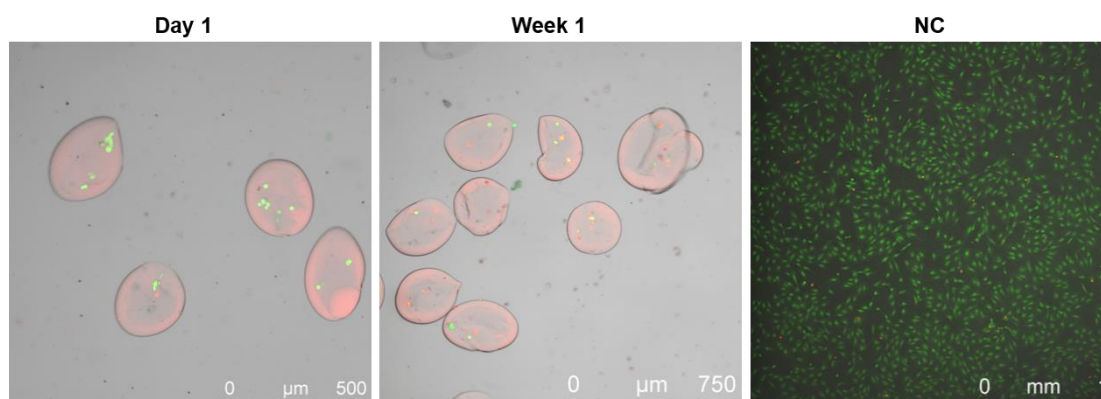


**Figure 36.** Encapsulated NIH/3T3 cells in microgel particles **M3** monitored *via* confocal microscopy in a period of 7 days. The images were taken a day after and subsequently on a weekly basis after the microfluidic entrapment of the cells. Naked NIH/3T3s were used as a negative control. Excellent viabilities were observed for over 5 days with a low number of living cells one week after the encapsulation. The deformation and partial disruption of the integrity of the encapsulation membrane are seen. Interestingly, released cells from the disrupted hydrogels anchored on the remaining stable scaffolds and were still viable for one week in culture. The particles were stained with calcein AM and ethidium homodimer 1.

The conditions applied during fabrication were for all 3D artificial matrices identical to allow an objective comparison of the behavior of the generated microgels. It is obvious from the obtained results that this set of parameters was not suitable for macromonomers **P3** and **P4**, although highly stable pre-microgels were observed during the microfluidic templating. A further manifestation of the moderate mechanical properties of scaffold **M3** was the disruption of its network integrity resulting in a release of the encapsulated cells. Interestingly, some of the released cells could adhere onto the surface of the few intact microgels and thus remain viable. Our findings suggest that **M3** gels present a degree of elasticity too high to promote long-term viability of the used fibroblast cells. Such a synthetic matrix could eventually find use in biomedical applications after significant optimization of its biomechanical properties.

As documented for all microgel matrices, the NIH/3T3 fibroblasts after their microfluidic encapsulation adopted a spherical morphology, which they maintained throughout the respective time periods of this study. After immobilization in the microcapsules, cells should adapt to the new conditions provided from the bioinert material surrounding them. A spherical morphology suggests a lack of adherence or spreading in the inner microenvironment of the hydrogel particles and requires further optimization of scaffolds of the **M3** type for them to be implemented in biomedical applications of cell encapsulation.

### 2.1.3 Conclusions

This study presents the synthesis of azide-functionalized polymer precursors as well as of a cyclooctyne cross-linker for microfluidic templating of artificial 3D scaffolds for cell encapsulation. This approach was designed to involve three different polyglycerol architectures as building blocks for microgel cell carriers: a dendritic structure bearing highly active bicyclooctyne moieties (dPG-polyC), a six-membered, star-shaped (S-PG-hexaazide), and a linear ( $\alpha$ ,  $\omega$ -bisazido-IPG) bearing azide functionalities at their ends. The first two have been prepared for the purposes of this strategy for the first time, whereas  $\alpha$ ,  $\omega$ -bisazido-linear polyglycerol had been already established in our group. The specific functional groups were introduced in the macromonomers to facilitate a bioorthogonal strain-promoted azide-alkyne cycloaddition (SPAAC) in the presence of cells.

The multistep syntheses of polymeric precursors **P1**, **P2**, and **P4** proceeded uneventfully and afforded the desired products in overall yields exceeding 50 %. The acetal protection of the monomer utilized for the development of both **P1** and **P2** allows a controlled polymerization and can be readily removed under mild acidic conditions. Although it constitutes a favorable feature, this acid lability presents the potential of transacetalization, which can even partially lead to inter-cross-linking of the polymer chains. The key transformation of the applied synthetic protocols is the introduction of vinyl sulfone or mesyl moieties into the star-shaped and linear polyglycerol, respectively. The ease of incorporation as well as the advantageous properties as a leaving group (mesyl) or a Michael acceptor (vinyl sulfonates), facilitate straightforward conversions to the corresponding azides necessary for the SPAAC with poly(bicyclooctyne) **P4**. The employed procedures, the linear syntheses of which do not exceed 4 (**P1** and **P2**) or 5 (**P4**) steps make use of commercially available materials and generate the end products on multigram scales. In general, the established synthetic strategy is a very efficient and elegant approach that could also be implemented to address more complex synthetic challenges.

The cytotoxicity potential of the prepared polymers was evaluated through an assay with a cell counting kit 8 (CCK-8). Very low or moderate toxicities were recorded for the cells incubated in the presence of low, medium, and high concentration solutions of the polymers. After 24 hours of inoculation, a slight decreasing tendency in the cell viabilities was reported for the higher polymer concentrations. A similar trend was observed, even after 3 days in culture, with only moderate or no toxicities, especially upon increasing polymer content. In this context, the developed macromonomers exhibited extremely cytocompatible

profiles for the chosen cell line and under the conditions of the conducted assay. Particularly outstanding results were documented for the cells in solutions of S-PG-hexaazide.

As proof of concept, mouse fibroblasts of the NIH/3T3 cell line were encapsulated in polyglycerol-based hydrogel matrices fabricated by bioorthogonal microfluidic templating. By varying the implemented polymeric materials, specific properties were introduced to each system corresponding to the viability profiles of the encapsulated cells. In particular, the performance of the newly developed cell-laden beads was compared with that of hydrogels composed of  $\alpha$ ,  $\omega$ -bisazido-linear polyglyethylene glycol ( $\alpha$ ,  $\omega$ -bisazido-PEG) and dPG-poly(bicyclooctyne). Due to PEG's highly advantageous features, it is a widely used material in numerous biomedical applications.<sup>[121]</sup> It was included in the building blocks of this study, as it was envisioned to generate hydrogel cellular vehicles with universally favorable attributes. Three different microgels were constructed, in which cells were enclosed with fully retained viability. In case of the particles composed of S-PG-hexaazide, fibroblasts remained vital up to three weeks post encapsulation. As a result, these microcapsules could be used for long-term immobilization of cells with the possibility to further study and manipulate their biological cargo. Thus, this approach could contribute to the ongoing efforts for the understanding of the immunoisolation and cellular survival in synthetic 3D networks. Additionally, it should be noted that polyglycerol-based scaffolds are amenable to the incorporation of a plethora of therapeutics. In our hands, similar types of carriers have been prepared that bear various therapeutically relevant payloads.<sup>[136–139]</sup> Especially due to their high-end functionality, dPG-based microgels could be easily modified for future therapeutic delivery. As such, the investigated S-PG-hexaazide-gels are promising for the entrapment and *de novo* and *in vivo* release of biologically interesting content such as drugs, proteins, and even genetic material.

The second ( $\alpha$ ,  $\omega$ -bisazido-IPG) and third ( $\alpha$ ,  $\omega$ -bisazido-PEG) type of developed hydrogels demonstrated markedly lower cell viabilities, which were limited to 14 and 7 days, respectively. This behavior could be attributed to the properties derived from the polymer constituents, in association with their individual cytotoxicity data but not for the PEG-based gels, because  $\alpha$ ,  $\omega$ -bisazido-PEG outperformed the assay with CCK-8. Furthermore, due to poor microcapsule stability, it was assumed that the applied conditions for the microfluidic templating of  $\alpha$ ,  $\omega$ -bisazido-PEG were not suitable and should be optimized to generate robust microbeads. In general, the versatility of this strategy is reflected in the diversity of the overall behavior of the generated mammalian-cell-laden microgels. This study could demonstrate that properties of the surrounding matrices, such as stiffness and hydrophilicity

and not only the inherent exquisitely cytocompatible profile of the utilized polymeric building blocks determine cell survival.

As a future perspective, a wider range of parameters for the microfluidic cell encapsulation should be examined, to extend the versatility of the developed biomaterials. In this regard, the functional survival of the enclosed cells could also benefit. As was observed, after their microfluidic embedment the NIH/3T3 fibroblasts, exhibited a spherical morphology that suggests no adherence or spreading due to the bioinert material surrounding them. To expand the potential of the studied microgels as three-dimensional cell cultures, which enable confluency and further proliferation of the entrapped cells, the introduction of cyclic RGD peptide sequences as recognition and cellular adhesion sites would be necessary.<sup>[140]</sup> Moreover, as cell encapsulation therapies are growing into a significant biomedical field,<sup>[5-8,15-17,20-23,130]</sup> there is crucial need for the introduction of new biocompatible materials to ensure definitive treatments for various chronic diseases. As an alternative, it would be a good idea to thoroughly characterize and further optimize existing synthetic or naturally occurring polymers to establish their application in cell immunoisolation.<sup>[49]</sup>

## 2.2 Dendritic Polyglycerol-Based Microgels and Bulk Hydrogels for Transplantation of Pancreatic Islet Cells

### 2.2.1 Objective

To extend the scientific goals of the first part of this work, the developed polyglycerol macromonomers would be used to facilitate the bioorthogonal microfluidic templating of 3D scaffolds for encapsulation of  $\beta$ -TC-6 mouse insulinoma cells. These efforts are encouraged not only by the initial promising results of this study but also by the current limitations of the available biomaterials and fabrication processes in the research for potential cell-based treatments of T1D.

Star-shaped polyglycerol-hexaazide and dendritic polyglycerol-poly(bicyclooctyne) would be utilized to produce micro- and bulk gels *via* strain-promoted alkyne-azide cycloaddition. The favorable features of this hydrogel formation have highly reduced potential cytotoxicity risks and could promote long-term functional survival of the enclosed cells. Apart from the application of microfluidic devices (Figure 37) to achieve highly reproducible, fine-tuned geometries,<sup>[109,110]</sup> this strategy include the generation of larger synthetic matrices. To evaluate the performance of the obtained cell-laden microcapsules and macrogels, the viability of the immobilized  $\beta$ -TC-6 cells would be appraised at specific time intervals after the encapsulation. Additionally, the glucose-stimulated insulin secretion of the embedded cells would be quantified through the related immunoassay.

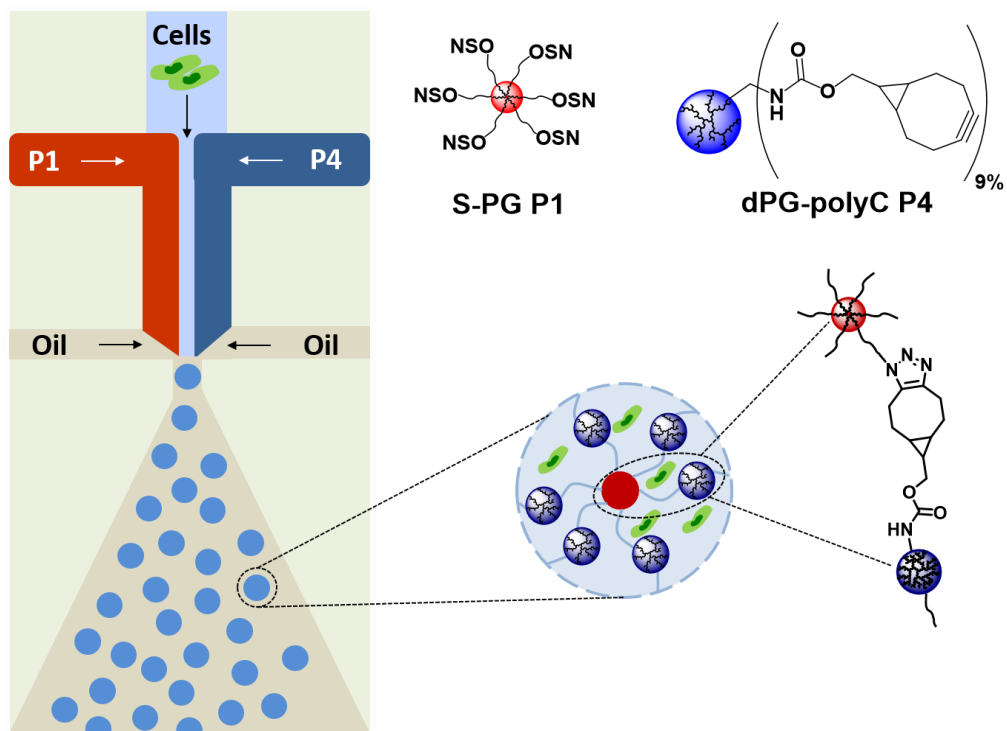


**Figure 37.** Simplified illustration of microfluidic templating of  $\beta$ -TC-6 cell-laden dPG-based 3D scaffolds.

## 2.2.2 Results and discussion

### 2.2.2.1 Encapsulation of $\beta$ -TC-6 cells in microgels and bulk hydrogels

Although several different pancreatic  $\beta$ -cell lines have been established, only a few achieved a normal regulation of insulin secretion. Of the latter even less have been widely used in diabetes research due to significant shortcomings, including poor sensitivity to glucose or a substantial shift of their concentration-dependence curves to hypersensitivity.<sup>[188]</sup> This tendency has been especially noted with passages in tissue culture exceeding 60 cell cycles.<sup>[189]</sup> Additionally, the data of related studies suggested that culture in lower glucose concentrations (up to 1 g/L) could prevent adverse effects on insulin gene expression.<sup>[190]</sup> Among the reported cells lines, mouse insulinoma  $\beta$ -TC-6 was shown to highly resemble insulin secretion profiles of primary cells without discrepancies for a considerably prolonged passage<sup>[188]</sup> and was thus employed for the purposes of this study.

Prior to encapsulation mouse insulinoma  $\beta$ -TC-6 cells, cells were cultured in DMEM culture medium containing low glucose (1 g/L), 15 % FCS and 1 % PS (penicillin/streptomycin) in a humidified incubator at 37 °C under 5.0 % CO<sub>2</sub>. They were grown in 182.5 cm<sup>2</sup> cell culture flasks and their medium was changed every second day after a rinsing step with DPBS (2 x 10.0 mL). Upon confluency of 70 % the culture was 1:2 subcultured.

To create monodisperse pre-microgel droplets as templates for the particle synthesis, identical PDMS microchannels were used, to those described in Section 2.1.2.7 of this study. Upon mixing of S-PG-hexaazide, dPG-polyC, and a suspension of  $\beta$ -TC-6 cells inside the droplets (Figure 38A, lower part), the precursors reacted in a SPAAC and formed cell-laden microgels within a few minutes. To monitor the droplet formation the microtemplate was operated on an inverted optical microscope equipped with a digital camera. After a sequence of collection, preincubation, and work up, the preformed microgels were allowed to gel overnight at 37 °C under 5.0 % CO<sub>2</sub>.

The fabricated microgels swelled to 200  $\mu$ m, were monodisperse in sizes and shapes and exhibited high stability not only directly upon collection but also 24 hours after microencapsulation. Nevertheless, as was observed in the confocal images recorded 24 hours after microgel production (Figure 38B and C), the majority of enclosed cells were dead, which suggests that the surrounding synthetic matrices were unsuitable for the longevity of this type of pancreatic  $\beta$ -cells. This could be attributed to the mechanical properties of the hydrogels which might either be too elastic or too viscous for the entrapped cells.<sup>[119]</sup> Apart

from that, the associated degree of hydrophilicity presented to the cells from the enclosing membrane network could be inappropriate for long-term viabilities of the  $\beta$ -TC-6 cells.<sup>[131,132]</sup>

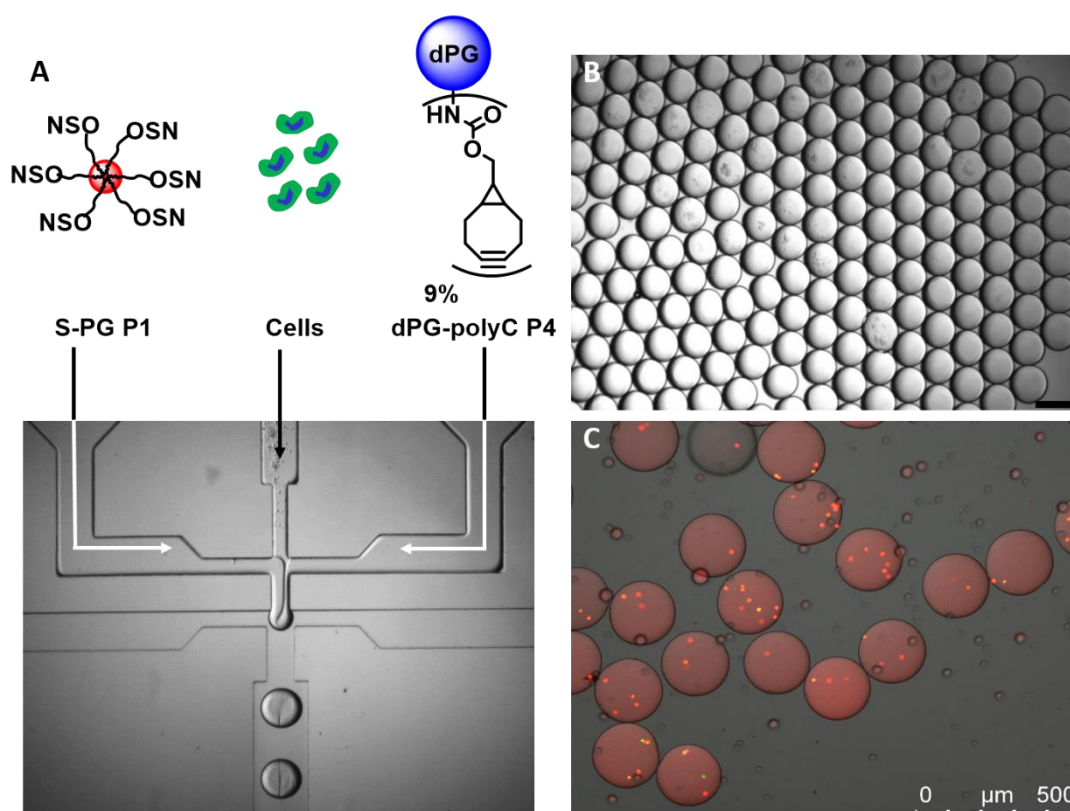


**Figure 38.** Droplet-templated encapsulation of  $\beta$ -TC-6 cells: (A) S-PG-hexaazide (**P1**), dPG-polyC (**P4**), and a suspension of  $\beta$ -TC-6 cells were loaded on a microfluidic device that allowed the SPAAC inside monodisperse, micrometer-sized precursor capsules. (B) Stable pre-microgel particles collected directly after fabrication. (C) The majority of the pancreatic  $\beta$ -cells 24 hours post encapsulation were dead as observed *via* confocal microscopy after staining with calcein AM and propidium iodide. The black scale bar denotes 150  $\mu$ m.

To circumvent this problem, the envisioned 3D scaffolds were supposed to be optimized to bear a higher resemblance to the natural ECM of pancreatic islets. The latter was found to constitute a supramolecular organization consisting of a branching network of collagen IV with end-to-end and lateral associations as well as a mesh of short interconnecting struts of laminin polymers.<sup>[191]</sup> This combined laminin/collagen network is interlaced with proteoglycans, especially heparan and chondroitin sulfates.<sup>[192]</sup> These negatively charged sites are responsible for the sieving properties of the ECM, which enable binding and sequestration of growth factors and cytokines with a function as a reserve to be released on demand. Detailed knowledge of the matrix molecular composition and of how it guides cell function still remains incomplete.<sup>[192]</sup>

As mimics of naturally occurring biomacromolecules, dendritic polyglycerol-based, polysulfated heparin analogs that were established in our group have exhibited exceptional biocompatibilities. Being non-cytotoxic and anti-inflammatory, dPGS has also recently proved to promote cellular metabolic activity.<sup>[193]</sup> Furthermore, its incorporation in hydrogels for the cell encapsulation has been associated with long-term cell viabilities favored by higher gel swelling.<sup>[106]</sup> The presented excess of negative charges led to expansion of the polymeric networks due to increased repulsion and subsequently to diffusion of large amounts of water. This suggested, a more dynamic influx of nutrients and oxygen with a simultaneous outflux of metabolic waste promoting cellular longevity. On the other hand, a net negative charge allowed the infiltration of various proteins or factors crucial for the regulation of cell adhesion, proliferation, or differentiation.<sup>[106]</sup>

Therefore, a new system of macromonomers, which included sulfated dPG-polyazide **P5** and homobifunctionalized bicyclooctyne PEG **P6** was utilized to improve the viability profiles of encapsulated  $\beta$ -TC-6 cells. These polymers with average molecular weight of 10000, and 6000 g mol<sup>-1</sup>, respectively, were kindly contributed by Dr. P. Dey.<sup>[106–108]</sup> Bearing the same set of functionalities as precursors **P1** and **P4**, they also could facilitate a bioorthogonal SPAAC-based cross-linking in the presence of living cells (Figure 39). The desired cellular vehicles (**M4**) were developed *via* microfluidic templating, employing the appropriate set of conditions for the utilized polymers, determined prior to cell encapsulation.

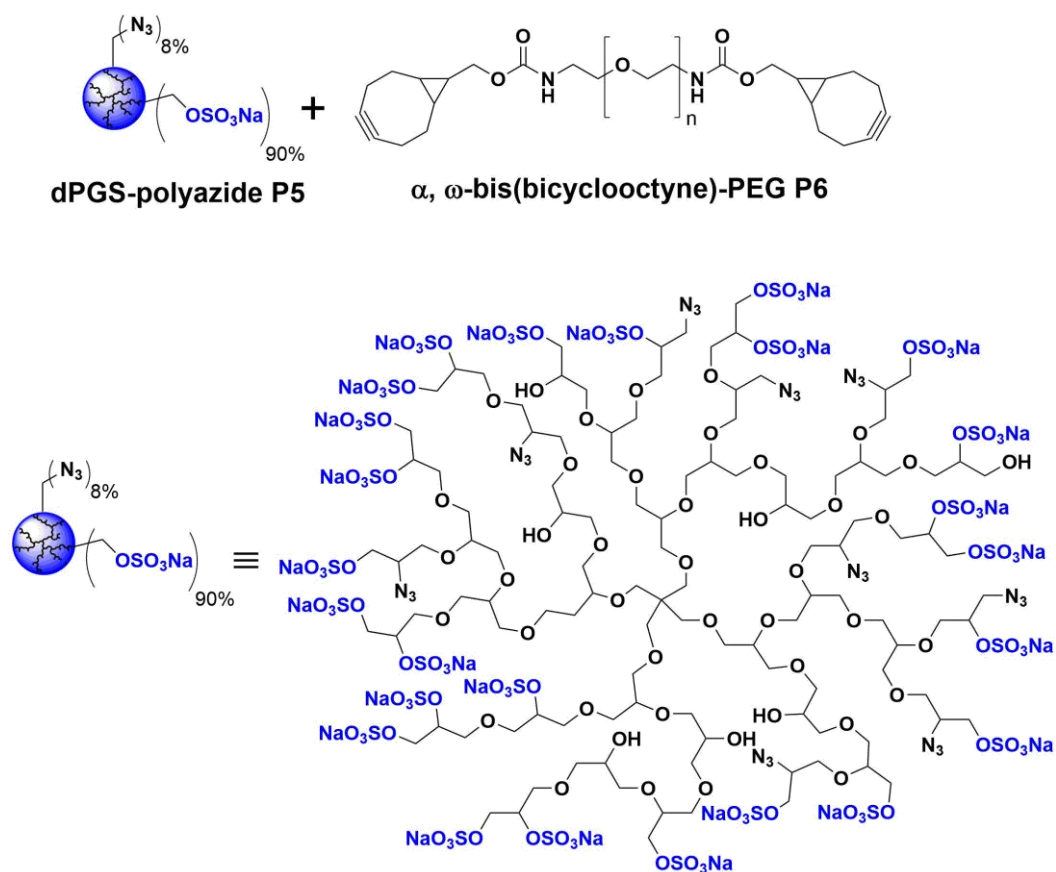


**Figure 39.** SPAAC of macromonomers **P5** and **P6**.

The generated cell-laden pre-microgels exhibited very high stability and were monodisperse in sizes and shapes shortly after their fabrication (Figure 40A). Typical water-swollen product particles (415  $\mu\text{m}$ ) bearing encapsulated cells are shown in Figure 39B and C.  $\beta$ -TC-6 cells enveloped in these cell carriers showed excellent viabilities as observed in the recorded confocal images 24 hours post encapsulation. Although these systems produced very promising results, it is not possible to accurately determine the number of pancreatic  $\beta$ -cells immobilized in each microcapsule. The natural behavior of these cells to form aggregates that ensure their survival, only allows an approximation of their number by use of the conventional staining methods. Additionally, the pore sizes as well as the durability of the constructed microgels do not support quantification of the enclosed cell population by means of immune staining.

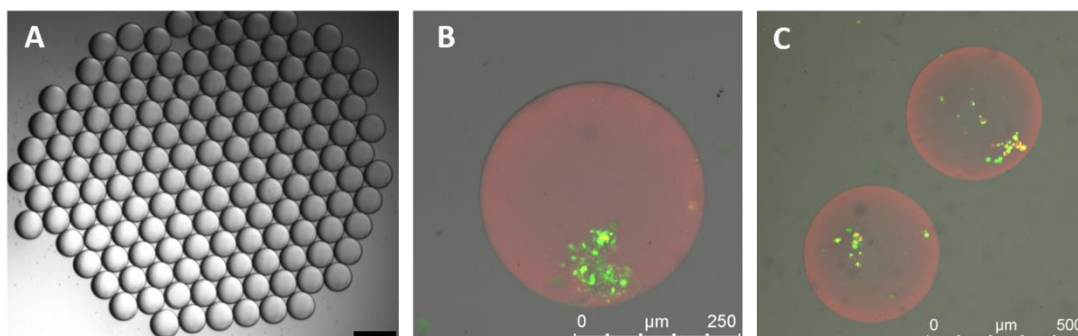


**Figure 40.** Encapsulated  $\beta$ -TC-6 cells. (A) Pre-microgel droplets recorded immediately after fabrication. The black scale bar denotes 150  $\mu\text{m}$ . Micrometer-sized dPGS-capsules (**M4**) with living cells 24 hours post microfluidic templating at (B) higher and (C) low enlargements. The cells and their carriers were stained with calcein AM and propidium iodide.

Thus, apart from  $\beta$ -TC-6 cell-laden micrometer-sized particles, bulk hydrogels were prepared carrying a specific number of pancreatic islet cells, which were also utilized for the necessary quantification of GSIS. These immune-isolation scaffolds were also prepared by gelation of polymers **P5** and **P6**. To this aim, the wells of a 96-well-plate served as templates for the formed macrogels. To avoid erroneous results and allow the comparison of the related biocompatibility profiles, semi-dilute solutions of polymers **P5** and **P6** were prepared in the same concentrations as for the microfluidic encapsulation of pancreatic  $\beta$ -cells. They were applied in a volume ratio corresponding to the respective flow rate ratio on the microfluidic platform. Each well was loaded consecutively with specific aliquots of a polymer solution, the cell suspension (counting  $4.00 \cdot 10^4$  cells/well), and the remaining polymer solution. Upon gentle mixing the SPAAC was initiated and the 96-well-plate was incubated for 20 minutes at 37  $^{\circ}\text{C}$  under 5.0 %  $\text{CO}_2$  to allow further gelation. Subsequently, culture medium (DMEM 1 g/L glucose, 15 % FCS, 1 % P/S) was added to a final volume of 100  $\mu\text{L}$  per well. After a 24-hour incubation and a rinsing step, fresh medium was added to each well and the macrogels were further incubated. The supernatants of each well were collected one and eight days after encapsulation and stored at -25  $^{\circ}\text{C}$  for the following quantification of secreted insulin.

To simulate the natural glucose metabolism, the produced hydrogels bearing pancreatic  $\beta$ -cells were incubated in three different glucose containing culture media with: no, low, and high glucose content, respectively, whereas pure low glucose DMEM (15 % FCS, 1 % P/S) was used as a negative control. Each of the applied conditions were investigated in a triplicate with an overall number of three repetitions. To compare the performance of bulk hydrogels regarding the insulin secretion capacity of the utilized cell-line, naked  $\beta$ -TC-6 cells were incubated under identical conditions with the cell-laden macrogels. Moreover, to estimate the

encapsulation limits of this specific polymer system, three bulk gels were prepared of the same overall polymer concentration as in each well, carrying  $4.00 \cdot 10^4$  (**G1**),  $1.00 \cdot 10^5$  (**G2**), and  $1.00 \cdot 10^6$  (**G3**) cells, respectively. The viabilities of the encased cells in each dPGS-gel carrier (**G1-G3**) were determined *via* confocal imaging after treatment with a mixture of calcein AM and propidium iodide staining reagents.

#### 2.2.2.2 Cytocompatibility profile of cell-laden microcapsules and bulk gels

This step of the strategy involved the investigation of the viability profiles of the encapsulated  $\beta$ -TC-6 cells in the dPGS-based microgels (**M4**) and bulk hydrogels (**G1 - G3**). To this end, a set of calcein AM and propidium iodide (PI) was utilized to allow specimen visualization *via* confocal microscopy. The first, an inherently non-fluorescent staining reagent, can penetrate living cells, in which upon action of intracellular esterases its acetoxymethylester undergoes hydrolysis to produce the green fluorescing calcein. With excitation/emission maxima of 495/515 nm, this reagent stains living cells green. The second, cannot permeate intact cellular membranes and is thus commonly used to detect dead cells. PI binds to DNA by intercalating between the bases with little or no sequence preference and has in aqueous solutions excitation/emission maxima of 493/636 nm. Upon binding to DNA, the dye's fluorescence is enhanced 20- to 30-fold, its fluorescence excitation maximum is shifted  $\sim 30 - 40$  nm to the red and the fluorescence emission maximum is shifted  $\sim 15$  nm to the blue (Ex/Em maxima of 538/617 nm) staining dead cells red. The pretreated aliquots of cell-laden microgels **M4** and bulk gels **G1 - G3** were observed each one day after and at weekly intervals after microfluidic encapsulation. At least three pictures at different positions of each gel were recorded scanning  $200 \mu\text{m}$  on the  $z$  axis.

In case of the dPGS-microgels, excellent cell viabilities for up to five weeks were recorded (Figure 41). The enclosed pancreatic cells were arranged into aggregates, which is their natural behavior as repeatedly reported<sup>[49,190]</sup> and also observed in the 2D culture. As for microgels **M1 - M3** examined in the first part of this study, the calcein/PI mixture appeared to react with the polymeric networks of microgels **M4** which therefore were seen as dark or pale red spheres in the confocal images. To rule out the interference of the particle fluorescence with the expected from their biological cargo, encapsulated  $\beta$ -TC-6 cells were treated with a 70 % ethanol solution for 30 minutes and then stained with the calcein/PI mixture. Based on this confocal image (Figure 41, NC EtOH 70 %), it is possible to distinguish dead cells from the fluorescence of the matrix surrounding them.

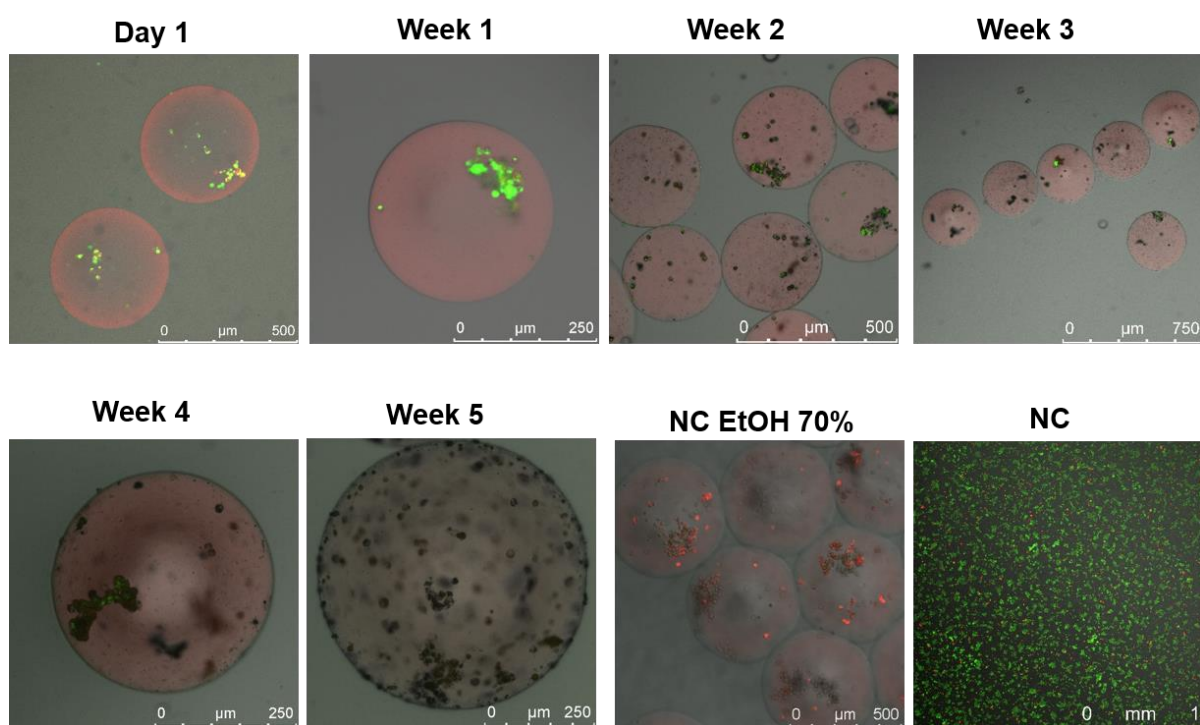


**Figure 41.** Encapsulated  $\beta$ -TC-6 cells in dPGS-based microgels **M4** were monitored *via* confocal microscopy in a period of 35 days. The images were taken a day after and subsequently on a weekly basis after the microfluidic entrapment of the cells. Naked  $\beta$ -TC-6 cells were used as a negative control. To distinguish between the fluorescence of dead cells and microcapsules, cell-bearing particles were treated with an ethanolic solution (NC EtOH 70 %). Excellent viabilities were observed for over 21 days with a low number of living cells even four weeks after the encapsulation. The particles were stained with calcein AM and PI.

A decrease in the viability of the enclosed  $\beta$ -TC-6 cells was first detected at the beginning of the fifth week post microfluidic encapsulation. A complementing observation to this finding is that the microscale spherical gels, which initially were transparent and could be recognized by bare sight from their margins, gradually turned opaque. It was thus assumed that the immobilized pancreatic cells had deposited matrix macromolecules that, in turn, either partially or extensively clogged the pores of the 3D scaffolds. As a result, it could be suggested that the staining reagents could not fully permeate the microgels and reach their cellular content (Figure 41, Week 5).

In case of the  $\beta$ -TC-6 cells encapsulated in dPGS-macrogels, exceptional viabilities of almost 100 % were monitored for all gels of type **G1** 24 hours and up to four weeks after embedment (Figure 42). The bulk hydrogels were shaped like pies and swelled up to 13 mm measured one day after their formation. The cells appeared to assemble in aggregates and were distributed throughout the hydrogel. Different regions of each specimen were recorded and observed at various levels of 200  $\mu\text{m}$  depth. The high viabilities were also detected in

sites of the gels containing defects, which highlighted the exquisite biocompatibility of these cellular vehicles.

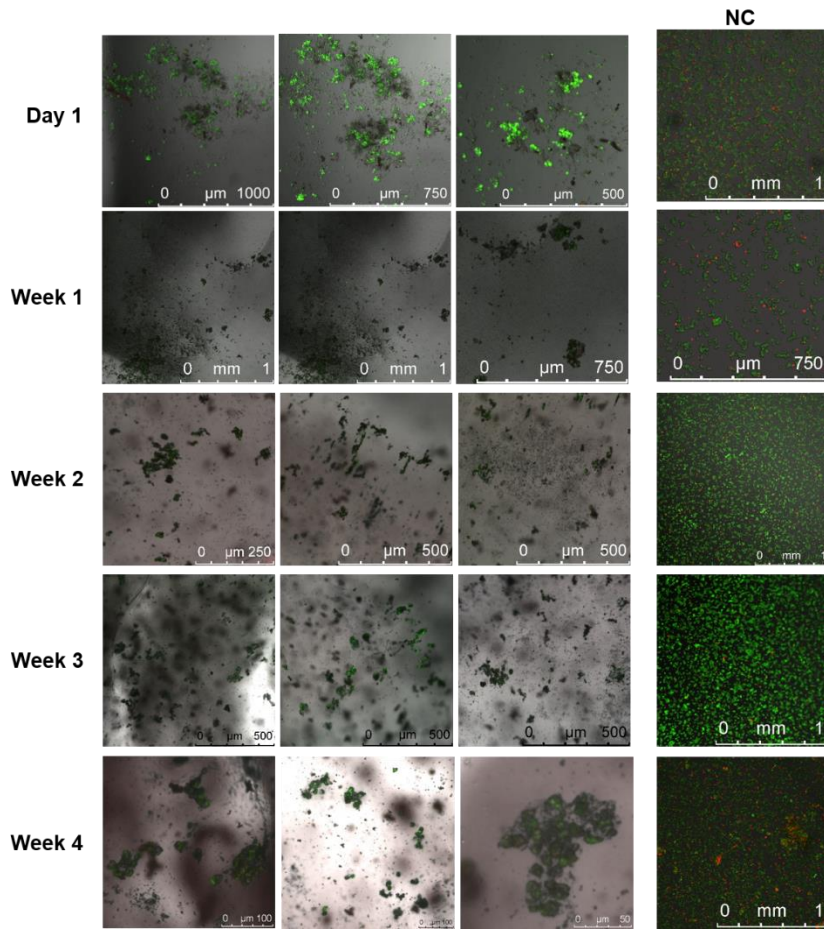


**Figure 42.** Encapsulated  $\beta$ -TC-6 cells in dPGS-based macrogel **G1** were monitored *via* confocal microscopy in a period of 31 days. Various gel regions were recorded a day after and subsequently on a weekly basis after the microfluidic entrapment of the cells. Naked  $\beta$ -TC-6 cells were used as a negative control. Excellent viabilities were observed for over 30 days in culture in bulk hydrogels **G1**. The particles were stained with calcein AM and PI.

The more densely populated hydrogels **G2** and **G3** also demonstrated very high viabilities already one day after encapsulation. This behavior was globally documented for gel **G2** extending to four weeks, the full duration of this assay (Figure 43). In the largest cell masses present in macrogel **G3**, however, cells were viable only at layers closer to the surface of the hydrogel and dead in its deeper areas (Figure 44). This viability profile observed throughout the study suggests that the encapsulating capacity of such a hydrogel carrier was reached already at less than  $1.00 \cdot 10^6$  cells. Additionally, the detected tendency of vital cells in the periphery but necrotic cells in the cores of the available aggregates was a reflection of the inadequate nutrients and oxygen supply and pointed to spatial optimization of these capsules to support the encapsulation of larger cell populations.

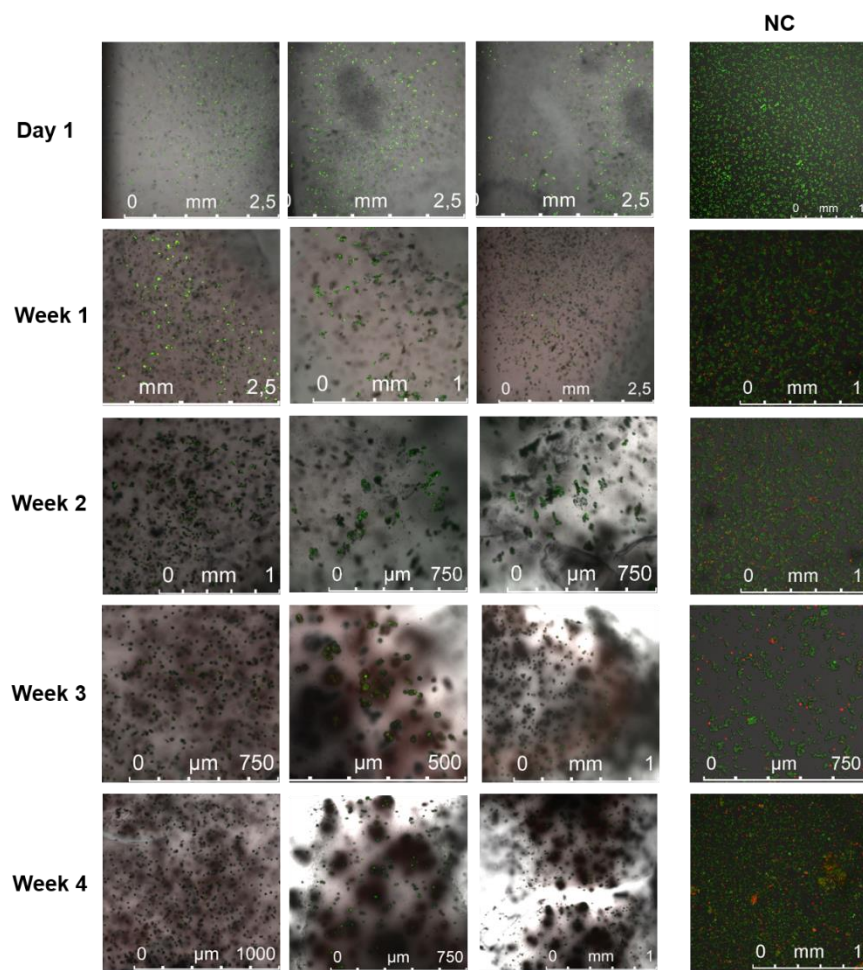


**Figure 43.** Encapsulated  $\beta$ -TC-6 cells in dPGS-based macrogel **G2** were monitored *via* confocal microscopy in a period of 31 days. Various gel regions were recorded a day after and subsequently on a weekly basis after the microfluidic entrapment of the cells. Naked  $\beta$ -TC-6 cells were used as a negative control. Excellent viabilities were observed for over 30 days in culture in bulk hydrogels **G2**. The particles bore  $1.00 \cdot 10^5$  cells and were stained with calcein AM and PI.

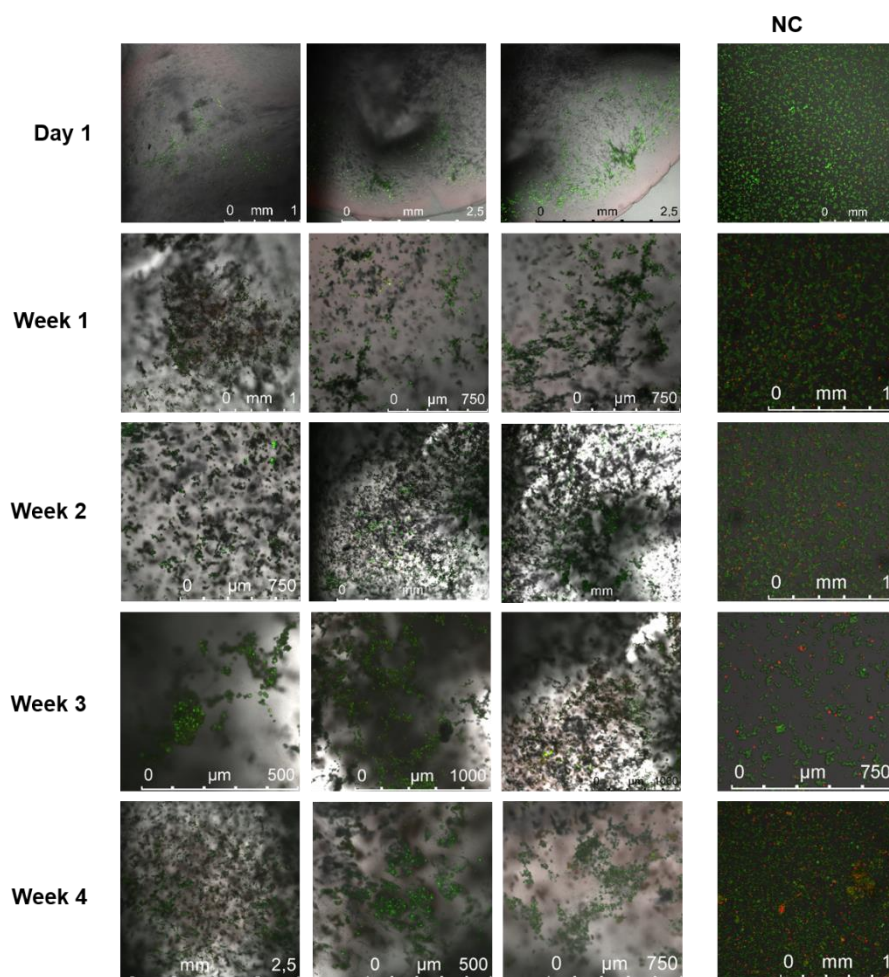


**Figure 44.** Encapsulated  $\beta$ -TC-6 cells in dPGS-based macrogel **G3** were monitored *via* confocal microscopy in a period of 31 days. Various gel regions were recorded a day after and subsequently on a weekly basis after the microfluidic entrapment of the cells. Naked  $\beta$ -TC-6 cells were used as a negative control. Excellent viabilities were observed for over 30 days in culture in bulk hydrogels **G3**. Cells appeared viable only at layers closer to the surface of the hydrogel and dead in its deeper regions. The particles bore  $1.00 \cdot 10^6$  cells and were stained with calcein AM and PI.

In general, the long-term high viabilities monitored for the various cell populations in the prepared dPGS-based bulk hydrogels indicated that not only the materials but also the applied chemistry did not impair the functional survival of this type of pancreatic cells. Contrary to the first microgels fabricated from macromonomers **P1** and **P4**, the system utilizing polymers **P5** and **P6** (dPGS-polyazide and  $\alpha, \omega$ -bis(bicyclooctyne)-PEG) is suitable for the  $\beta$ -TC-6 cells most probably due to more favorable viscoelasticity and hydrophilicity as well as the presence of negative charge. Thus, this system is highly promising for the encapsulation of other sensitive cell types or after specific modifications for its implementation in *in vivo* studies of cell-based therapies of T1D.

### 2.2.2.3 Quantitative determination of insulin secretion via ELISA

To complete the performance evaluation of the developed cell-laden hydrogels, this study included the assessment of their potential to support glucose-stimulated insulin secretion of the encapsulated  $\beta$ -TC-6 cells. Therefore, the developed cell-bearing dPGS-based bulk hydrogels as well as bare  $\beta$ -TC-6 cells seeded in separate 96-well-plates were incubated at 37 °C under 5.0 % CO<sub>2</sub> in the presence of three different glucose containing culture media (DMEM, 15 % FCS, 1 % P/S): 0, 1, and 4.5 g/L, respectively. As a negative control, pure DMEM (15 % FCS, 1 % P/S) of medium glucose content was used. After incubating under the conditions detailed in Section 2.2.2.1 of this thesis, the supernatants of each well were collected at days one and eight after encapsulation or inoculation of the  $\beta$ -TC-6 cells. Their insulin content was thereafter determined by means of a mouse insulin enzyme-linked immunosorbent assay (ELISA).

A series of solutions were prepared from each supernatant after dilution to a previously specified degree respective for naked and encapsulated cells. These as well as the provided standards were loaded on the ELISA kit and treated with the available enzyme conjugate solution. After incubation and subsequent addition of the substrate, the assay was completed upon treatment with an acidic stop solution. Thus, an enzymatically catalyzed fluorescence alteration took place, which is directly dependent on the amount of insulin present in the supernatant solutions. The optical density of the ELISA-plate was then read out at 450 nm followed by the square spline regression of the generated absorption data (Figure 46).

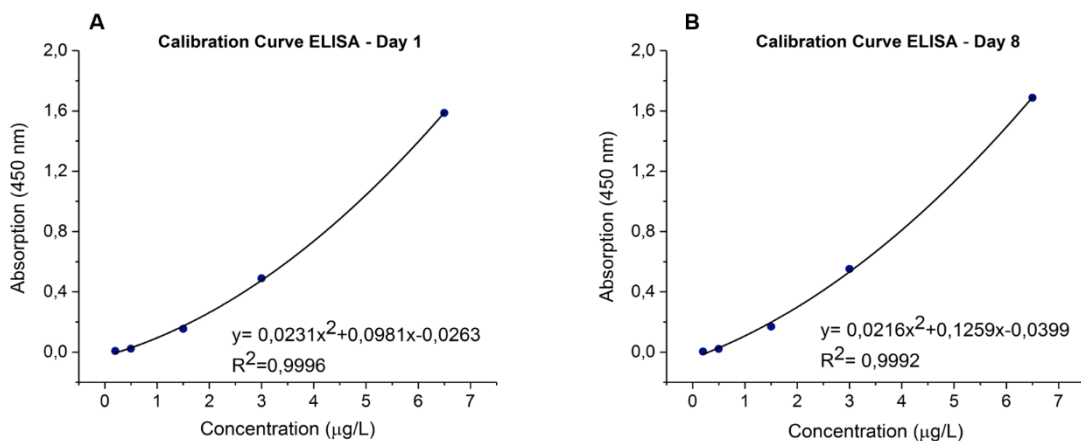


**Figure 45.** Calibration curves of conducted ELISAs on days (A) one and (B) eight of  $\beta$  TC 6 cells encapsulated in dPGS-based bulk hydrogels **G1**.

Both bare and encapsulated pancreatic  $\beta$ -cells in dPGS-hydrogels **G1** produced insulin one day after embedment as well as after eight days in culture (Figure 46), under the applied

conditions for this assay. This suggests that the hydrogel matrices did not impair the insulin secretory function of the enclosed cells. Interestingly, it appears that bare  $\beta$ -TC-6 cells produced insulin 24 hours after initiation of the investigation not only upon low and high glucose stimulus but also in the absence of the latter (34.2, 12.3, and 0.435 nM in 0, 1, and 4.5 g/L glucose, respectively). On the eighth day, the amounts of diffused hormone were significantly higher, due to its concentration in the respective wells, with the highest value (0.278  $\mu$ M) determined as expected for the highest glucose content. Nevertheless, a much higher insulin amount was detected in glucose lacking wells (0.226  $\mu$ M) than in the presence of 1 g/L glucose (0.093  $\mu$ M). This could be attributed to the origin of the selected pancreatic  $\beta$ -cells.  $\beta$ -TC-6 cells were generated from an insulinoma tumor and were thus by nature programmed to produce insulin even in the lowest available glucose concentrations. This lack of the fine sensor mechanisms with which primary, physiological pancreatic beta cells had been equipped led to a different conception of the external glucose stimuli. Additionally, as has been previously noted, this type of cell line is known for a shift in their concentration dependency curves to hypersensitivity.<sup>[188,190]</sup>

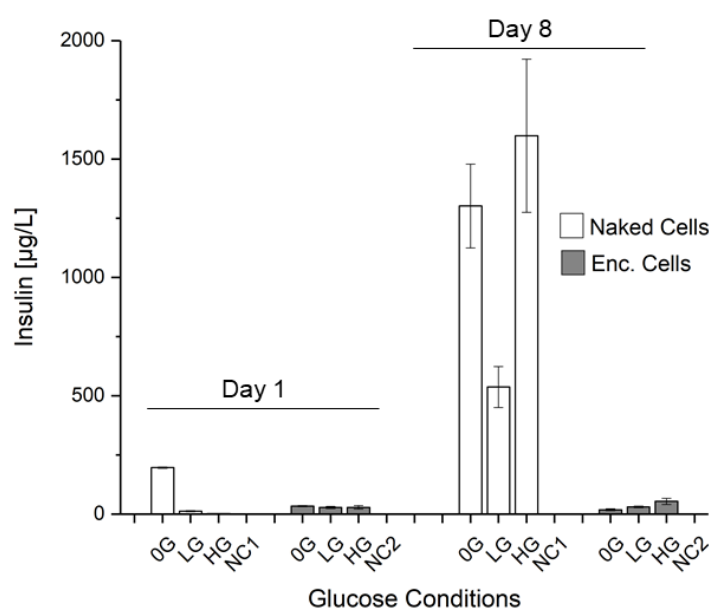


**Figure 46.** Bar diagram of glucose-stimulated insulin secretion from naked and encapsulated  $\beta$ -TC-6 cells in bulk dPGS-gels **G1**. Both naked and encapsulated cells were cultured in 0 g/L (0G), 1 g/L (1G), and 4.5 g/L (hG) glucose, respectively. The concentrations of released insulin were determined *via* ELISA on days one and eight in the two cultures. NC1 and NC2 stand for negative control 1 and 2, respectively, which was DMEM (15 % FCS, 1 % P/S) used for the naked and encapsulated cells, respectively.

The immobilized  $\beta$ -TC-6 cells in the bulk hydrogels, 24 hours after encapsulation secreted similar amounts of insulin with the naked cells (Figure 43). This finding is highly

promising for the further application of our sulfated-polyglycerol-based scaffolds as artificial 3D matrices in *in vivo* studies of therapeutic cell-transplantations. The absolute determined values did not significantly differ between 0, 1, and 4.5 g/L glucose (5.90, 4.86, 4.96 nM, respectively) which could be related to the reasons explained above. As was initially envisioned, the quantities of insulin released after eight days in culture in the hydrogel matrices, exhibited an increasing tendency at higher glucose concentrations (3.18, 5.27 and 9.31 nM in the presence of 0, 1, and 4.5 g/L glucose, respectively). However, the detected insulin amounts were much lower than the respective amounts secreted from naked  $\beta$ -TC-6 cells at the same time point. Additionally, they were not substantially higher than the corresponding ones released only one day after encapsulation. This could be associated with the presence of the surrounding polymeric matrix, which was assumed to limit the release kinetics of insulin. At this preliminary phase of their development, these hydrogels have produced very promising data for a variety of potential applications, which nonetheless entails a series of further optimizations.

### 2.2.3 Conclusions

The second part of this work presented the development of polyglycerol-based carriers of pancreatic  $\beta$ -TC-6 cells for their eventual transplantation as a potential treatment of autoimmune type 1 diabetes. The highly promising performance of the cellular vehicles, established in the first part of this study, inspired their application for immune isolation of insulin-producing  $\beta$ -cells. Therefore, microfluidic templating of droplet microreactors was employed, which allowed the bioorthogonal SPAAC of S-PG-hexaazide and dPG-poly(bicyclooctyne) in the presence of cells.

Unfortunately, most  $\beta$ -TC-6 cells were already dead 24 hours after encapsulation in the microgels. Due to the outstanding results of the applied chemistry in various biologic systems,<sup>[105–108]</sup> this finding could be only attributed to the properties of the artificial 3D scaffolds surrounding the cells. As detailed previously, the cytocompatible nature of the polymeric constituents alone did not suffice to promote long-term viabilities of the encapsulated cells. To be fully biocompatible for the enclosed cells, the fabricated matrices should have presented specific viscoelastic properties and hydrophilicity.

To achieve longevity of the embedded  $\beta$ -cells, the capsules were redesigned to bear a higher resemblance to the natural extracellular matrix supporting the pancreatic islets. Thus, the non-cytotoxic and anti-inflammatory<sup>[106,193]</sup> sulfated dPG-polyazide (dPGS-polyazide) was implemented in this approach to simulate the negatively charged proteoglycans of the targeted physiological ECM.<sup>[191,192]</sup> Additionally, cytocompatible, homobifunctional linear PEG bearing bicyclooctyne moieties at both its ends ( $\alpha, \omega$ -bis(bicyclooctyne)-PEG) was the utilized cross-linker chosen on grounds of PEG's highly advantageous properties as a biomaterial and especially due to its slightly lower hydrophilicity compared to polyglycerol.

The microfluidic templating of these two polymer precursors proceeded with exquisite control over the sizes and shapes of the produced cell-laden microgels, which were highly monodisperse and stable. Their observed durability could be related to the presence of carbamate functionalities at focal points of their networks. The majority of immobilized cells remained viable longer than four weeks as evidenced *via* confocal microscopy imaging. Nevertheless, at the beginning of the fifth week in culture, only poor staining of the cell-bearing microgels and subsequent monitoring was possible. This as well as the opaque appearance of the collected micrometer-sized beads, most probably signified an extended deposition of ECM-macromolecules and eventual clogging of the particles' pores. Furthermore, the lack of a way to accurately determine the number of enclosed cells in each microcapsule substantially limited the outlined strategy. The natural tendency of  $\beta$ -TC-6 cells

to form aggregates and the non-degradable, immune-isolating character of the developed microgels hindered the quantification of cell masses *via* conventional or immune staining. As a result, this approach could not support the assessment of potential cell proliferation or functional survival through appraisal of secreted insulin.

To circumvent these limitations, dPGS-polyazide and  $\alpha, \omega$ -bis(bicyclooctyne)-PEG were utilized to construct bulk hydrogels as artificial 3D matrices for  $\beta$ -TC-6. For comparison purposes, these scaffolds had the same composition as their micrometer-sized counterparts and bore a defined number of pancreatic  $\beta$ -cells. Three such immune-isolating carriers were developed to enclose a low ( $4.00 \cdot 10^4$ ), a medium, ( $1.00 \cdot 10^5$ ) and a high ( $1.00 \cdot 10^6$ ) cell population, respectively. Already 24 hours after gel development the embedded cells adapted to the surrounding matrices by forming aggregates, which was a natural tendency observed in their 2D cultures. This behavior constituted a first positive outcome pointing to the superior biocompatibility of the dPGS bulk hydrogels.

Exceptional viabilities for four weeks were observed in the confocal images of all encapsulated  $\beta$ -TC-6 cells. The low and medium cell masses appeared to be vital in all documented regions in the corresponding dPGS hydrogels. On the contrary, throughout the duration of this study,  $\beta$ -TC-6 cells remained viable in the most densely populated dPGS gel at the surface layers but not in the cores of their aggregates. This behavior indicated an insufficient supply of nutrients and oxygen and highlighted the capacity limits of these cell carriers. In general, in order to promote long-term functional survival of the encased cells, the designed dPGS hydrogels should be improved to meet the requirements as islet transplantation devices, especially regarding the detailed space limitations of all animal models in *in vivo* studies. As such, the potential optimizations of the scaffolds should support a large cell mass in a confined site in the host.<sup>[185,186]</sup>

The insulin secretory function of the enclosed pancreatic  $\beta$ -cells was evaluated through the related mouse enzyme-linked immunosorbent assay. The hormone release was quantified both prior to as well as on days one and eight post encapsulation in the dPGS bulk hydrogels bearing the lowest number of cells. The applied assay conditions were designed to mimic the physiological insulin release in the cases of low and high blood glucose concentrations. The cellular behavior was also investigated in the presence of no glucose. After one day in culture, both naked and encapsulated cells were found to diffuse similar amounts of insulin, which is significant evidence for the exquisite biocompatibility of dPGS-based cellular vehicles. Nevertheless, this trend was not concluded after eight days in culture. As expected, bare cells had produced in this time period substantial amounts of insulin, which were not observed for

encased pancreatic cells. It was thus assumed that the hydrogel network surrounding the cells compromised the release kinetics of the hormone. Moreover, there were no notable differences in the quantified insulin at low or high glucose concentration neither for naked nor for encapsulated  $\beta$ -cells. Interestingly, large insulin quantities were also detected in the absence of a glucose stimulus. These findings could be attributed to the tumorous origin of the cells, which is responsible for a hypersensitivity towards scarce amounts of glucose in their microenvironments.

Overall, this study has demonstrated the potential to immune-isolate pancreatic cells in artificial 3D dPGS scaffolds of either micrometer sizes generated *via* microfluidic templating or of higher dimensions present in bulk hydrogels. Both synthetic extracellular matrices were designed to serve as devices for potential islet transplantation strategies towards the treatment of T1D. The biocompatibility of the dPGS-based cell carriers was determined for both micrometer-sized and bulk gel particles. The established insulin secretion prior to and post encapsulation in bulk gels augments the exceptional documented cellular viabilities and holds great promise for their application in *in vivo* studies of islet transplantation. Nevertheless, future efforts should focus on considerably optimizing the properties of the developed enclosing systems to support even longer graft lifetimes. A potential modification could be the introduction of amino-acid sequences, such as RGD<sup>[140]</sup> or IKVAV,<sup>[185]</sup> in the polymeric networks to promote cell adhesion and eventually extended long-term viabilities. Further improvements could include routes to the accurate determination of cell masses enveloped in microgels as well as procedures that would allow an exact appraisal of the viscoelastic features of the produced encapsulating systems. Additionally, to properly define the influence of the hydrogel networks on the release of insulin, the developed enclosing systems should be applied for primary pancreatic  $\beta$ -cells, which would respond with their fine sensory mechanisms to glucose stimuli different from the employed tumor-isolated cells.

## 2.3 Summary

### Abstract

Cell encapsulation is a very promising therapeutic strategy for the controlled and sustained delivery of biologically relevant agents. This thesis has contributed to the field with the bioorthogonal, microfluidic templating of cell-laden polyglycerol-based matrices. The latter were constructed *via* strain-promoted alkyne-azide cycloaddition of the newly synthesized azide-functionalized star-shaped polyglycerol and dendritic polyglycerol (dPG) with cyclooctyne moieties tethered on its surface. Linear polyglycerol as well as polyethylene glycol (PEG) bearing both azides at their ends were also utilized to fabricate overall three types of artificial 3D matrices that enclosed fibroblast cells. By varying the implemented polymeric materials, specific properties were introduced to each system that resulted in different viability profiles of the encased cells. A type of microgel scaffolds was distinguished, in which cells were cultured that retained full viability extending to three weeks. As a result, these polyglycerol-particles could be used for long-term immobilization of cells with the possibility to be studied and manipulated during encapsulation.

The established dPG-microgels were also used to immune-isolate pancreatic  $\beta$ -cells for islet transplantation as a treatment of type 1 diabetes. Due to the poor cell viabilities detected already one day after embedment the cellular vehicles were redesigned to bear a higher resemblance to the physiological extracellular matrix of pancreatic islets. Therefore, negatively charged sulfated dPG-polyazide (dPGS-polyazide) as well as homobifunctional PEG with cyclooctynes at its ends ( $\alpha$ ,  $\omega$ -bis(bicyclooctyne)-PEG) were employed for the generation of both microgels and bulk hydrogels as encapsulation systems. Whether at a range of micrometer sizes or in bulk the dPGS-based hydrogel scaffolds presented highly biocompatible environments to the enclosed pancreatic  $\beta$ -cells. These remained vital exceeding one month of culture in the gels. The determined insulin secretion prior to and post encapsulation in bulk gels augments the exceptional documented cellular viabilities and holds great promise for their application in *in vivo* studies of islet transplantation.

On the whole, the developed gels present significant potential not only for cell immobilization but also for enveloping and *de novo* release of various therapeutic, biologic payloads such as drugs, proteins, and even genetic material. Dendritic polyglycerols constitute outstanding candidates for these applications due to their globally favorable properties as well as their amenability to a series of modifications that could optimize the gels' performance and support even longer graft lifetimes.

## Kurzzusammenfassung

Die Zellverkapselung ist eine vielversprechende therapeutische Strategie für die kontrollierte und nachhaltige Freisetzung von biologisch aktiven Substanzen. Die vorliegende Arbeit beschäftigt sich mit der bioorthogonalen mikrofluidischen Herstellung zellbeladener Polyglycerinkapseln und deren Evaluierung in biologisch relevanten Systemen. Der Tröpfchenbasierte Aufbau der Kapseln wird durch eine Alkin-Azid-Zykloadditionsreaktion, zwischen einem erstmalig beschriebenen Azid funktionalisierten sternförmigen Polyglycerin und einem mit Cyclooctin-Einheiten dekoriertem dendritischem Polyglycerin (dPG), durchgeführt. Des Weiteren wurde mit Aziden funktionalisiert lineares Polyglycerin sowie Polyethylenglykol (PEG) verwendet um insgesamt drei Arten künstlicher 3D-Matrizen zu synthetisieren mit denen Fibroblasten verkapselt wurden. Durch Variation der verwendeten Polymere wurden spezifische Eigenschaften in jedes System eingeführt, die zu unterschiedlichen Zellviabilitäten führten. Es wurden Mikrogele identifiziert in denen die kultivierten Zellen eine volle Lebensfähigkeit von bis zu drei Wochen aufwiesen. Die generierten Mikrogele eignen sich für die Langzeitimmobilisierung von Zellen, wobei sich die Zellen während der Verkapselung studieren und manipulieren lassen.

Die etablierten dPG-Mikrogele wurden daraufhin zur Immunisolierung von Pankreas- $\beta$ -Zellen verwendet, dass einen vielversprechenden Ansatz zur Therapie von Typ-1-Diabetes darstellt. Wegen der schlechten Zellüberlebensraten, die bereits einen Tag nach der Einbettung festgestellt wurden, wurden die Polymere neugestaltet, um eine höhere Ähnlichkeit mit der physiologischen extrazellulären Matrix von Pankreasinseln aufzuweisen. Daher wurde negativ geladenes sulfatiertes dPG-Polyazid (dPGS-polyazid) sowie homobifunktionelles PEG mit Cyclooctinen an seinen Enden ( $\alpha, \omega$ -bis(bicyclooctyn)-PEG) zur Erzeugung von beiden Mikro- und Makrogelen als Verkapselungssysteme eingesetzt. Ob im Mikrometer- oder Makrometerbereich, boten die dPGS-basierten Hydrogelgerüste den eingeschlossenen pankreatischen  $\beta$ -Zellen hoch biokompatible Umgebungen an. Die Zellen blieben vital über einen Monat in Kultur. Die ermittelte Insulinsekretion der Zellen vor und nach der Verkapselung in dPGS Makrogelen ergänzt die außergewöhnlich dokumentierten zellulären Viabilitäten und ist vielversprechend für ihre Anwendung für *in vivo* Studien der Inseltransplantation.

Insgesamt können sich die entwickelten Gele nicht nur für die Zellimmobilisierung eignen, sondern auch für die Umhüllung und die *de novo* Freisetzung von verschiedenen therapeutischen, biologischen Ladungen wie Medikamenten, Proteinen und sogar genetischem Material. Dendritische Polyglycerine stellen aufgrund ihrer inhärenten

günstigen Eigenschaften hervorragende Kandidaten für diese Anwendungen dar. Darüber hinaus weisen sie sich durch eine exzellente Modifizierbarkeit aus, die die Leistung der Gele optimieren und sogar noch längere Transplantatlebensdauer unterstützen könnten.

### 3 Experimental

#### 3.1 Materials and methods

##### 3.1.1 Reagents

Reagent grade chemicals and anhydrous solvents (dimethylformamide (DMF), dimethyl sulfoxide (DMSO), pyridine and toluene) were purchased from Sigma-Aldrich (Darmstadt, Germany) and ThermoFisher Scientific (Darmstadt, Germany) respectively and used without further purification. 1*H*, 1*H*, 2*H*, 2*H*-perfluoro-1-octanol (Sigma Aldrich, Darmstadt, Germany), 1*H*, 1*H*, 2*H*, 2*H*-perfluorooctyltriethoxysilane (Sigma Aldrich, Darmstadt, Germany), OptiPrep™ (Sigma Aldrich, Darmstadt, Germany), Sylgard® 184 Silicon Elastomer Kit (Dow Corning, Michigan, USA), Novec™ 7100 (3M™, Neuss, Germany),  $\alpha,\omega$ -bis-amino PEG<sub>600</sub> (Huntsman Corporation, Hamburg, Germany), Krytox® 157FS(H) (DuPont™, Hamm, Germany),  $\alpha,\omega$ -bis-bromo-PEG 6000 (Rapp POLYMERE, Tübingen, Germany), Ultracel regenerated cellulose membranes (MWCO = 5000 g mol<sup>-1</sup>, Millipore, Darmstadt, Germany), Spectra/Por® dialysis tubings (MWCO = 2000, 1000, 500 g mol<sup>-1</sup>, Carl Roth GmbH, Karlsruhe, Germany) NIH/3T3 (ATCC® CRL-1658™) mouse fibroblast cells NIH/3T3 (ATCC LGC Standards, Wesel, Germany), mouse insulinoma cells  $\beta$ -TC-6 (ATCC LGC Standards, Wesel, Germany), Dulbecco's Modified Eagle Medium (DMEM) containing 1 (low glucose, lG) or 4.5 g/L glucose (high Glucose, hG), L-Glutamine and phenol red (ThermoFisher Scientific, Darmstadt, Germany), DPBS (ThermoFisher Scientific, Darmstadt, Germany), Cell Counting Kit-8 (CCK-8, Sigma-Aldrich, Darmstadt, Germany), LIVE/DEAD™ Viability/Cytotoxicity Kit for mammalian cells (ThermoFisher Scientific, Darmstadt, Germany), Mercodia mouse insulin ELISA kit (Mercodia AB, Uppsala, Sweden), microscope glass slides (ThermoFisher Scientific, Darmstadt, Germany) were used as received. Ethoxy ethyl glycidyl ether (EEGE),<sup>[115]</sup> bicyclo[6.1.0]non-4-yn-9ylmethyl(4-nitrophenyl)carbonate (BCN)<sup>[125]</sup> as well as the surfactant<sup>[194]</sup> used for the droplet-based microfluidic templating were synthesized in our group based on already known procedures.

##### 3.1.2 Measurements

All moisture sensitive reactions were performed in flame-dried glassware under a positive argon pressure. Organic solvents were removed using a rotary evaporator, which is referred as concentrated *in vacuo*. <sup>1</sup>H NMR and <sup>13</sup>C NMR spectra were recorded on an ECX400 (Jeol Ltd, Tokyo, Japan), an AMX 500 (Bruker, Fällanden, Switzerland) and a Bruker AVANCE

III 700 (Bruker, Massachusetts, USA) spectrometer. NMR chemical shifts were reported as  $\delta$  values in ppm and were referenced to the indicated solvents: deuterated water ( $D_2O$ ), deuterated acetone (Acetone- $d_6$ ), deuterated methanol (MeOH- $d_4$ ), and deuterated chloroform ( $CDCl_3$ ). NMR data were reported as follows: chemical shift, multiplicity (s = singlet, d = doublet, t = triplet, m = multiplet, br = broad), coupling constants in Hertz (Hz) and integration. Multiplets (m) were reported over the range (ppm) at which they appear at the indicated field strength. Infrared spectra were obtained using a JASCO FTIR-4100 spectrophotometer (JASCO Inc, Gross-Umstadt, Germany), which was equipped with a PIKE diamond (PIKE Technologies Fitchburg, USA). The vibration bands were reported as  $\nu$  values in  $cm^{-1}$  (w = wide, s = sharp). Confocal laser scanning microscopy (cLSM) was performed with a Leica TCS SP8 microscope (Leica, Mannheim, Germany), using a 5x objective and the Argon laser with wavelengths of 488 and 514 nm, as set by the AOBs® beam splitter software (Leica, Mannheim, Germany). Analysis of the images was performed with the Leica Application Suite X software (Leica, Mannheim, Germany). Optical density was measured using a Tecan Infinite® 200PRO (Tecan Trading AG, Männedorf, Switzerland) plate reader, which was equipped with a Tecan i-control software (Tecan Trading AG, Männedorf, Switzerland) for the data acquisition.

Gel permeation chromatography was performed using an Agilent HPLC system with a G1362A refractive index detector, a G1310A IsoPump and a G1328B manual injection unit (Agilent 1100 Series, PSS, Mainz, Germany) and a system of three Suprema size exclusion columns (modified acrylacto polymer network with a porosity of 100, 1000 and 3000 Å respectively, dimensions of 8 x 300 mm, particle size of 10  $\mu m$  from PSS, Mainz, Germany) for the water-soluble polymers. For the latter the mobile phase consisted of ultrapure water with 0.1 M  $NaNO_3$  p.a. in a flow rate of 1 mL/min. Samples were prepared at a concentration of 3.5 mg/mL in the running buffer and were filtered using CA- or PA-filters (0.2  $\mu m$ , from VWR, Darmstadt, Germany) prior to the measurement. GPC traces of the synthesized polymers are shown in Schemes 25 and 26. For the non-water-soluble samples the same GPC-facility was used but with a G1328C manual injection unit (Agilent 1260 Infinity, PSS, Mainz, Germany) with three linear size exclusion columns (PLgel, a highly crosslinked, porous polystyrene/divinylbenzene matrix, with dimensions of 7.5 x 300 mm and particle size of 5  $\mu m$ , Agilent, Santa Clara, CA). Tetrahydrofuran for HPLC, 0.2  $\mu m$  filtered, non-stabilized was employed as the mobile phase with a flow rate of 1 mL/min. Samples were prepared at a concentration of 3.5 mg/mL in the running buffer and were filtered using PTFE-filters (0.2  $\mu m$ , from VWR, Darmstadt, Germany) prior to the analysis. Molecular weights

were calculated using the WinGPC software (PSS, Mainz, Germany). A calibration curve was obtained using narrow pullulan (342 to 708000 Da) or polystyrene (474 to 2520000 Da) for the aqueous and non-aqueous samples respectively.

## 3.2 Synthesis

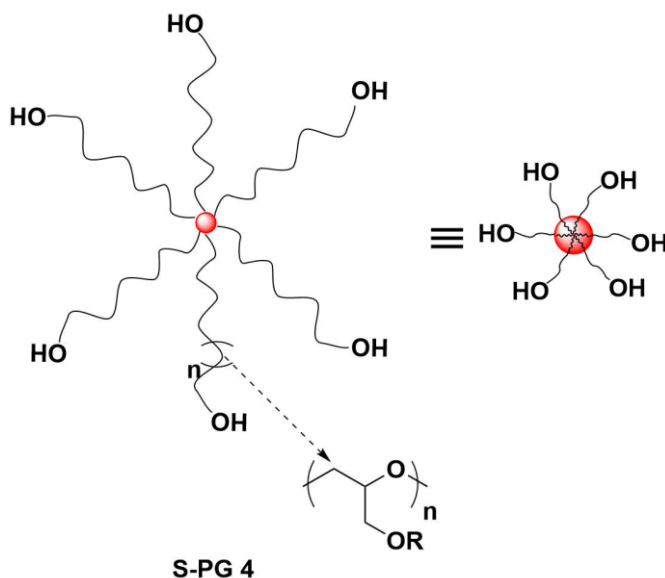
### 3.2.1 Synthesis of ethoxyethyl glycidyl ether EEGE 5



Glycidol (50.0 mL, 0.771 mol, 1.00 equiv.) was added to ethyl vinyl ether (295 mL, 3.08 mol, 4.00 equiv.) and the resulting mixture was cooled down to 0 °C. Subsequently, slow, portionwise addition of *p*-TsOH (1.47 g, 7.71 mmol, 0.01 equiv.) under vigorous stirring followed during which, the temperature in the reaction mixture was maintained at 10 °C. Upon completion of this addition, the reaction mixture was allowed to gradually warm up to room temperature whereby, it stirred for 4 hours. Thereafter, the reaction was quenched by the addition of a saturated NaHCO<sub>3</sub> aqueous solution (75 mL). The organic layer was extracted with NaHCO<sub>3</sub>, dried over Na<sub>2</sub>SO<sub>4</sub>, filtered and the solvent was removed *in vacuo*. The obtained crude product was further dried over CaH<sub>2</sub> and distilled under high vacuum. The desired product was isolated, as a colorless liquid at 40 °C, purged with Ar and stored over CaH<sub>2</sub>. Due to its storage under fully inert conditions, it was not possible to weigh the final product and a complete conversion of the starting material was assumed.

<sup>1</sup>H NMR (400 MHz, CDCl<sub>3</sub>,  $\delta$  (ppm)) 4.41 (t, J = 6.5, 1H), 3.42 (m, 1H), 3.34 - 3.26 (m, 1H), 3.21 - 3.10 (m, 2H), 3.05 (dd, J = 11.5, 6.1, 1H), 2.78 (m, 1H), 2.43 (dd, J = 5.1, 4.1, 1H), 2.26 (m, 1H), 0.97 (t, J = 6.4, 3H), 0.86 (t, J = 7.1, 3H).

### 3.2.2 Synthesis of six-arm-star-shaped polyglycidol S-PG 4



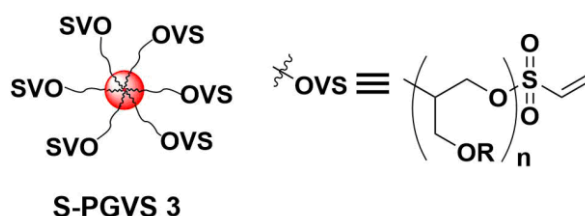
Dipentaerythritol (**6**, 236 mg, 0.928 mmol, 1.00 equiv.) was dried under vacuum at 60 °C for 2 hours, it was allowed to cool down to room temperature and dissolved in DMSO (60.0 mL). Thereafter, KO<sup>t</sup>Bu (557 μL of a 1.0 M THF solution, 0.557 mmol, 0.100, equiv. per hydroxy-group) was added slowly, dropwise under an Argon atmosphere and vigorous stirring. The resulting mixture was thereby, stirred for 20 minutes after which, the formed <sup>t</sup>BuOH was removed under high vacuum. The obtained solution was then heated to 60 °C, EEGE (**5**, 10.0 mL, 66.8 mmol, 72.0 equiv.) was added under vigorous stirring. The resulting reaction mixture was stirred at 60 °C under Argon for 5 days. The reaction was terminated by the addition of a few drops of EtOH. The resulting mixture was dissolved in DCM and washed twice with saturated NaHCO<sub>3</sub> (20.0 mL). The collected organic phases were dried over Na<sub>2</sub>SO<sub>4</sub>, filtered and the solvents were removed *in vacuo*. The obtained crude product was dissolved in MeOH and purified *via* ultrafiltration for 3 days with addition of fresh MeOH every 30 minutes. The desired product was isolated as a highly viscous, dark yellow oil in 69 % yield (7.00g,  $M_n = 11695 \text{ g mol}^{-1}$ ).

<sup>1</sup>H NMR (500 MHz, MeOH-d<sub>4</sub>, δ (ppm)): 1.21 - 1.31 (m, 6H), 3.52 - 3.70 (m, 7H), 4.75 (d, 1H).

<sup>13</sup>C NMR (500MHz, MeOH-d<sub>4</sub>, δ (ppm)): 14.6 (40C, CH<sub>3</sub>), 19.1 (40C, CH<sub>3</sub>); 45.7 (1C, C<sub>initiator</sub>), 60.7 (40C, CH<sub>2</sub>), 65.0 (39C, CH<sub>2</sub>), 70.4 (40C, CH<sub>2</sub>), 71.7 (4C, CH<sub>2, end group</sub>) 78.9 (37C, CH<sub>2</sub>), 99.9 (40C, CH). The number average molecular weight as calculated through

integration of the inverse gated  $^{13}\text{C}$  NMR spectrum amounted to approximately:  $11695 \text{ g mol}^{-1}$ .  
 $^1\text{H}$  GPC (THF):  $M_n = 7767$ ,  $M_w = 8025$ , PDI = 1.03.

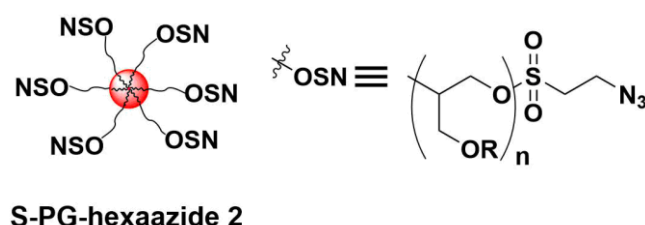
### 3.2.3 Synthesis of six-arm-star-shaped polyglycidol-hexavinyl sulfonate S-PGVS 3



S-PG **4** (3.67 g, 0.314 mmol, 1.00 equiv.) dissolved in DCM (35.0 mL) was cooled down to  $0\text{ }^\circ\text{C}$ ,  $\text{Et}_3\text{N}$  (1.05 mL, 7.54 mmol, 24.0 equiv.) was added in one portion and the resulting mixture was stirred for 10 minutes. Subsequently, 2-chloroethylsulfonyl chloride (0.39 mL, 3.77 mmol, 12.0 equiv.) was slowly added dropwise under vigorous stirring. The reaction mixture was stirred 15 minutes at  $0\text{ }^\circ\text{C}$  and then at room temperature for 1 hour. The reaction was stopped by addition of a saturated  $\text{NaHCO}_3$  aqueous solution (5.00 mL). The resulting mixture was extracted from DCM (3 x 20.0 mL) and washed with distilled  $\text{H}_2\text{O}$  (2 x 20.0 mL) and a saturated  $\text{NaHCO}_3$  solution (2 x 20.0 mL). The collected organic phases were dried over  $\text{Na}_2\text{SO}_4$ , filtered and the solvents were removed *in vacuo*, affording the name-product as a brown, viscous oil in a quantitative yield (3.67 g).

$^1\text{H}$  NMR (400 MHz, Acetone- $d_6$ ,  $\delta$  (ppm)): 1.13 - 1.24 (m, 6H), 3.46 - 3.65 (m, 7H), 4.70 (s, 1H), 6.17 (s, 0.1H), 6.34 (s, 0.1H), 6.89 (s, 0.1H).

### 3.2.4 Synthesis of six-arm-star-shaped polyglycidol hexaazide S-PG-hexaazide 2



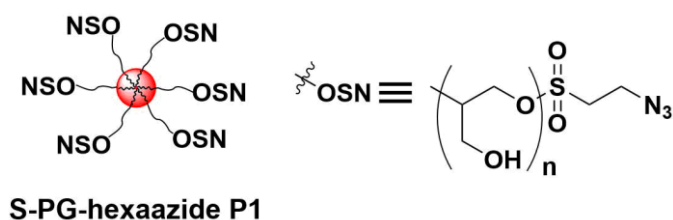
A solution of vinylsulfone **3** (3.67 g, 0.314 mmol, 1.00 equiv.) in DMF (35.0 mL) was heated to  $120\text{ }^\circ\text{C}$  whereby  $\text{NaN}_3$  (612 mg, 9.42 mmol, 30.0 equiv.) was added in one portion under vigorous stirring and the resulting reaction mixture was stirred for 4 hours under reflux and

an argon atmosphere. It was then cooled down to 60 °C and continued stirring overnight. The obtained crude product was purified *via* dialysis against MeOH for 3 days with a frequent exchange of the dialysate (2 times a day). The solvent was removed *in vacuo* affording the desired product as a yellow viscous oil in 90 % yield (3.32 g).

$^1\text{H}$  NMR (400 MHz, Acetone- $d_6$ ,  $\delta$  (ppm)): 1.14 - 1.23 (m, 6H), 3.46 - 3.66 (m, 7H), 4.70 (s, 1H).

IR (Dry film):  $\nu = 2976, 2874, 2360, 2342, 2100$  ( $\text{N}_3$ ), 1715, 1682, 1444, 1379, 1339, 1299, 1271, 1219, 1130, 1081, 1053, 998, 945, 929, 874, 667  $\text{cm}^{-1}$ .

### 3.2.5 Synthesis of six-arm-star-shaped polyglycidol hexaazide S-PG-hexaazide P1



S-PG-hexaazide **2** (3.32 g, 0.284 mmol, 1.00 equiv.) was dissolved in EtOH (35.0 mL) and treated with  $\text{HCl}_{\text{conc}}$ . (37 wt %, 17.6 mL) at room temperature and stirred overnight. The deprotected polymer was purified *via* dialysis against distilled water for 3 days with an exchange of the dialysate every 8 hours. The solvent was removed *via* freeze drying giving the name product (yield = 1.22 g, 87 %). as a highly viscous oil.

$^1\text{H}$  NMR (500 MHz,  $\text{D}_2\text{O}$ ,  $\delta$  (ppm)): 3.36 – 3.73 (m, 5H);

$^{13}\text{C}$  NMR (500 MHz,  $\text{D}_2\text{O}$ ,  $\delta$  (ppm)): 45.7 (2C,  $\text{C}_{\text{initiator}}$ ), 60.9 - 61.4 (101C), 62.7 (5C), 62.9 (5C), 68.9 - 69.4 (89C), 70.4 (5C), 70.9 (19C), 79.7 - 80.1 (89C).

IR (Dry film):  $\nu = 3348$  (w), 2925 (s), 2876 (s), 2359 (s), 2341 (s), 2110 (s,  $\text{N}_3$ ), 1650 (w), 1458 (s), 1407 (s), 1346 (s), 1303 (s), 1260 (s), 1037 (w), 914 (s), 839 (w)  $\text{cm}^{-1}$ .

GPC ( $\text{H}_2\text{O}$ ):  $M_n = 4919 \text{ g mol}^{-1}$ ,  $M_w = 5443 \text{ g mol}^{-1}$ , PDI = 1.10.

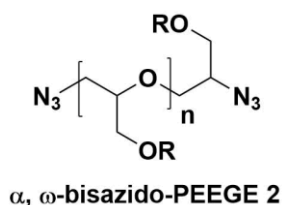


equiv.) was added slowly, dropwise under vigorous stirring and the reaction mixture stirred initially at 0 °C and then at room temperature for 16 hours. The obtained crude product was purified *via* dialysis against distilled acetone for 3 days with a frequent exchange of the dialysate (twice a day). *In vacuo* removal of the solvent gave the name product as a slightly yellow, viscous oil in 86 % yield (8.23 g).

<sup>1</sup>H NMR (400 MHz, CDCl<sub>3</sub>, δ (ppm)): 1.15 - 1.19 (t, 3H), 1.26 - 1.27 (d, 3H), 3.42 - 3.66 (m, 7H), 4.67 (d, 1H).

<sup>13</sup>C NMR (500 MHz, CDCl<sub>3</sub>, δ (ppm)): 15.4, 19.9, 60.9, 64.9, 70.2, 85.5, 99.8.

### 3.2.8 Synthesis of linear α, ω-bisazido-poly(ethoxyethyl glycidyl ether) (α, ω-bisazido-PEEGE 2)

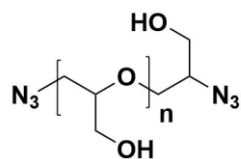


PEEGE 3 (8.23 g, 0.735 mmol, 1.00 equiv.) was dissolved in DMF (50.0 mL) and heated to 80 °C. NaN<sub>3</sub> (239 mg, 3.68 mmol, 5.00 equiv.) was added in one portion and the resulting mixture was refluxed 72 hours. The excess of NaN<sub>3</sub> was filtered and the obtained crude product was purified *via* dialysis against MeOH for 3 days with a frequent exchange of the dialysate (twice a day). *In vacuo* removal of the solvent resulted in the isolation of the name product as a yellow, viscous oil with 97 % yield (8.00 g).

<sup>1</sup>H NMR (400 MHz, CDCl<sub>3</sub>, δ (ppm)): 1.16 - 1.19 (m, 3H), 1.27 - 1.28 (m, 3H), 3.45 - 3.63 (m, 7H), 4.68 (m, 1H).

IR (Dry film):  $\nu = 2975$  (s), 2874 (s), 2100 (s, N<sub>3</sub>), 1444 (w), 1379 (s), 1299 (w), 1130 (s), 1080 (s), 1053 (s), 998 (s), 945 (s), 929 (s), 874 (w), 731 (s), 665 (w) cm<sup>-1</sup>.

### 3.2.9 Synthesis of linear $\alpha,\omega$ -bis-azido-PG ( $\alpha,\omega$ -bis-azido-IPG P2)



$\alpha, \omega$ - bis azido-IPG P2

PEEGE **2** (8.00 g, 0.715 mmol, 1.00 equiv.) was dissolved in EtOH (50.0 mL) at room temperature whereby,  $\text{HCl}_{\text{conc.}}$  (37 wt %, 3.43 mL) was added in one portion and the resulting mixture was vigorously stirred overnight. The obtained crude product was purified *via* dialysis against distilled  $\text{H}_2\text{O}$  for 3 days with a frequent exchange of the dialysate (twice a day). The solvent was removed *via* freeze drying affording the name product as a pale yellow, viscous oil (yield = 4.09 g, 83 %).

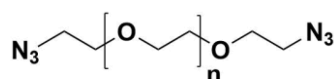
$^1\text{H}$  NMR (400 MHz,  $\text{D}_2\text{O}$ ,  $\delta$  (ppm)): 3.46 - 3.64 (m, 463H).

$^{13}\text{C}$  NMR (500 MHz,  $\text{D}_2\text{O}$ ,  $\delta$  (ppm)): 60.7, 68.7, 79.7.

IR (Dry film):  $\nu = 3348$  (w), 2923 (s), 2876 (s), 2101 (s,  $\text{N}_3$ ), 1648 (w), 1459 (s), 1407 (s), 1345 (s), 1038 (s), 915 (s), 836 (w), 651(w)  $\text{cm}^{-1}$ .

GPC ( $\text{H}_2\text{O}$ ):  $M_n = 4919 \text{ g mol}^{-1}$ ,  $M_w = 5443 \text{ g mol}^{-1}$ , PDI = 1.10.

### 3.2.10 Synthesis of linear $\alpha,\omega$ -bis-azido-PEG P3



$\alpha, \omega$ - bis azido-PEG P3

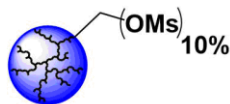
Homobifunctional  $\alpha,\omega$ -bis-bromo-PEG with a  $M_n$  of 6000  $\text{g mol}^{-1}$  (750 mg, 0.123 mmol, 1.00 equiv.) was dissolved in DMF (10.0 mL) and heated to 120  $^\circ\text{C}$  and  $\text{NaN}_3$  (80.0 mg, 1.23 mmol, 10.0 eq) was added in one portion under vigorous stirring. The resulting reaction mixture was refluxed for 4 hours under argon flow, then cooled down to 60  $^\circ\text{C}$ , and stirred overnight. The obtained crude product was purified *via* dialysis against water for 3 days with a frequent exchange of the dialysate (twice a day). The solvent was removed *via* freeze drying giving the title compound (yield = 693 mg, 92 %) as a white non-crystalline solid.

$^1\text{H}$  NMR (700 MHz,  $\text{D}_2\text{O}$ ,  $\delta$  (ppm)): 3.44 (s, 1H), 3.64 (s, 151H), 4.70 (s, 14H).

$^{13}\text{C}$  NMR (700 MHz,  $\text{D}_2\text{O}$ ,  $\delta$  (ppm)): 50.2, 69.6.

IR (Dry film):  $\nu = 2881$  (s), 2101 (s,  $\text{N}_3$ ), 1960 (w), 1463 (s), 1341 (s), 1279 (s), 1147 (s), 1095 (s), 1062 (s), 958 (s), 840 (s)  $\text{cm}^{-1}$ .

### 3.2.11 Synthesis of dPG-polymesylate 4

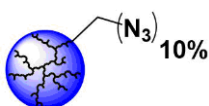


**dPG-polymesylate 4**

dPG **5** with an  $M_n$  of  $10000 \text{ g mol}^{-1}$  (5.52 g, 0.552 mmol, 7.46 mmol hydroxy-groups, 1.00 equiv.) was dissolved in pyridine (50.0 mL), cooled down to  $0 \text{ }^\circ\text{C}$  and MsCl (693  $\mu\text{L}$ , 8.95 mmol, 1.20 equiv. to hydroxy-groups) was added dropwise. The resulting reaction mixture was stirred twenty minutes at  $0 \text{ }^\circ\text{C}$  and then at room temperature overnight under an argon atmosphere. The solvent was removed *in vacuo* and the obtained crude product was purified *via* dialysis for 3 days against distilled acetone, with a frequent exchange of the dialysate (twice a day). After rotary evaporation of the solvents, the name product was isolated as a yellow viscous oil (yield = 5.52 g, quantitative, 10 % degree of functionalization).

$^1\text{H NMR}$  (500 MHz,  $\text{D}_2\text{O}$ ,  $\delta$  (ppm)): 1.15 - 1.19 (0.30H), 1.46 - 2.05 (5H).

### 3.2.12 Synthesis of dPG-polyazide 3



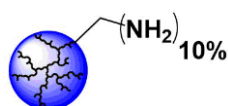
**dPG-polyazide 3**

dPG-polymesylate **4** (5.52 g, 0.552 mmol, 7.46 mmol mesyloxy-groups, 1.00 equiv.) was dissolved in DMF (50.0 mL), heated to  $120 \text{ }^\circ\text{C}$  and  $\text{NaN}_3$  (2.42 g, 37.3 mmol, 5.00 equiv. to mesyloxy-groups) was added in one portion under Ar and vigorous stirring. The reaction mixture stirred 4 hours at  $120 \text{ }^\circ\text{C}$  under reflux and then at  $60 \text{ }^\circ\text{C}$  overnight. Subsequently, the excess of  $\text{NaN}_3$  was removed by filtration and the obtained crude product was purified *via* dialysis against MeOH for 3 days, with a frequent exchange of the dialysate (twice a day). After rotary evaporation of the solvents, the name product was isolated as a yellow viscous oil (yield = 5.40 g, 98 %, 10 % degree of functionalization).

$^1\text{H}$  NMR (500 MHz,  $\text{D}_2\text{O}$ ,  $\delta$  (ppm)): 3.37 - 3.97 (5H).

IR (Dry film):  $\nu = 3357$  (w), 2872 (s), 2358 (s), 2100 (s), 1651 (w), 1455 (w), 1270 (w), 1070 (w), 1026 (w), 932 (s), 868 (s) 666 (s)  $\text{cm}^{-1}$ .

### 3.2.13 Synthesis of dPG-polyamine 2

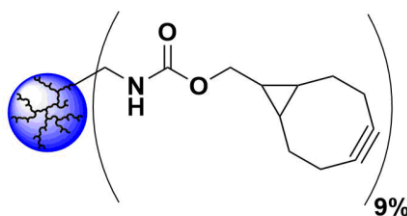


dPG-polyamine 2

To a solution of dPG-polyazide **3** (5.40 g, 0.540 mmol, 7.46 mmol azide-groups, 1.00 equiv.) in distilled  $\text{H}_2\text{O}$  (25.0 mL) a solution of  $\text{PPh}_3$  (2.54 g, 9.70 mmol, 1.30 equiv.) in THF (25.0 mL) was added at room temperature and the resulting reaction mixture was stirred for 16 hours. The formed white salt was removed by filtration. The solvents were removed *via* rotary evaporation and the obtained crude product was purified *via* dialysis against MeOH for one day with two times of dialysate exchange. It was then further dialyzed against distilled  $\text{H}_2\text{O}$  for 3 days with a frequent exchange of the dialysate (twice a day). The solvent was concentrated *in vacuo*, leaving the desired product as a pale yellow, viscous oil (yield = 3.51 g, 64 %, 10 % degree of functionalization).

$^1\text{H}$  NMR (500 MHz,  $\text{D}_2\text{O}$ ,  $\delta$  (ppm)): 3.36 - 3.96 (5H).

### 3.2.14 Synthesis of dPG-poly(bicyclooctyne) (dPG-polyC P4)



dPG-polyC P4

BCN (773 mg, 2.45 mmol, 1.50 equiv. to ammine-groups) was added to a solution of dPG-polyamine, **2** (1,49 g, 0,149 mmol, 1.63 mmol  $\text{NH}_2$ -groups, 1.00 eq) in DMF (50.0 mL) in one portion under an argon atmosphere and vigorous stirring. The resulting reaction mixture was stirred at room temperature for 1.5 hours. The obtained crude product was purified *via*

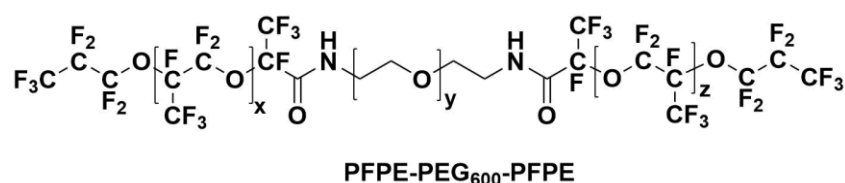
dialysis initially against MeOH and thereafter distilled H<sub>2</sub>O for two days each with a frequent exchange of the dialysate (2 times a day). The purified product (yield = 1.39 g, 93 %, 9 % cyclooctyne moieties) was stored as a pale yellow aqueous stock solution and water was removed by freeze drying only for characterization. The conversion was determined by the disappearance of the NH<sub>2</sub> signal in the <sup>1</sup>H-NMR spectrum.

<sup>1</sup>H-NMR (700 MHz, D<sub>2</sub>O,  $\delta$  (ppm)): 0.73 - 0.91 (m, 3H), 1.33 - 1.54 (m, 4H), 2.10 - 2.38 (m, 4H), 3.13 - 3.95 (m, 135H).

<sup>13</sup>C-NMR (700 MHz, D<sub>2</sub>O,  $\delta$  (ppm)): 21.2 (2C, CH of the three membered ring), 22.8, 23.6 (2C CH<sub>2</sub>-C $\equiv$ C-CH<sub>2</sub>), 29.0(2C CH<sub>2</sub>-C $\equiv$ C-CH<sub>2</sub>), 43.2 (CH of the three-membered ring), 60.9 (dPG-core), 62.7 (dPG-core), 68.9 (dPG-core), 69.2 (dPG-core), 70.5 (dPG-core), 70.7 (dPG-core), 70.9 (dPG-core), 72.2 (dPG-core), 78.1 (OCO-CH<sub>2</sub>), 79.5 (dPG-core), 99.6 (2C, C $\equiv$ C), 157.9 (1C, OCO).

BCN was kindly contributed by Anja Stöhsel.

### 3.2.15 Synthesis of surfactant KBT



The perfluorinated-triblock-copolymer-based surfactant was synthesized according to a modified procedure reported by Weitz and coworkers.<sup>[194]</sup> This product was kindly contributed by S. M. Chowdhury.

### 3.2.16 Synthesis of dPGS-polyazide P5



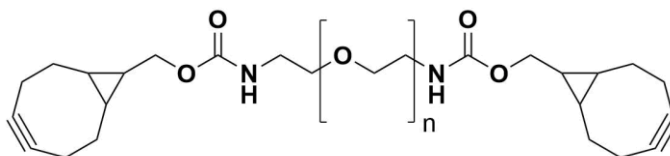
The name product was synthesized starting from a dPG with an average molecular weight of  $10000 \text{ g mol}^{-1}$ , as reported previously<sup>[106]</sup> and was kindly contributed by Dr. P. Dey.

$^1\text{H-NMR}$  (500 MHz,  $\text{D}_2\text{O}$ ,  $\delta$  (ppm)): 0.94 (s, 0.05H), 1.45 (s, 0.04H), 3.44 - 4.36 (m, 5H).

IR (Dry film):  $\nu = 2873, 2361, 2102 (\text{N}_3), 1457, 1273, 1122, 668 \text{ cm}^{-1}$ .

The Sulfur content was determined by elemental analysis (CHN) and the degree of sulfation was found to be 90 %. The degree of functionalization with azide-moieties was found to be 8 %.

### 3.2.17 Synthesis of $\alpha, \omega$ -bis(bicyclooctyne)-PEG P6



**$\alpha, \omega$ -bis(bicyclooctyne)-PEG P6**

The name product, with an average molecular weight of  $6000 \text{ g mol}^{-1}$  was synthesized as reported previously<sup>[106]</sup> and was kindly contributed by Dr. P. Dey.

$^1\text{H-NMR}$  (500 MHz,  $\text{D}_2\text{O}$ ,  $\delta$  (ppm)): 0.48 - 0.60 (m, 4H), 0.80 (s, 6H), 1.44 (m, 4H), 1.64 (s, 1H), 2.18 - 2.46 (m, 12H), 3.36 (s, 4H), 3.59 - 4.24 (m, 762H).

### **3.3 *In Vitro* studies**

#### **3.3.1 Cytotoxicity assay of NIH/3T3 cells by use of Cell Counting Kit-8 (CCK-8)**

A suspension of NIH/3T3 fibroblasts in DMEM (hG, 10 % FCS, 1 % PS) was seeded in a transparent 96 well plate with a density of  $1.00 \cdot 10^4$  cells in an overall volume of 100  $\mu$ L per well. After culture for 24 hours at 37 °C under 5.0 % CO<sub>2</sub>, 10  $\mu$ L of each solution **S1 - S3** of each polymer **P1 - P4** (Table 1, Section 2.1.2.6 of the first part of this work) were added to the respective wells and the plate was incubated for another day. Thereafter, 10  $\mu$ L of the pre-mixed CCK-8 solution, containing the proprietary WST-8 tetrazolium salt, were added to each well. Two hours after addition of the CCK-8 solution, the absorbance was read at 450 nm for samples after 24 and 72 hours, using a Tecan Infinite® 200PRO microplate reader. Three independent experimental runs were performed, which tested three triplicates per polymer solution (n = 3).

#### **3.3.2 Treatment of mammalian NIH/3T3 cells prior to microfluidic encapsulation**

A suspension of NIH/3T3 cells was prepared. Following removal of the culture medium, adherent cells were rinsed with DPBS and trypsinized to detach them from the culture flask. After centrifugation for 4 minutes at 140 RCF, the supernatant was discarded and the cell pellet was resuspended in 10 mL of fresh medium (DMEM 10 % FCS, 1 % P/S). Cells were counted in a hemacytometer and the cell density was adjusted to approximately  $1.00 \cdot 10^7$  cells mL<sup>-1</sup> by another centrifugation step and resuspension in fresh medium containing 18 vol % OptiPrep™.

#### **3.3.3 Treatment of mouse insulinoma $\beta$ -TC-6 cells prior to microfluidic encapsulation**

A suspension of pancreatic  $\beta$ -TC-6 cells was prepared as detailed above for the NIH/3T3 fibroblasts. Cells were counted in a hemacytometer and the cell density was adjusted to approximately  $7.00 \cdot 10^7$  cells mL<sup>-1</sup> by another centrifugation step and resuspension in fresh medium (DMEM 1G, 15 % FCS, 1 % P/S) containing 15 vol % OptiPrep™.

### **3.3.4 Treatment of mouse insulinoma $\beta$ -TC-6 cells prior to encapsulation in bulk hydrogels**

Following the procedure described above, three suspensions of  $\beta$ -TC-6 cells in DMEM (1G, 15 % FCS, 1 % P/S) were prepared, that contained  $6.70 \cdot 10^6$  cells mL<sup>-1</sup>,  $1.70 \cdot 10^6$  cells in 100  $\mu$ L, and  $1.70 \cdot 10^7$  cells in 100  $\mu$ L respectively.

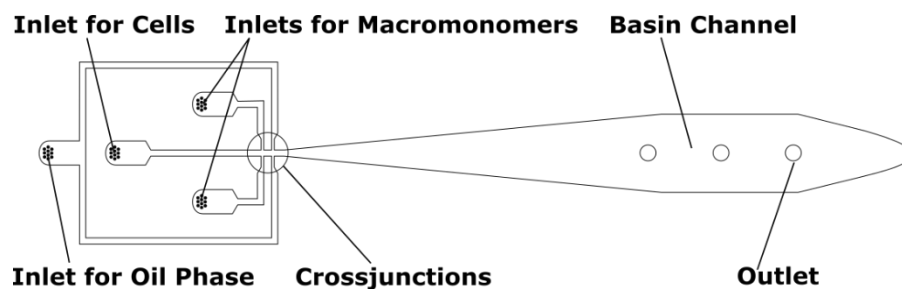
## **3.4 Microfluidic templating**

### **3.4.1 Microfluidic devices**

To produce the microfluidic devices soft lithography<sup>[195]</sup> was employed, whereby, PDMS along with cross-linker (Sylgard<sup>®</sup> 184 Silicon Elastomer Kit) were mixed in a 10:1 weight ratio and then poured onto a silicon wafer patterned with SU-8 photoresist. After degassing and solidifying the material overnight at 60 °C, PDMS replicas were obtained, which were washed with isopropanol (3 x 20.0 mL) and dried with compressed air. Thereafter, devices were fabricated by oxygen plasma bonding of the PDMS replicas onto glass slides. To render the devices hydrophobic, and hence, suitable for water-in-oil emulsification, they were treated with 1*H*, 1*H*, 2*H*, 2*H*-perfluorooctyltriethoxysilane, a commercial windshield treatment. Therefore, the latter was injected into the channels, allowed to sit for a few minutes, and then removed by thorough air drying.

### **3.4.2 Microfluidic encapsulation of mouse fibroblast NIH/3T3 cells**

NIH/3T3 cell-laden microgels were prepared according to a modified procedure, already established in our group.<sup>[105]</sup> In detail, microchannels with four different inlets and a double cross-junction were produced using the soft lithography procedure detailed above. The microchannels had a rectangular cross-section with a uniform height of 180  $\mu$ m. The channel width was 100  $\mu$ m at the first cross-junction and 150  $\mu$ m at the second cross-junction. A wide basin channel was patterned downstream of the second cross-junction to allow observation of the resultant droplets, as illustrated in Scheme 1.



**Scheme 1.** Inkscape illustration of the microfluidic channels used in this work (Kind contribution of Dr. J. Moschner).

The concentrations of all macromonomer solutions and the density of the NIH/3T3-cell suspension in cell medium as well as the composition of the used oil are summarized in Table 2, Section 2.1.2.7. All fluids were loaded to the microfluidic device using analytical plastic syringes and polyethylene tubing (Scientific Commodities). The flow rates were adjusted by syringe pumps (Harvard Apparatus PHD Ultra). To monitor the droplet formation, the microfluidic device was operated on an inverted optical microscope (Zeiss Primo Vert) equipped with a digital camera (ABS UK1155). The two precursor solutions were injected into two separate inlets, whereas the cells were introduced into the middle inlet serving as a blocker for the reactive macromonomers. At the first cross-junction, these three fluids formed a laminar coflowing stream in the microchannel. This stream was broken to form monodisperse pre-microgel droplets with diameters of 140  $\mu\text{m}$  in the second cross-junction by flow focusing with the immiscible Novec<sup>TM</sup> 7100 oil. By mixing the three liquids inside the droplets, the precursors rapidly cross-linked by SPAAC in the presence of NIH/3T3 cells, thereby encapsulating them. Varying the flow rates of the three phases adjusts their respective volume fractions in the laminar coflowing stream that forms downstream of the first cross-junction. Subsequent flow focusing by the continuous phase, a mixture of Novec<sup>TM</sup> 7100 oil (98.7 wt %), and hyperfluorinated KBT-surfactant (1.3 wt %) led to droplet formation. The following volume flow rates were used for the **P1 - P3** and dPG-polyC phases, the cell phase, and the continuous oil phase, respectively: 200:200:80:1000  $\mu\text{L h}^{-1}$ .

To transfer the collected cell-laden microgel particles into cell medium a four-step procedure was applied. The supernatant organic phase was removed using a pipette and 1*H*, 1*H*, 2*H*, 2*H*-perfluoro-1-octanol (50  $\mu\text{L}$ ) was added as a scavenger of the remaining oil phase traces. Then the sediment-microgels were suspended in cell medium (500  $\mu\text{L}$ ) and densified by centrifugation at 3500 rpm. An organic layer was formed, which was subsequently removed using a pipette. The sedimented microgels in medium were

centrifuged again and the remaining organic phase was discarded with a pipette. This procedure was repeated three times and the resulting suspension of microgels in medium was transferred in a Petri dish where fresh cell medium was added to a final culture volume of 2000  $\mu\text{L}$ . The encapsulated cells in dPG-based microgels were then cultured in a humidified incubator at 37 °C under 5.0 %  $\text{CO}_2$ .

### 3.4.3 Microfluidic encapsulation of mouse insulinoma $\beta$ -TC-6 cells

For the encapsulation of the pancreatic  $\beta$ -TC-6 cells the same microfluidic devices and procedure were applied as detailed above. The following volume flow rates were used for the **P1** and **P4** phases, the cell and the continuous oil phase, respectively: 200:200:80:1000  $\mu\text{L h}^{-1}$ . The corresponding flow rates of **P5**, **P6**, the cell and oil phase for the generation of microgels **M4** were: 67:133:40:1000  $\mu\text{L h}^{-1}$  respectively. The concentrations of the precursor solutions and the density of the  $\beta$ -TC-6-cell suspension in cell medium as well as the composition of the used oil are summarized in Tables 3 and 4. The obtained microgel particles were transferred in the respective culture medium DMEM (1G, 15 % FCS, 1 % P/S) following the procedure described above. The encased  $\beta$ -cells in dPG-based microgels were then cultured in a humidified incubator at 37 °C under 5.0 %  $\text{CO}_2$ .

**Table 3.** Detailed description of microfluidic-templated dPG-based microgels: concentration and composition of all involved components (annotation **P1** as in Table 1, Section 2.1.2.6 of this work).

Microgel	Polymer	Concentration of <b>P1</b> in DMEM solution ( $\text{g L}^{-1}$ )	Concentration of dPG-polyC <b>P4</b> in DMEM solution ( $\text{g L}^{-1}$ )	Macromonomer Concentration in Microgels ( $\text{g L}^{-1}$ )	Density of $\beta$ -TC-6-cell-suspension	Consistency of Oil (wt %)
<b>M1</b>	<b>P1</b>	200	200	200	$7.00 \times 10^7$ in 1.00 mL DMEM of 15 vol % OptiPrep <sup>TM</sup>	Novec 7100 1.3 wt % KBT

**Table 4.** Detailed description of microfluidic-templated dPGS-based microgels: concentration and composition of all involved components.

Microgel	Polymer	Concentration of <b>P6</b> in DMEM solution ( $\text{g L}^{-1}$ )	Concentration of dPGS-polyazide <b>P5</b> in DMEM solution ( $\text{g L}^{-1}$ )	Macromonomer Concentration in Microgels ( $\text{g L}^{-1}$ )	Density of $\beta$ -TC-6-cell-suspension	Consistency of Oil (wt %)
<b>M4</b>	<b>P6</b>	200	200	200	$7.00 \times 10^7$ in 1.00 mL DMEM of 15 vol % OptiPrep™	Novec 7100 1.3 wt % KBT

### 3.5 Encapsulation of mouse insulinoma $\beta$ -TC-6 cells in dPGS-based bulk hydrogels

Bulk hydrogels **G1** - **G3** with the same composition and polymer content but bearing three different  $\beta$ -cell populations were prepared. Low ( $4.00 \cdot 10^4$ ), medium ( $1.00 \cdot 10^5$ ) and high ( $1.00 \cdot 10^6$ ) cell masses were encapsulated in gels **G1** - **G3** respectively. Solutions of macromonomers **P5** and **P6** in DMEM (1G, 15 % FCS, 1 % P/S) with a concentration of  $200 \text{ g L}^{-1}$  were utilized. The volume ratio of **P5/P6**/ $\beta$ -cell-suspension, 10:20:6 was the corresponding as defined by the flow rates employed for the microfluidic templating of microgels **M4**. The cell-laden bulk gels that were used for the evaluation of insulin secretion *via* ELISA, were prepared in the wells of a transparent 96-well-plate. The more densely populated gels **G2** and **G3** were constructed in Petri-dishes with a diameter of 35 mm.

The applied procedure for the generation of cell-bearing bulk hydrogels involved three steps.  $20 \mu\text{L}$  of **P6**-solution were added to each well, followed by  $6 \mu\text{L}$  of  $\beta$ -cell-suspension. After gentle mixing of the two fluids with a pipette  $10 \mu\text{L}$  of **P5**-solution were added and the resulting mixture was gently resuspended. Thus, each well contained a gelling mass that bore  $4.00 \cdot 10^4$  cells and the plate was incubated for 20 minutes at  $37 \text{ }^\circ\text{C}$  under 5.0 %  $\text{CO}_2$  to allow further cross-linking of the polymers. DMEM (1G, 15 % FCS, 1 % P/S) was then added to a final volume of  $100 \mu\text{L}$  per well and the cell-laden gels were incubated for 24 hours. Subsequently, the supernatants were removed, the gels were rinsed with DPBS  $\text{v/v}$  ( $2 \times 100 \mu\text{L}$ ) and fresh media ( $100 \mu\text{L}$ ) were added to each well. The latter were of three different glucose concentrations to facilitate the assessment of insulin release *via* ELISA. A no, low ( $1 \text{ g/L}$ ) and high ( $4.5 \text{ g/L}$ ) glucose DMEM (15 % FCS, 1 % P/S) were employed. The negative control consisted of empty bulk gels in DMEM (1G, 15 % FCS, 1 % P/S).

A second 96-well-plate was inoculated with bare  $\beta$ -cells under identical conditions as for the bulk gels. As a negative control pure DMEM (1G, 15 % FCS, 1 % P/S) was used. The supernatants of each well of the two plates were collected after one and eight, days of culture respectively and were investigated for the determination of their insulin content *via* ELISA.

To appraise the cytocompatibility of the developed encapsulation systems, bulk hydrogels **G1** ( $4.00 \cdot 10^4$  cells), **G2** ( $1.00 \cdot 10^5$  cells), and **G3** ( $1.00 \cdot 10^6$  cells) were prepared as described above and incubated in Petri-dishes in an overall DMEM (1G, 15 % FCS, 1 % P/S) volume of 2.00 mL.

### **3.6 Cytocompatibility of dPG-based hydrogels with NIH/3T3 *via* live-dead staining**

To assess the viability of NIH/3T3 cells encapsulated into dPG-based microgels, the LIVE/DEAD® Viability/Cytotoxicity Kit for mammalian cells was used. Calcein AM, which only fluoresces green inside living cells (Ex/Em 495/515 nm) and ethidium homodimer-1, which only penetrates dead cells staining them red (Ex/Em 495/635 nm), allowed specimen visualization *via* confocal microscopy. The dyes were mixed in a 1:4 (calcein AM/ethidium homodimer 1) volume ratio and diluted to 1.00 mL with DPBS  $\gamma^-$ . A 40  $\mu$ L-aliquot of each type of cell laden microgels (**M1** - **M3**) was treated with 40  $\mu$ L of staining mixture 30 minutes prior to confocal imaging. The bare cells used as negative control were cultured in Petri-dishes with a diameter of 35 mm, in an overall volume of 2.00 mL. Half an hour before microscopic visualization they were treated with 300  $\mu$ L of staining solution.

### **3.7 Cytocompatibility of dPGS-based hydrogels with $\beta$ -TC-6 cells *via* live-dead staining**

To evaluate the viability of  $\beta$ -TC-6 cells encapsulated into dPGS-based micrometer-sized and bulk hydrogels, calcein AM, which only stains living cells green (Ex/Em 495/515 nm) and PI, which only penetrates dead cells staining them red (Ex/Em 493/636 nm), allowed specimen visualization *via* confocal microscopy. The dyes were mixed in a 1:1.5 (calcein AM/PI) volume ratio and diluted to 1.00 mL with DPBS  $\gamma^-$ . A 40  $\mu$ L-aliquot of cell laden microgels **M4** was treated with 40  $\mu$ L of staining mixture 30 minutes prior to confocal imaging. The bare cells used as negative control were cultured in Petri-dishes with a diameter of 35 mm, in an overall volume of 2.00 mL. Half an hour before microscopic visualization they were treated with 300  $\mu$ L of staining solution. To stain the bulk hydrogels 300  $\mu$ L per specimen were employed. After each imaging session, the microgel samples were discarded

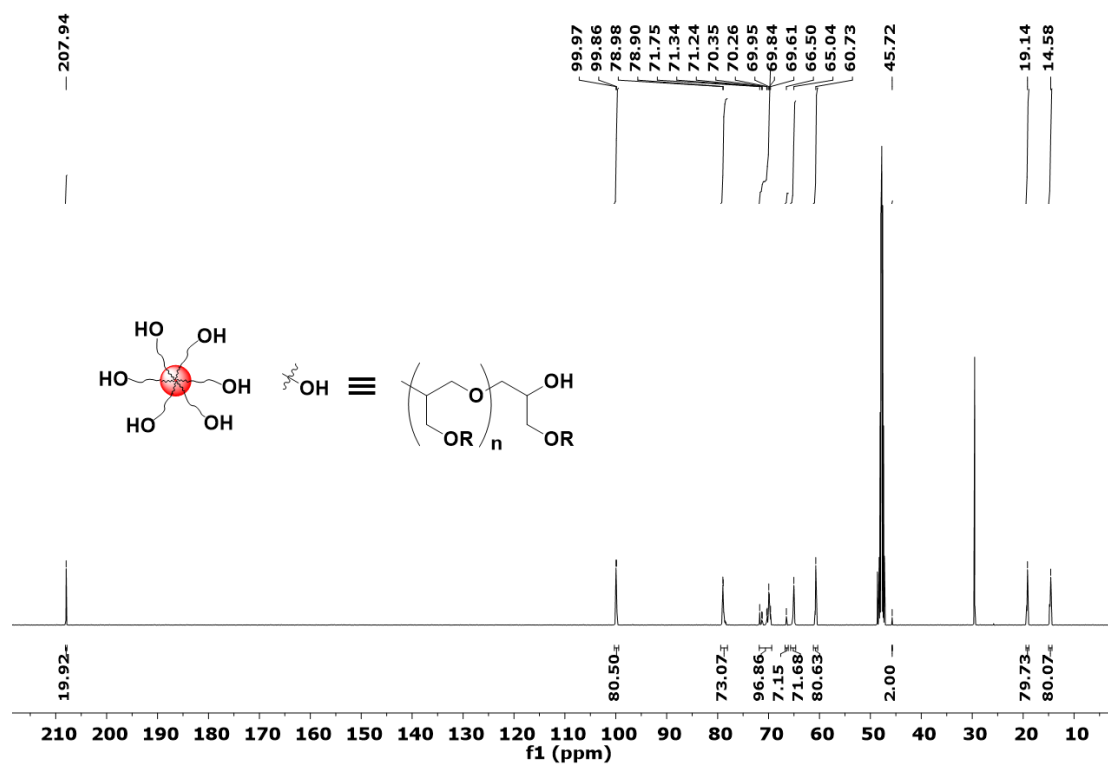
whereas the bulk hydrogels were rinsed repeatedly with DPBS  $\pm$  (4 x 1.00 mL) and further cultured in freshly added medium DMEM (1G, 15 % FCS, 1 % P/S) in a 2.00 mL volume.

### **3.8 Quantification of the released insulin from $\beta$ -TC-6 cell-laden dPGS bulk hydrogels *via* ELISA**

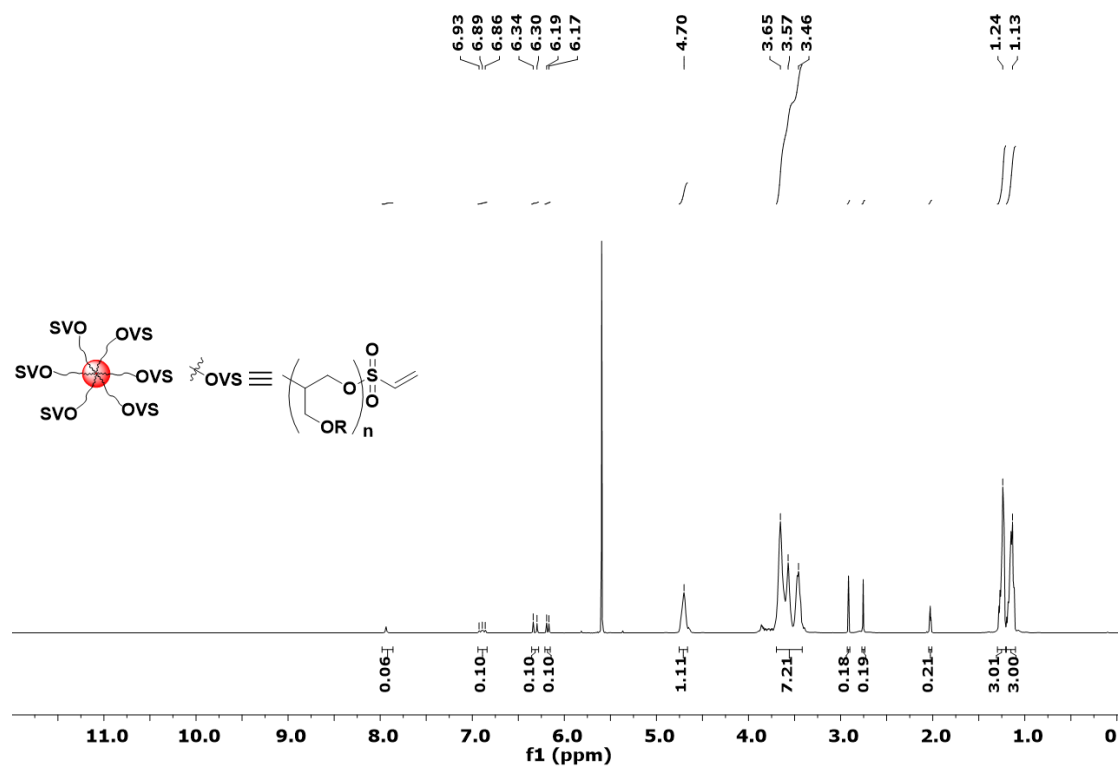
To quantify the secreted insulin from encapsulated  $\beta$ -TC-6 cells in bulk gels **G1** a Merckodia mouse insulin ELISA kit was employed. The assay was performed both prior to and after one and eight days post encapsulation. Diluted solutions were prepared for each of the collected supernatants. In case of the naked  $\beta$ -TC-6 cells on day one the dilution factor was equal to 1/25 as opposed to 1/5 for the cells enclosed in gels **G1**. The dilution coefficients for naked and immobilized cells on day eight amounted to 1/500 and 1/25 respectively. As negative controls, the supernatants from the corresponding wells (detailed in Section 3.5) were used after the related dilution.

10  $\mu$ L of each calibrator, control and sample solution were added in triplicates into the appropriate wells of the ELISA-kit. After pipetting in each well 100  $\mu$ L of the enzyme conjugate solution included in the kit, the plate was incubated on a plate shaker at 700 rpm for two hours at room temperature. Subsequently the reaction volumes were discarded and the wells were repeatedly rinsed with a wash buffer solution (6 x 350  $\mu$ L per well). 200  $\mu$ L of the kit's substrate solution were added to each well and the plate was incubated for 15 minutes on the bench at room temperature. The final steps of this protocol involved the addition of 50  $\mu$ L per well of the stop solution, short shaking (5 seconds) to ensure mixing and read out of the optical density at 450 nm within 30 minutes after the last addition. The assay was conducted three times in total and after each repetition the used kits were discarded.

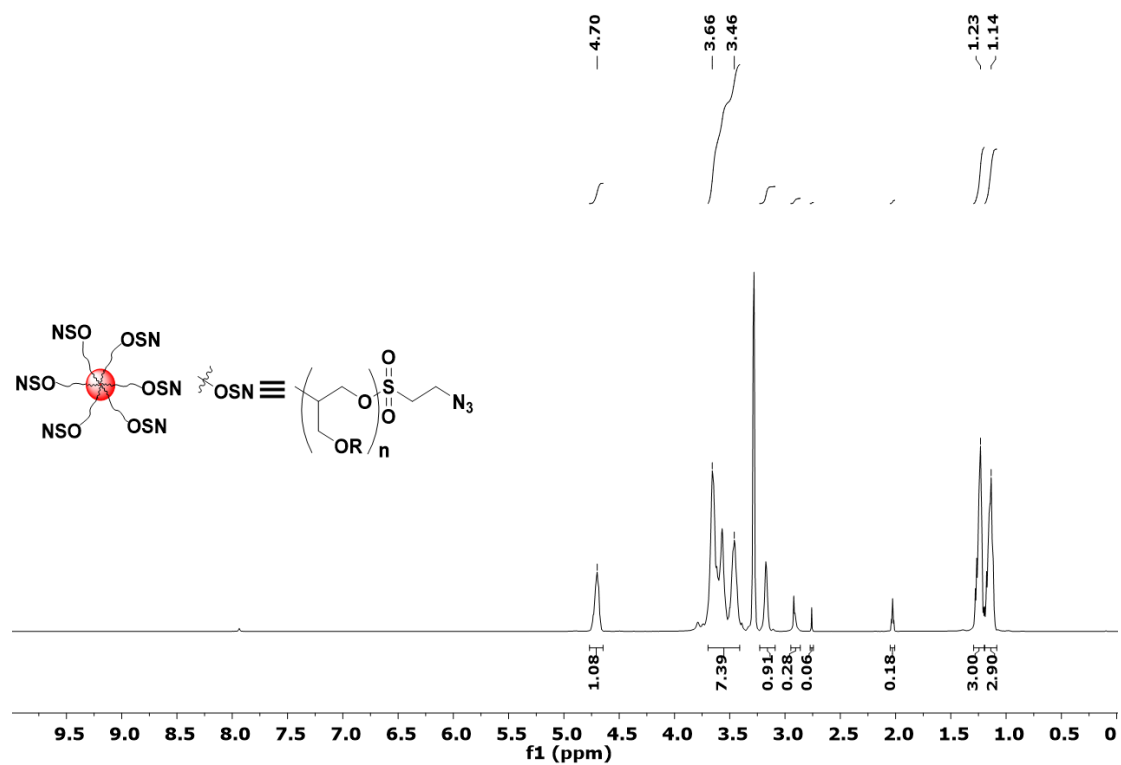




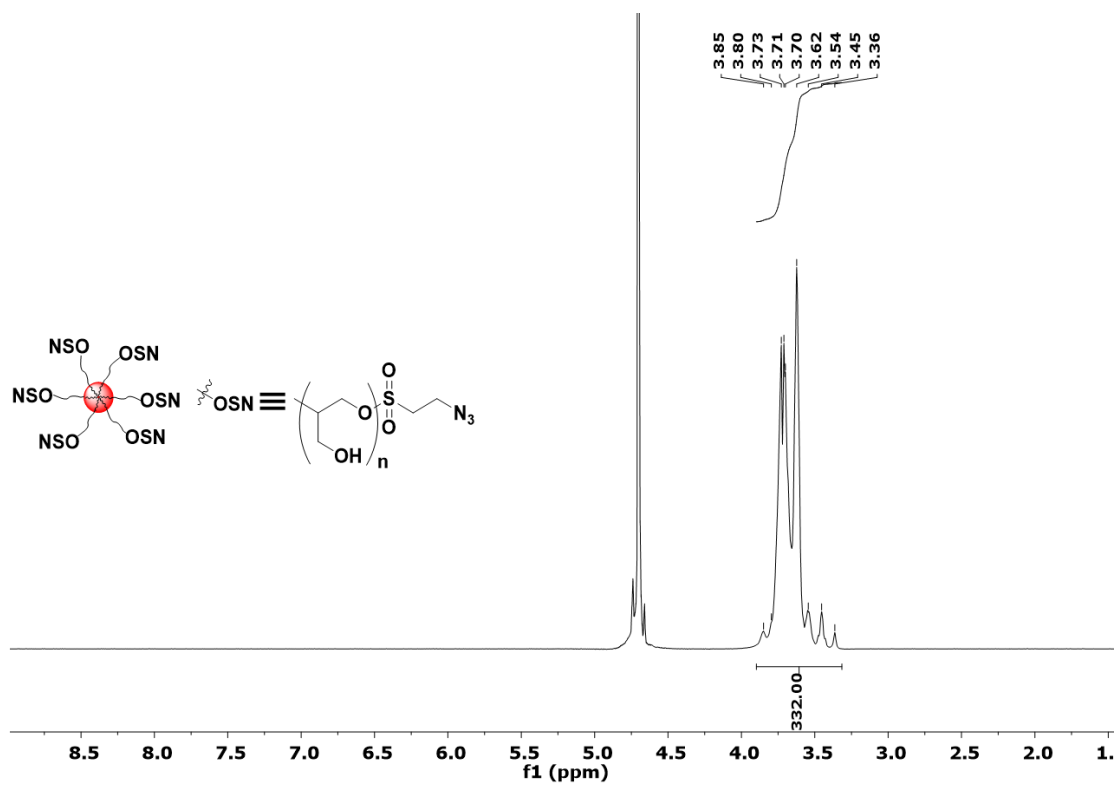
Scheme 4. Inverse gated  $^{13}\text{C}$  NMR (MeOH-d<sub>4</sub>, 700 MHz) S-PG 4.



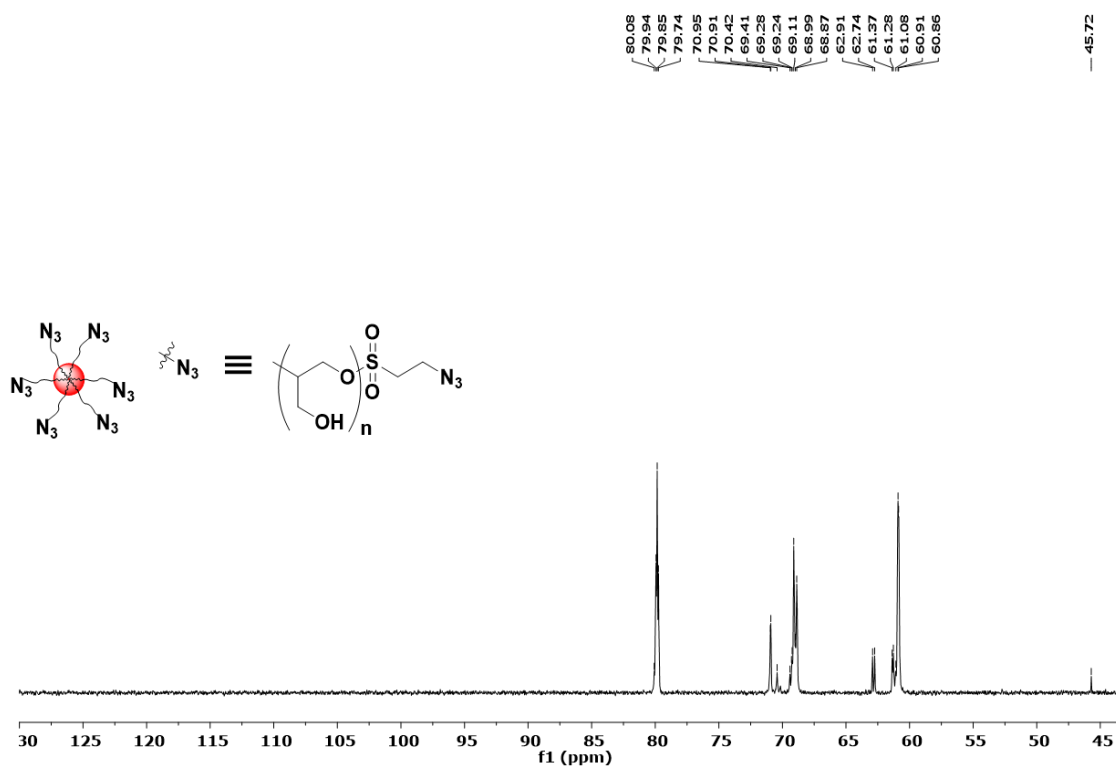
Scheme 5.  $^1\text{H}$  NMR (Acetone-d<sub>6</sub>, 400 MHz) S-PGVS 3.



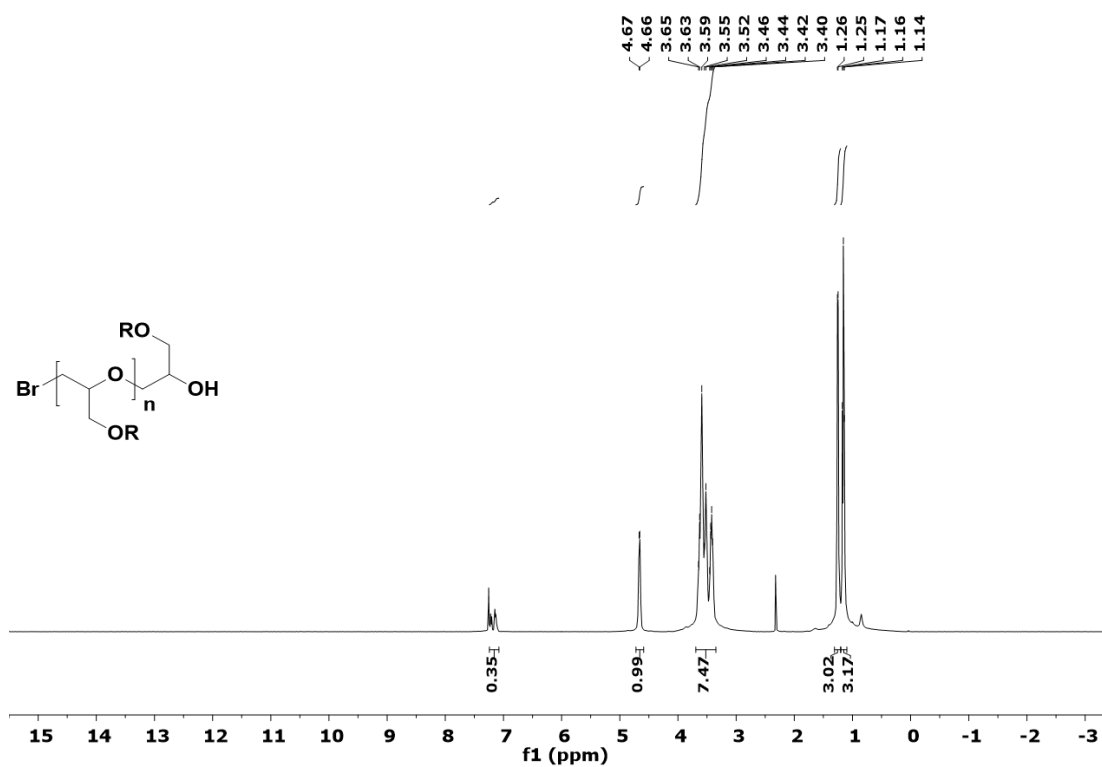
**Scheme 6.** <sup>1</sup>H NMR (Acetone-d<sub>6</sub>, 400 MHz) S-PG-hexaazide **2**.



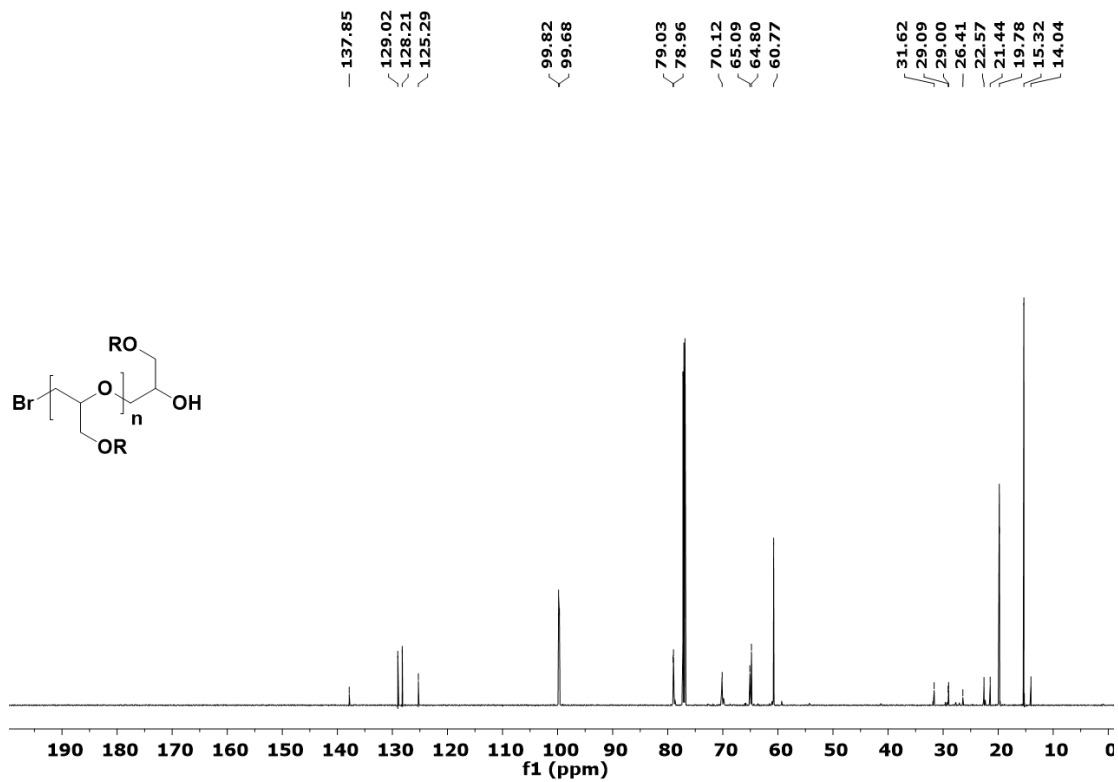
**Scheme 7.** <sup>1</sup>H NMR (D<sub>2</sub>O, 500 MHz) S-PG-hexaazide **P1**.



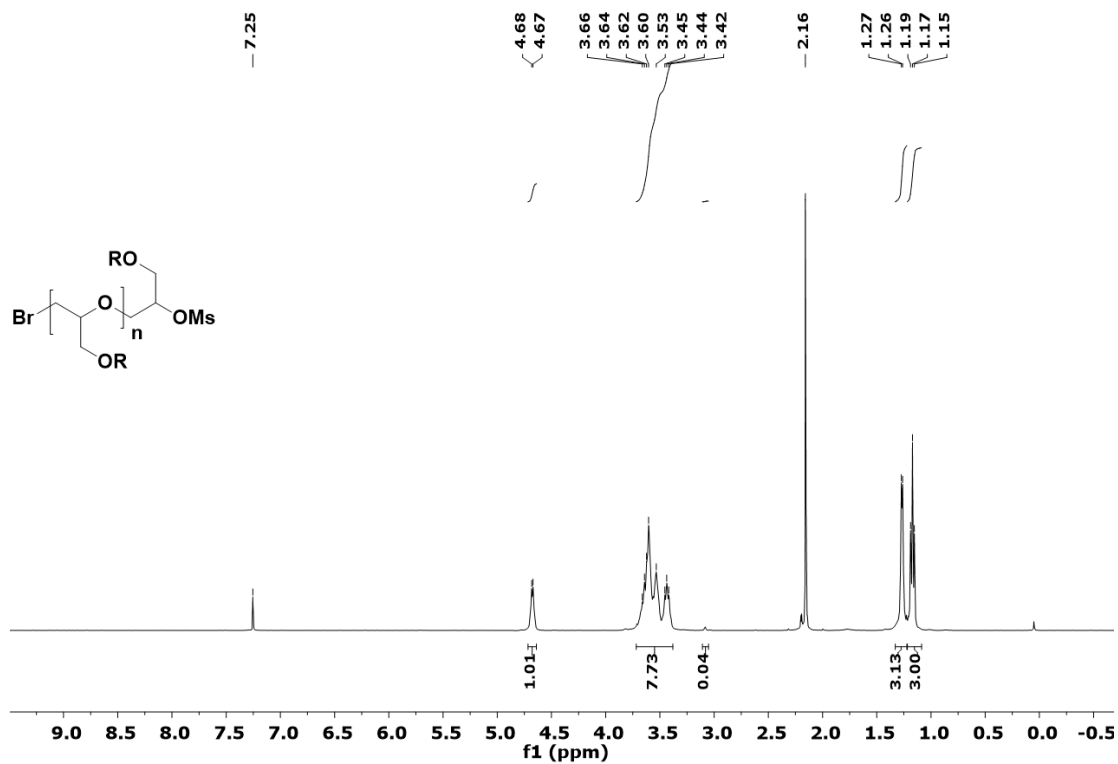
Scheme 8.  $^{13}\text{C}$  NMR ( $\text{D}_2\text{O}$ , 500 MHz) S-PG-hexaazide **P1**.



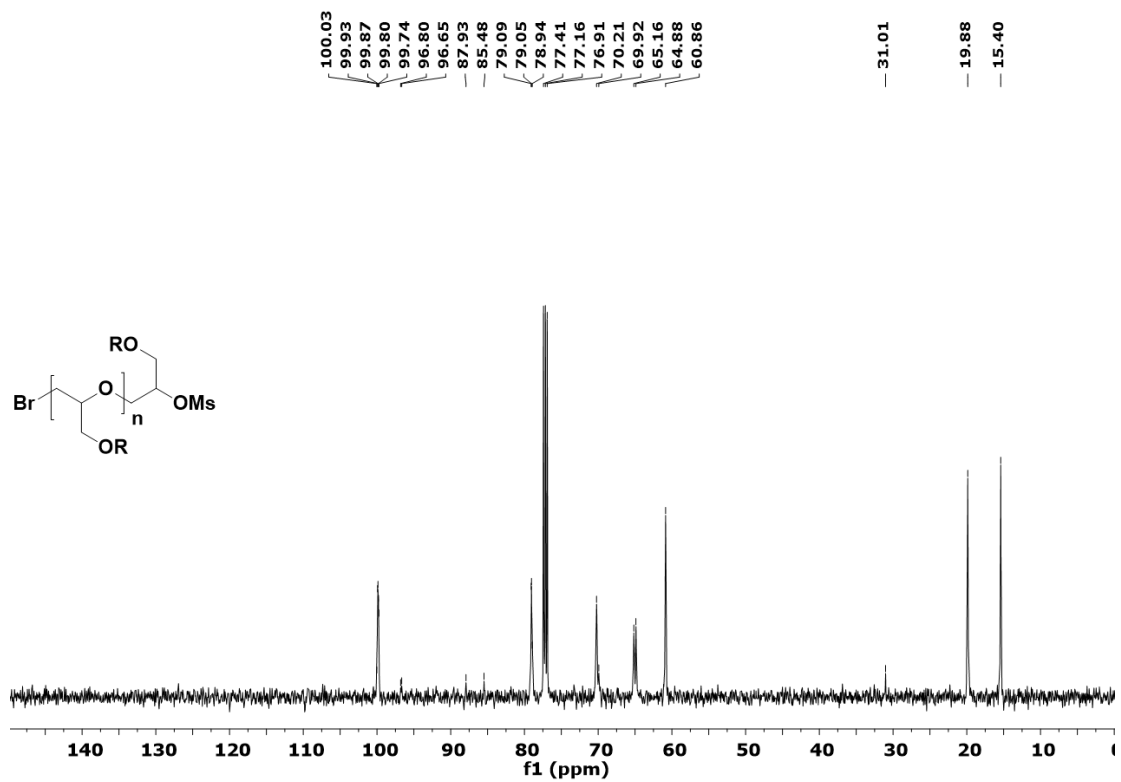
Scheme 9.  $^1\text{H}$  NMR ( $\text{CDCl}_3$ , 400 MHz) monobromo-PEEGE **4**.



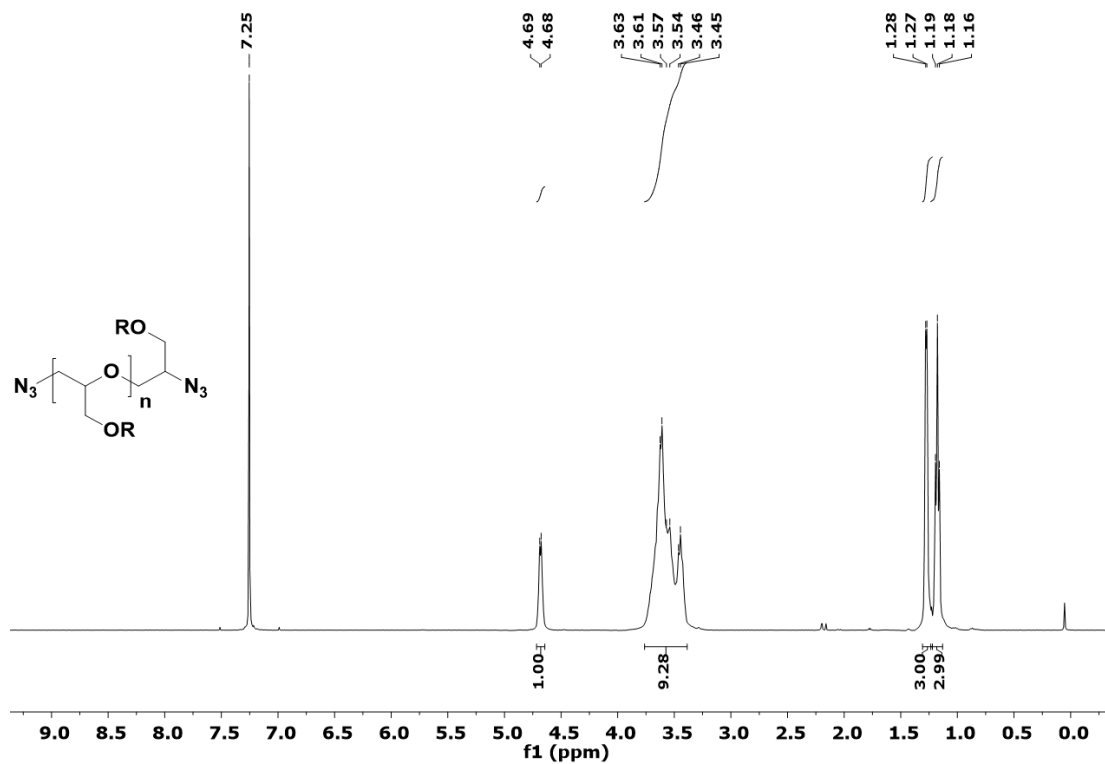
Scheme 10.  $^{13}\text{C}$  NMR (CDCl<sub>3</sub>, 400 MHz) monobromo-PEEGE 4.



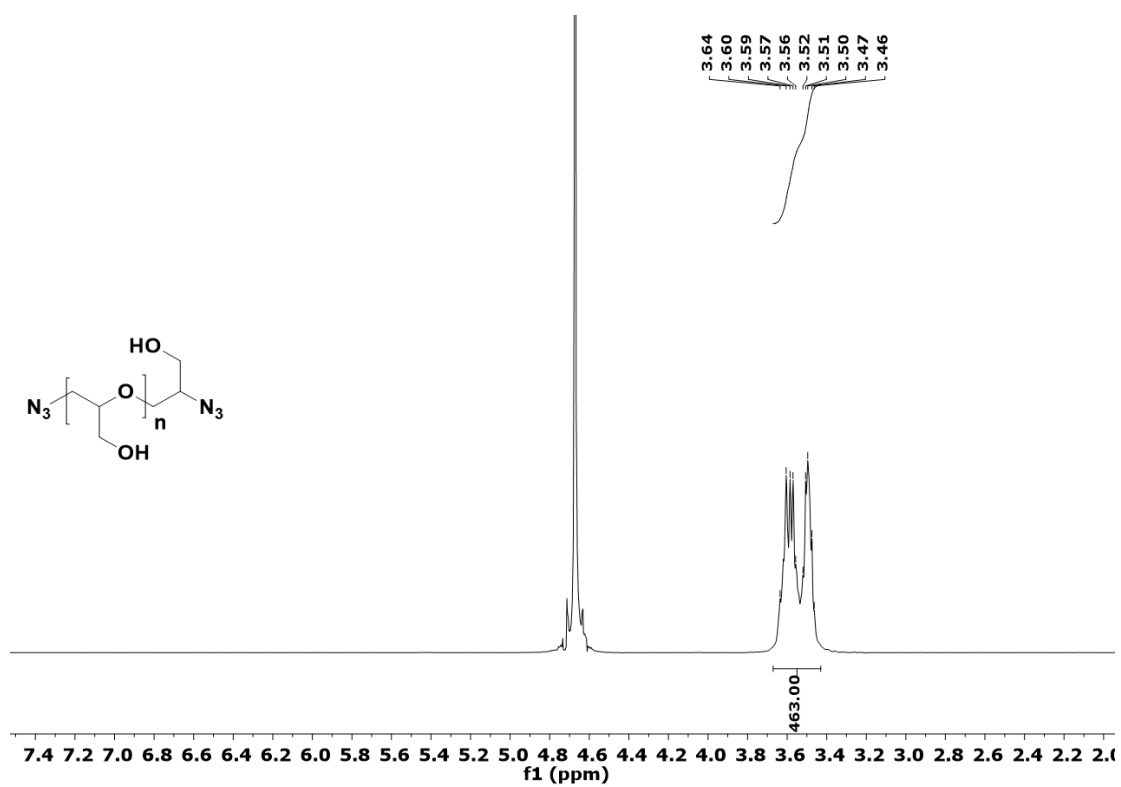
Scheme 11  $^1\text{H}$  NMR (CDCl<sub>3</sub>, 400 MHz)  $\alpha$ -bromo- $\omega$ -mesyloxy-PEEGE 3.



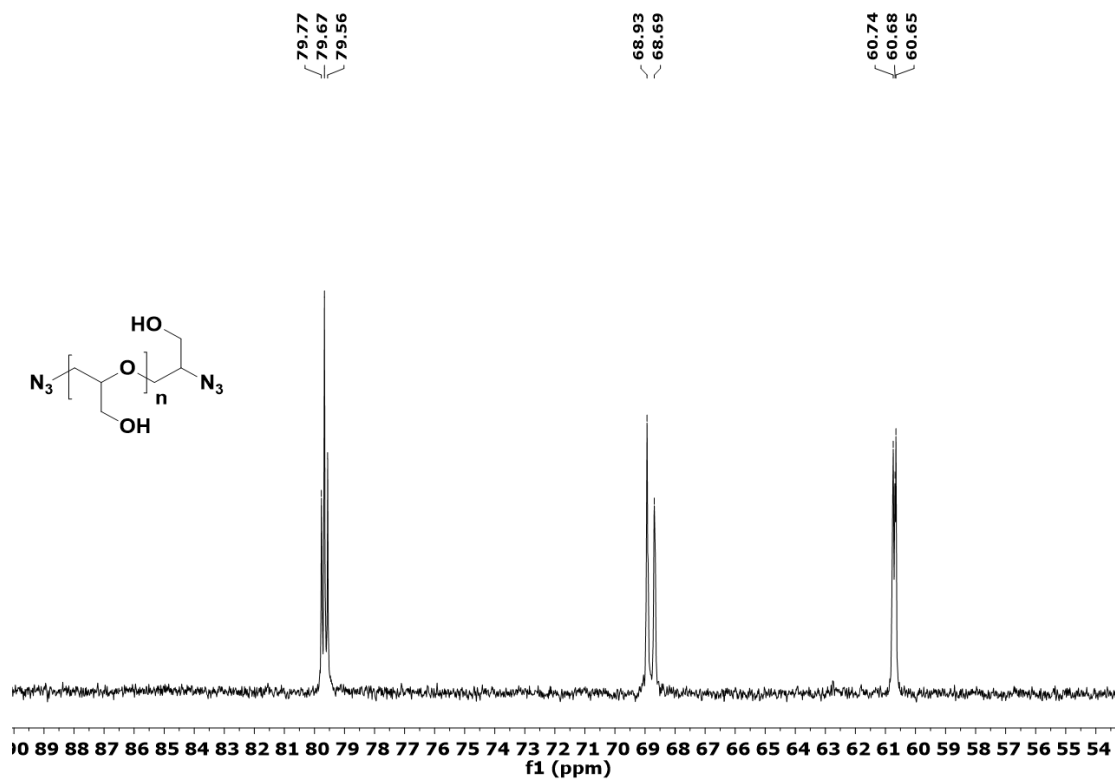
**Scheme 12**  $^{13}\text{C}$  NMR ( $\text{CDCl}_3$ , 400 MHz)  $\alpha$ -bromo- $\omega$ -mesyloxy-PEEGE **3**.



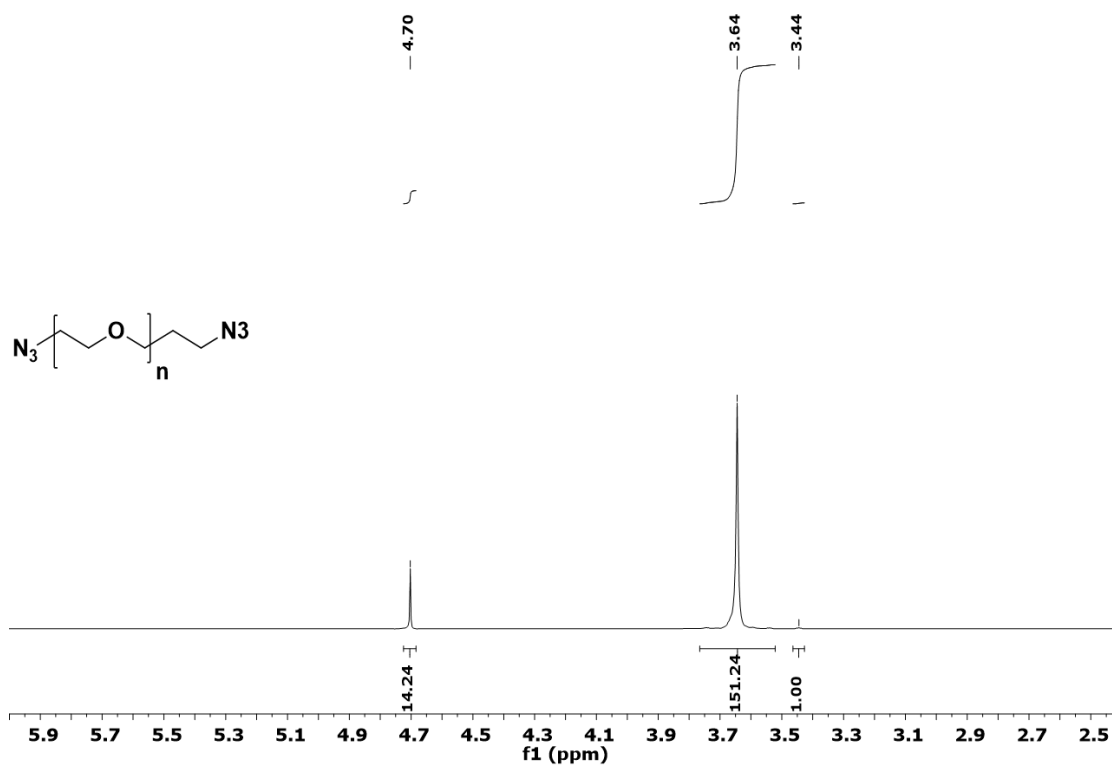
**Scheme 13.**  $^1\text{H}$  NMR ( $\text{CDCl}_3$ , 400 MHz)  $\alpha, \omega$ -bisazido-IPEEGE **2**.



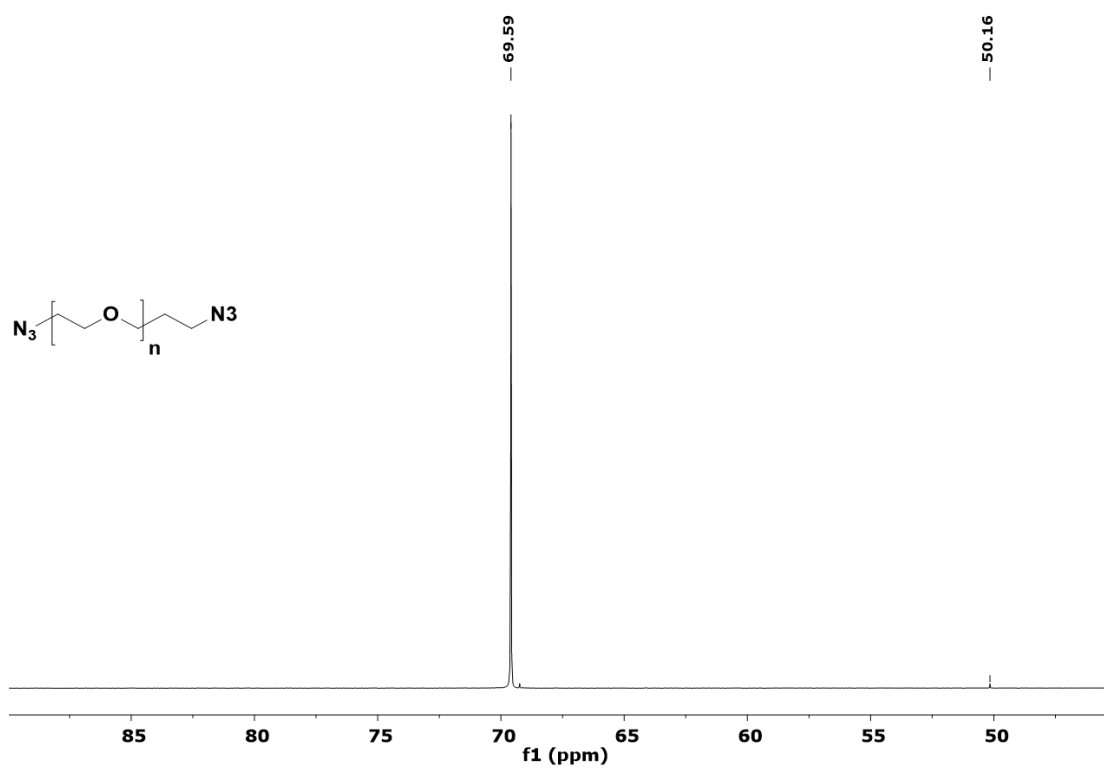
Scheme 14.  $^1\text{H NMR}$  (D<sub>2</sub>O, 700 MHz)  $\alpha, \omega$ -bisazido-IPG P2.



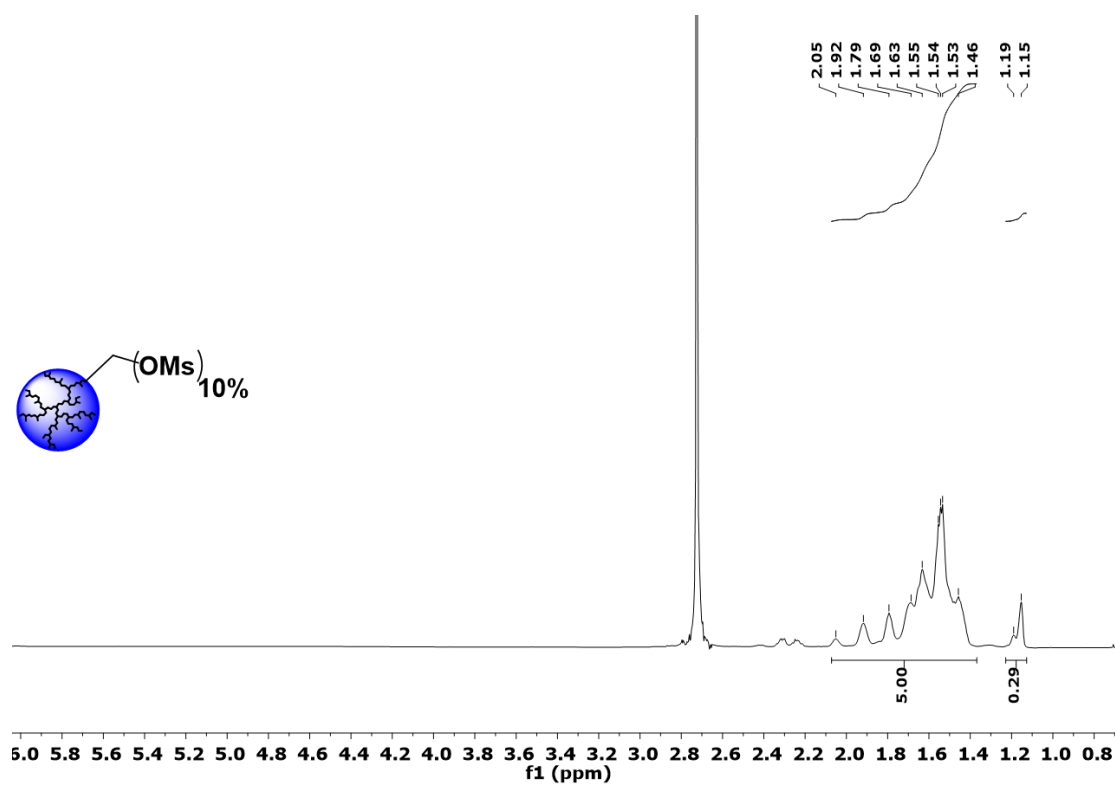
Scheme 15.  $^{13}\text{C NMR}$  (D<sub>2</sub>O, 700 MHz)  $\alpha, \omega$ -bisazido-IPG P2.



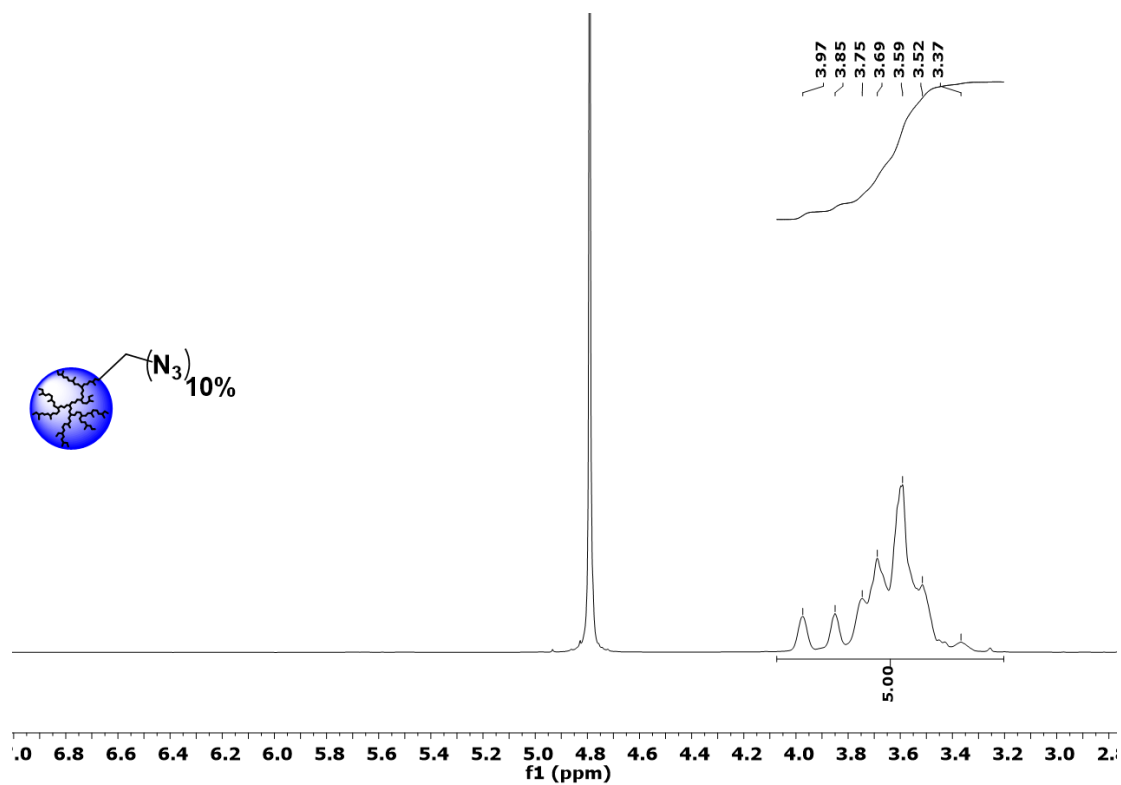
**Scheme 16.**  $^1\text{H NMR (D}_2\text{O, 700 MHz)}$   $\alpha, \omega$ -bisazido-PEG **P3**.



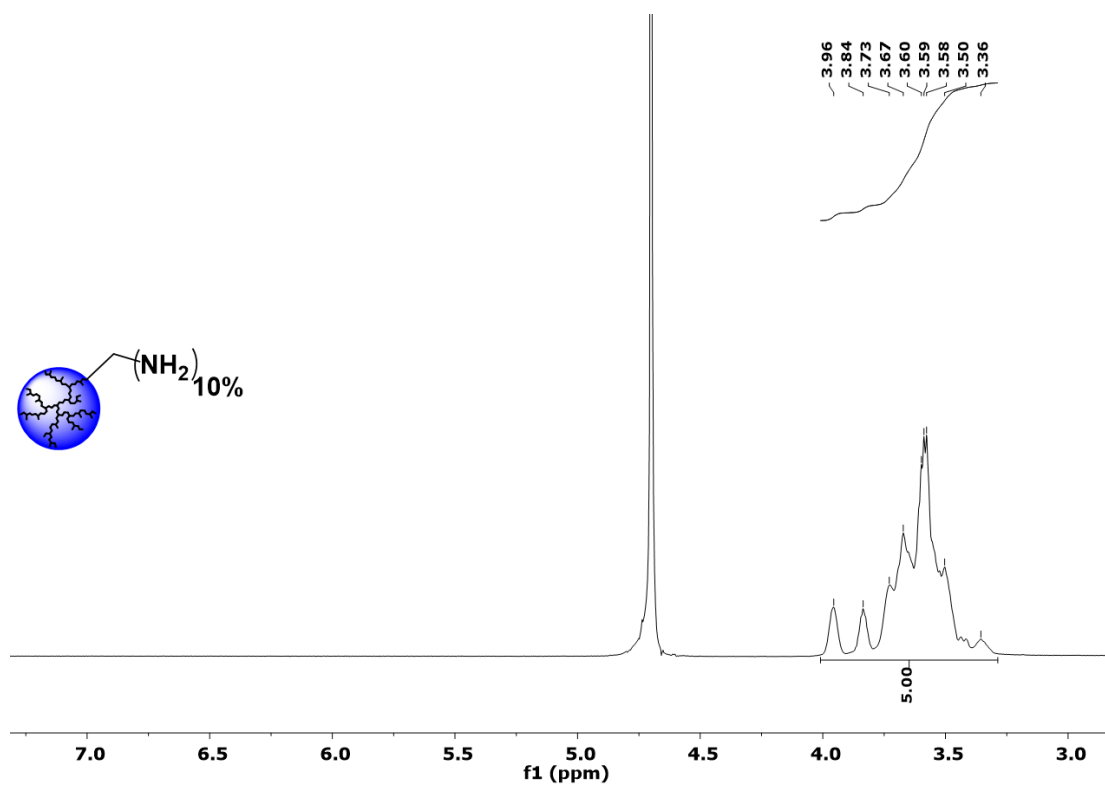
**Scheme 17.**  $^{13}\text{C NMR (D}_2\text{O, 700 MHz)}$   $\alpha, \omega$ -bisazido-PEG **P3**.



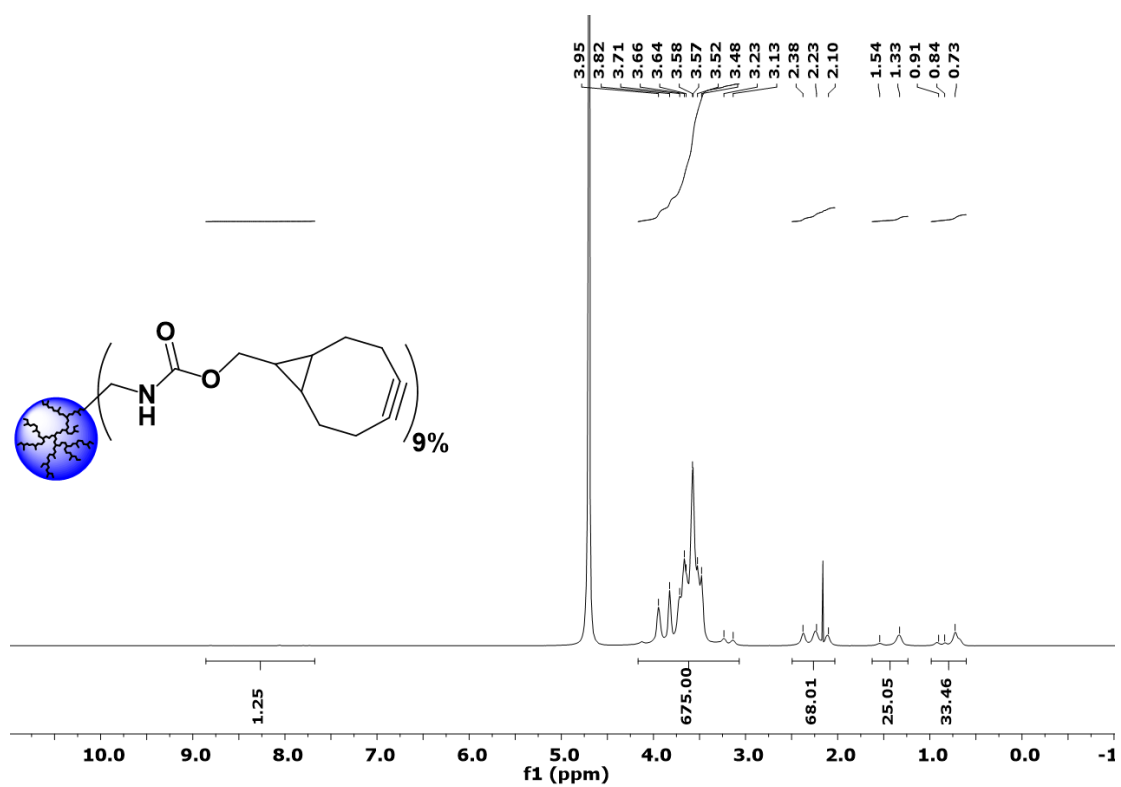
Scheme 18.  $^1\text{H}$  NMR ( $\text{D}_2\text{O}$ , 500 MHz) dPG-polymesylate 4.



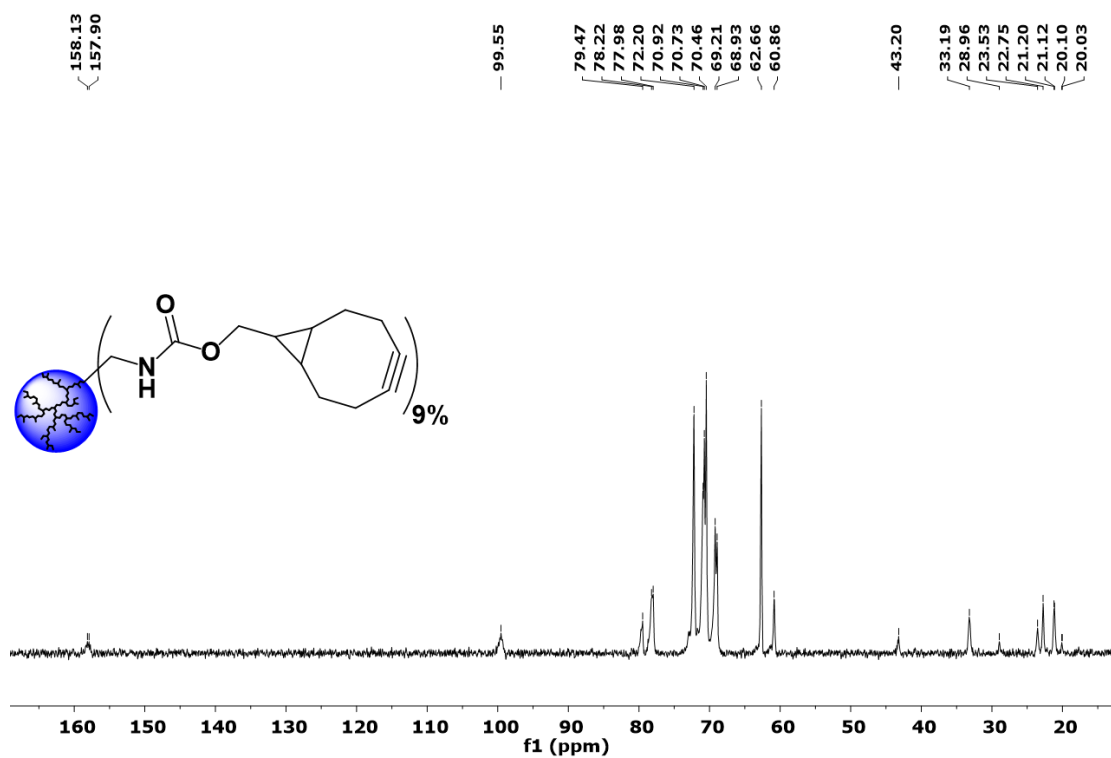
Scheme 19.  $^1\text{H}$  NMR ( $\text{D}_2\text{O}$ , 500 MHz) dPG-polyazide 3.



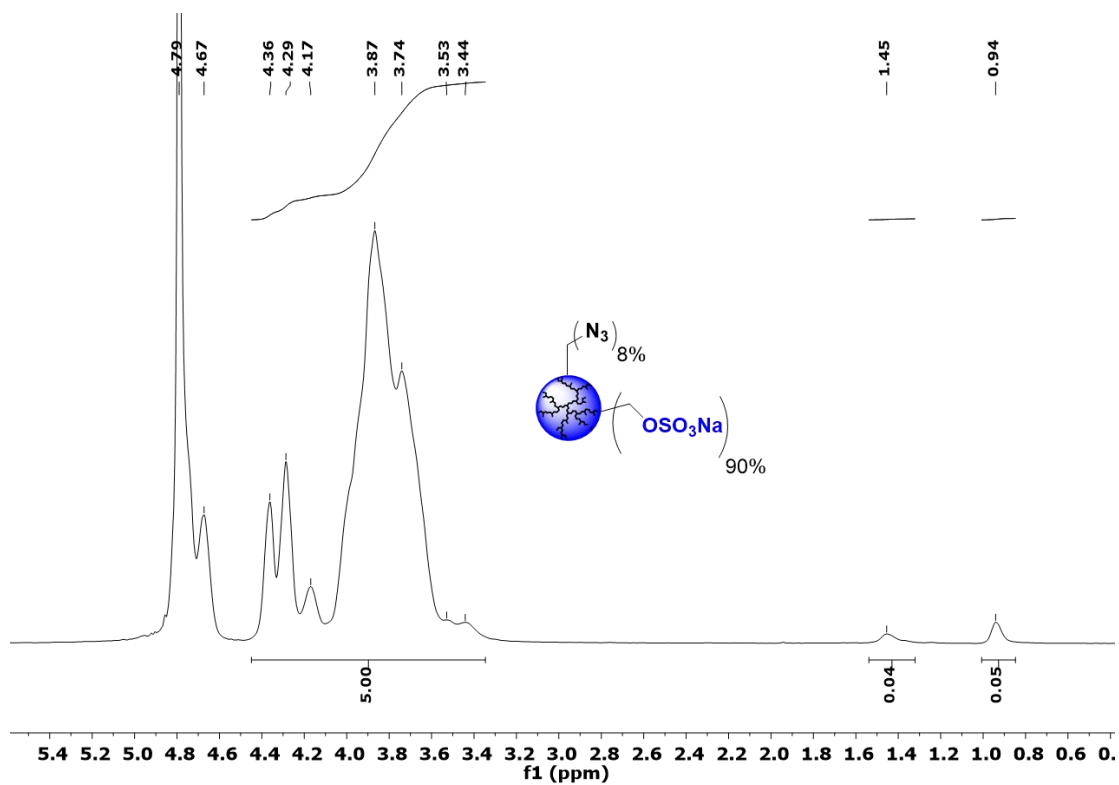
Scheme 20. <sup>1</sup>H NMR (D<sub>2</sub>O, 500 MHz) dPG-polyamine 2.



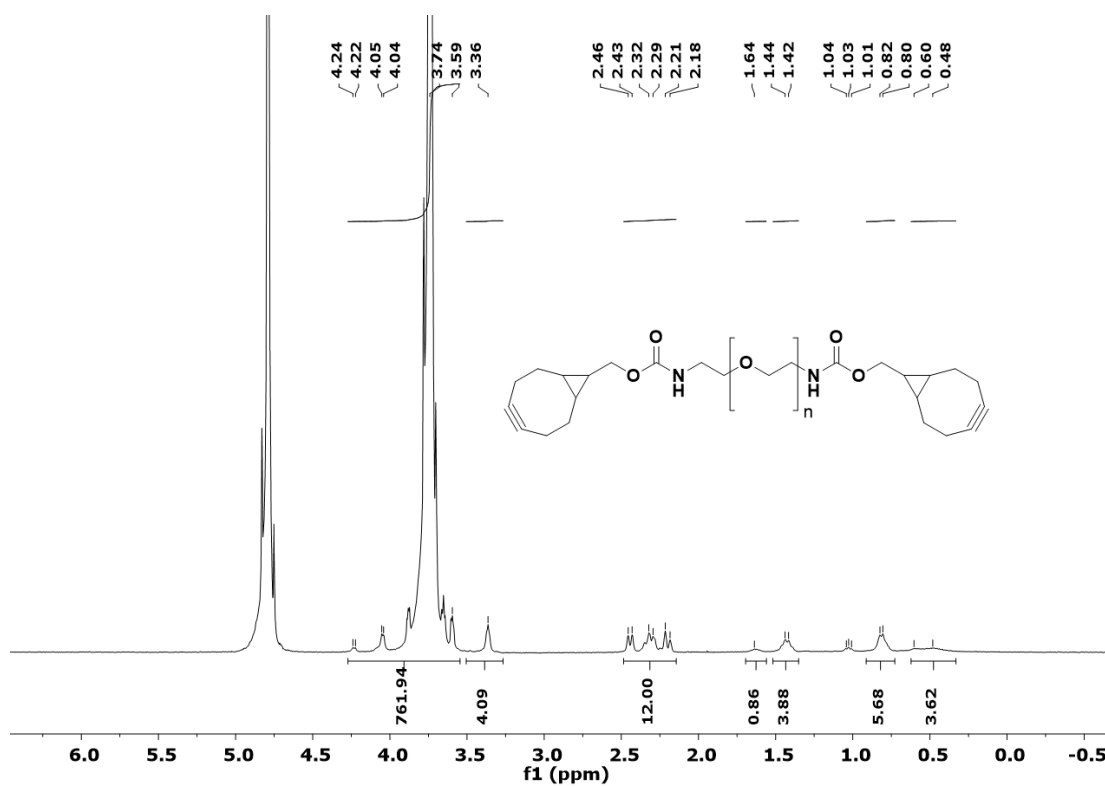
Scheme 21. <sup>1</sup>H NMR (D<sub>2</sub>O, 700 MHz) dPG-polyC P4.



Scheme 22.  $^{13}\text{C}$  NMR ( $\text{D}_2\text{O}$ , 700 MHz) dPG-polyC **P4**.

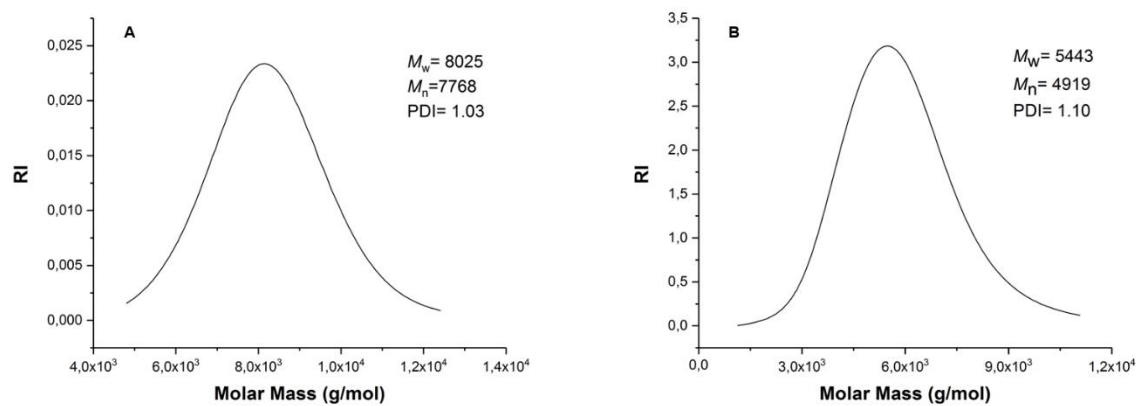


Scheme 23.  $^1\text{H}$  NMR ( $\text{CDCl}_3$ , 500 MHz) dPGS-polyazide **P5**.

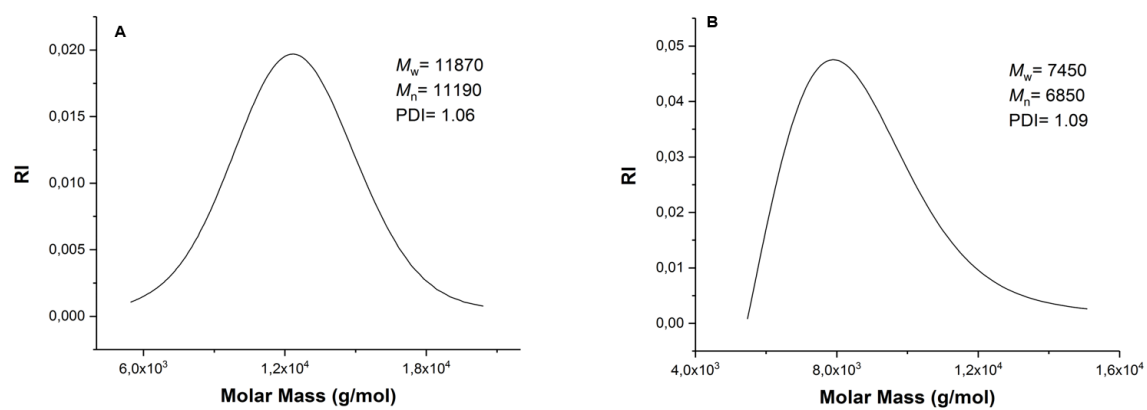


Scheme 24.  $^1\text{H}$  NMR ( $\text{D}_2\text{O}$ , 500 MHz)  $\alpha, \omega$ -bis(bicyclooctyne)-PEG P6.

## 4.2 GPC traces

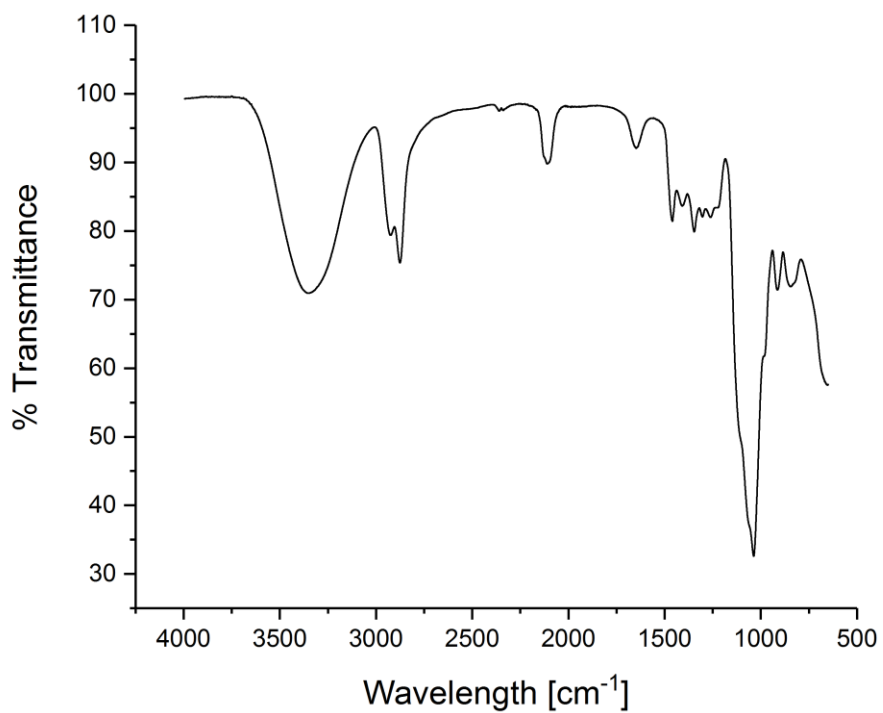


Scheme 25. GPC traces (A) S-PG 4 and (B) S-PG-hexaazide P1.

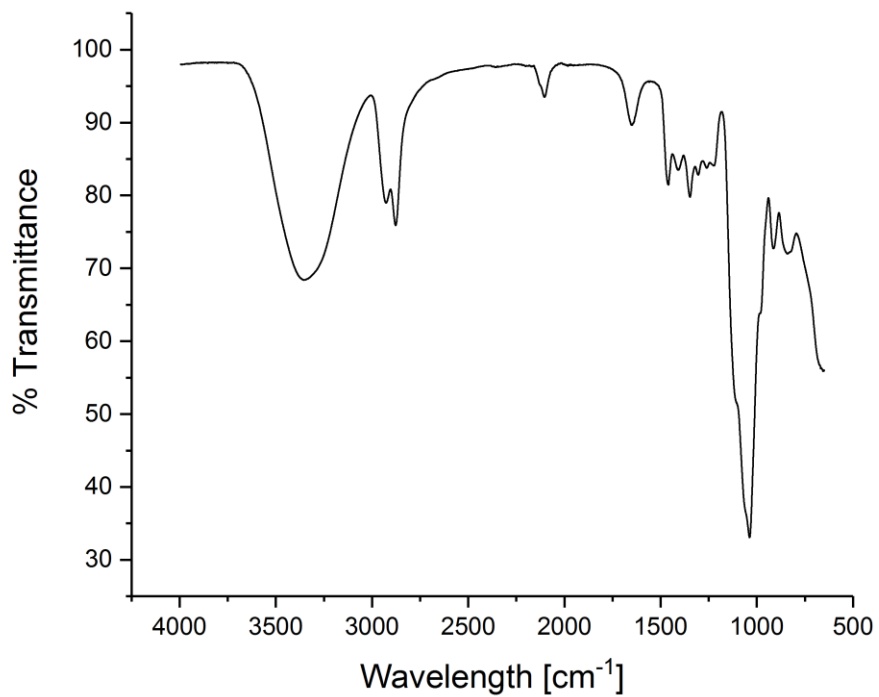


Scheme 26. GPC traces (A) monobromo-PEEGE 4 and (B)  $\alpha, \omega$ -bisazido-IPG P2.

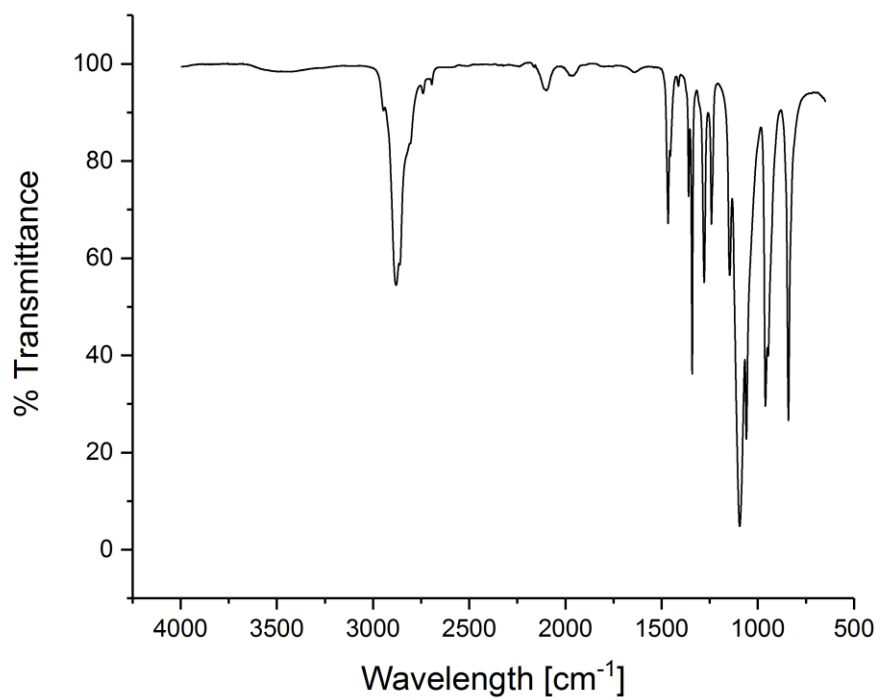
### 4.3 IR spectra



**Scheme 27.** IR spectrum of S-PG-hexaazide **P1**.



**Scheme 28.** IR spectrum of  $\alpha, \omega$ -bisazido-IPG **P2**.



**Scheme 29.** IR spectrum of  $\alpha, \omega$ -bisazido-PEG **P3**.

#### **4.4 Curriculum Vitae**

Due to reasons of data protection the *curriculum vitae* is not included in the online version.

## 5 References

- [1] T. M. S. Chang, *Science* **1964**, *146*, 1–2.
- [2] W. Chick, A. Like, V. Lauris, *Science* **1975**, *187*, 847–849.
- [3] R. Langer, J. P. Vacanti, *Science* **1993**, *260*, 920–926.
- [4] V. Bisceglie, *Zeitschrift für Krebsforsch.* **1934**, *40*, 122–140.
- [5] G. Orive, R. M. Hernández, A. R. Gascón, R. Calafiore, T. M. S. Chang, P. De Vos, G. Hortelano, D. Hunkeler, I. Lacík, A. M. J. Shapiro, J. L. Pedraz, *Nat. Med.* **2003**, *9*, 104–107.
- [6] G. Orive, R. M. Hernández, A. Rodríguez Gascón, R. Calafiore, T. M. S. Chang, P. De Vos, G. Hortelano, D. Hunkeler, I. Lacík, J. L. Pedraz, *Trends Biotechnol.* **2004**, *22*, 87–92.
- [7] P. de Vos, M. Bučko, P. Gemeiner, M. Navrátil, J. Švitel, M. Faas, B. L. Strand, G. Skjak-Braek, Y. A. Morch, A. Vikartovská, et al., *Biomaterials* **2009**, *30*, 2559–2570.
- [8] G. Orive, E. Santos, J. L. Pedraz, R. M. Hernández, *Adv. Drug Deliv. Rev.* **2014**, *67–68*, 3–14.
- [9] N. A. Peppas, J. Z. Hilt, A. Khademhosseini, R. Langer, *Adv. Mater.* **2006**, *18*, 1345–1360.
- [10] G. Orive, R. M. Hernández, A. R. Gascón, M. Igartua, J. L. Pedraz, *Trends Biotechnol.* **2002**, *20*, 382–387.
- [11] N. Sakata, S. Sumi, G. Yoshimatsu, M. Goto, S. Egawa, M. Unno, *World J. Gastrointest. Pathophysiol.* **2012**, *3*, 19–26.
- [12] A. Murua, A. Portero, G. Orive, R. M. Hernández, M. de Castro, J. L. Pedraz, *J. Control. Release* **2008**, *132*, 76–83.
- [13] D. F. Emerich, G. Orive, C. Thanos, J. Tornøe, L. U. Wahlberg, *Adv. Drug Deliv. Rev.* **2014**, *67–68*, 131–141.
- [14] S. V. Bhujbal, P. de Vos, S. P. Nicolou, *Adv. Drug Deliv. Rev.* **2014**, *67–68*, 142–153.
- [15] G. Orive, M. De Castro, S. Ponce, R. M. Hernández, A. R. Gascón, M. Bosch, J. Alberch, J. L. Pedraz, *Mol. Ther.* **2005**, *12*, 283–289.
- [16] B. P. Barnett, A. Arepally, P. V Karmarkar, D. Qian, W. D. Gilson, P. Walczak, V. Howland, L. Lawler, C. Lauzon, M. Stuber, et al., *Nat. Med.* **2007**, *13*, 986–991.
- [17] G. Orive, M. De Castro, H. J. Kong, R. M. Hernández, S. Ponce, D. J. Mooney, J. L. Pedraz, *J. Control. Release* **2009**, *135*, 203–210.
- [18] H. Oda, T. Konno, K. Ishihara, *Biomaterials* **2015**, *56*, 86–91.

- [19] A. T. Chan, M. F. Karakas, S. Vakrou, J. Afzal, A. Rittenbach, X. Lin, R. L. Wahl, M. G. Pomper, C. J. Steenbergen, B. M. W. Tsui, J. H. Elisseeff, M. R. Abraham *Biomaterials* **2015**, *73*, 1–11.
- [20] S. Zhao, Z. Xu, H. Wang, B. E. Reese, L. V Gushchina, M. Jiang, P. Agarwal, J. Xu, M. Zhang, R. Shen, et al., *Nat. Commun.* **2016**, *7*, 13306.
- [21] M. Liu, X. Zeng, C. Ma, H. Yi, Z. Ali, X. Mou, S. Li, Y. Deng, N. He, *Bone Res.* **2017**, *5*, 17014.
- [22] F. Schwenter, S. Zarei, P. Luy, V. Padrun, N. Bouche, J. S. Lee, R. C. Mulligan, P. Morel, N. Mach, *Cancer Gene Ther.* **2011**, *18*, 553–562.
- [23] N. E. Davis, L. N. Beenken-Rothkopf, A. Mirsoian, N. Kojic, D. L. Kaplan, A. E. Barron, M. J. Fontaine, *Biomaterials* **2012**, *33*, 6691–6697.
- [24] A. C. Lima, P. Batista, T. A. M. Valente, A. S. Silva, I. J. Correia, J. F. Mano, *Tissue Eng. Part A* **2013**, *19*, 1175–1187.
- [25] G. A. Silva, P. Ducheyne, R. L. Reis, *J. Tissue Eng Regen. Med.* **2007**, *1*, 4–24.
- [26] M. B. Oliveira, J. F. Mano, *Biotechnol. Prog.* **2011**, *27*, 897–912.
- [27] J. J. Moon, J. E. Saik, R. A. Poché, J. E. Leslie-Barbick, S. H. Lee, A. A. Smith, M. E. Dickinson, J. L. West, *Biomaterials* **2010**, *31*, 3840–3847.
- [28] O. Jeon, C. Powell, L. D. Solorio, M. D. Krebs, E. Alsberg, *J. Control. Release* **2011**, *154*, 258–266.
- [29] O. Jeon, D. S. Alt, S. M. Ahmed, E. Alsberg, *Biomaterials* **2012**, *33*, 3503–3514.
- [30] G. Chan, D. J. Mooney, *Trends Biotechnol.* **2008**, *26*, 382–392.
- [31] W. Chen, H. Zhou, M. D. Weir, C. Bao, H. H. K. Xu, *Acta Biomater.* **2012**, *8*, 2297–2306.
- [32] H. Zhou, W. Chen, M. D. Weir, H. H. Xu, *Tissue Eng Part A* **2012**, *18*, 1583–1595.
- [33] T. Boontheekul, H. J. Kong, D. J. Mooney, *Biomaterials* **2005**, *26*, 2455–2465.
- [34] O. Jeon, K. H. Bouhadir, J. M. Mansour, E. Alsberg, *Biomaterials* **2009**, *30*, 2724–2734.
- [35] M. P. Lutolf, J. L. Lauer-Fields, H. G. Schmoekel, A. T. Metters, F. E. Weber, G. B. Fields, J. A. Hubbell, *Proc. Natl. Acad. Sci. U. S. A.* **2003**, *100*, 5413–5418.
- [36] M. W. Tibbitt, K. S. Anseth, *Biotechnol. Bioeng.* **2009**, *103*, 655–663.
- [37] S. J. Bidarra, C. C. Barrias, M. A. Barbosa, R. Soares, P. L. Granja, *Biomacromolecules* **2010**, *11*, 1956–1964.
- [38] D. A. Kedziorek, L. V Hofmann, Y. Fu, W. D. Gilson, K. M. Cosby, B. Kohl, B. P. Barnett, B. W. Simons, P. Walczak, J. W. M. Bulte, K. Gabrielson, D. L. Kraitman

- Stem Cells* **2012**, *30*, 1286–96.
- [39] A. Gebler, O. Zabel, B. Seliger, *Trends Mol. Med.* **2012**, *18*, 128–134.
- [40] R. R. Rao, A. W. Peterson, J. Ceccarelli, A. J. Putnam, J. P. Stegemann, *Angiogenesis* **2012**, *15*, 253–264.
- [41] A. M. A. Rokstad, I. Lacík, P. de Vos, B. L. Strand, *Adv. Drug Deliv. Rev.* **2014**, *67–68*, 111–130.
- [42] A. A. Li, F. Shen, T. Zhang, P. Cirone, M. Potter, P. L. Chang, *J. Biomed. Mater. Res. - Part B Appl. Biomater.* **2006**, *77*, 296–306.
- [43] Y. Zhang, W. Wang, J. Zhou, W. Yu, X. Zhang, X. Guo, X. Ma, *Ann. Biomed. Eng.* **2007**, *35*, 605–614.
- [44] D. A. Cieslinski, H. David Humes, *Biotechnol. Bioeng.* **1994**, *43*, 678–681.
- [45] S. Bruni, T. M. Chang, *Biomater. Artif. Cells. Artif. Organs* **1989**, *17*, 403–11.
- [46] X. W. Fu, A. M. Sun, *Transplantation* **1989**, *47*, 432–435.
- [47] D. W. Scharp, P. Marchetti, *Adv. Drug Deliv. Rev.* **2014**, *67–68*, 35–73.
- [48] J. A. M. Steele, J. P. Hallé, D. Poncelet, R. J. Neufeld, *Adv. Drug Deliv. Rev.* **2014**, *67–68*, 74–83.
- [49] P. De Vos, H. A. Lazarjani, D. Poncelet, M. M. Faas, *Adv. Drug Deliv. Rev.* **2014**, *67–68*, 15–34.
- [50] P. De Vos, B. J. De Haan, G. H. J. Wolters, J. H. Strubbe, R. Van Schilfgaarde, *Diabetologia* **1997**, *40*, 262–270.
- [51] S. Kumar, H. Ingle, D. V. R. Prasad, H. Kumar, *Crit. Rev. Microbiol.* **2012**, *39*, 1–18.
- [52] H. Uludag, P. De Vos, P. A. Tresco, *Adv. Drug Deliv. Rev.* **2000**, *42*, 29–64.
- [53] H. Iwata, K. Kobayashi, T. Takagi, T. Oka, H. Yang, H. Amemiya, T. Tsuji, F. Ito, *J. Biomed. Mater. Res.* **1994**, *28*, 1003–1011.
- [54] B. Dupuy, H. Gin, C. Baquey, D. Ducassou, *J. Biomed. Mater. Res.* **1988**, *22*, 1061–1070.
- [55] T. Kobayashi, Y. Aomatsu, H. Iwata, T. Kin, H. Kanehiro, M. Hisanaga, S. Ko, M. Nagao, Y. Nakajima, *Transplantation* **2003**, *75*, 619–625.
- [56] S. Sakai, K. Kawakami, *Acta Biomater.* **2007**, *3*, 495–501.
- [57] E. Ruel-Gariépy, G. Leclair, P. Hildgen, A. Gupta, J. C. Leroux, *J. Control. Release* **2002**, *82*, 373–383.
- [58] M. Sobol, A. Bartkowiak, B. De Haan, P. De Vos, *J. Biomed. Mater. Res. - Part A* **2013**, *101 A*, 1907–1914.

- [59] G. Helenius, H. Bäckdahl, A. Bodin, U. Nannmark, P. Gatenholm, B. Risberg, *J. Biomed. Mater. Res. - Part A* **2006**, *76*, 431–438.
- [60] M. Briššová, I. Lacík, A. C. Powers, A. V. Anilkumar, T. Wang, *J. Biomed. Mater. Res.* **1997**, *39*, 61–70.
- [61] S. Schneider, P. J. Feilen, V. Slotty, D. Kampfner, S. Preuss, S. Berger, J. Beyer, R. Pommersheim, *Biomaterials* **2001**, *22*, 1961–1970.
- [62] C. H. Lee, A. Singla, Y. Lee, *Int. J. Pharm.* **2001**, *221*, 1–22.
- [63] C. Yin, S. M. Chia, C. H. Quek, H. Yu, R. X. Zhuo, K. W. Leong, H. Q. Mao, *Biomaterials* **2003**, *24*, 1771–1780.
- [64] B. J. De Haan, A. Rossi, M. M. Faas, M. J. Smelt, F. Sonvico, P. Colombo, P. De Vos, *J. Biomed. Mater. Res. - Part A* **2011**, *98 A*, 394–403.
- [65] J. Herzberger, K. Niederer, H. Pohlit, J. Seiwert, M. Worm, F. R. Wurm, H. Frey, *Chem. Rev.* **2016**, *116*, 2170–2243.
- [66] A. Sabnis, M. Rahimi, C. Chapman, K. T. Nguyen, *J. Biomed. Mater. Res. - Part A* **2009**, *91*, 52–59.
- [67] K. T. Nguyen, J. L. West, *Biomaterials* **2002**, *23*, 4307–4314.
- [68] C. Dulieu, D. Bazile, *Pharm. Res.* **2005**, *22*, 285–292.
- [69] G. B. M. N. E. Vrana, A. O’Grady, E. Kay, P. A. Cahill, *J. Tissue Eng. Regen. Med.* **2009**, *3*, 567–572.
- [70] M. G. Cascone, M. Tricoli, P. Cerrai, R. S. Del Guerra, *Cytotechnology* **1993**, *11*, 137–139.
- [71] G. D.T. Mathews, Y.A. Birney, P.A. Cahill, *J. Biomed. Mater. Res. B. Appl. Biomater.* **2007**, *84*, 531–540.
- [72] B. A Zielinski, P. Aebischer, *Biomaterials* **1994**, *15*, 1049–1056.
- [73] R. H. Li, *Adv. Drug Deliv. Rev.* **1998**, *33*, 87–109.
- [74] K.-Y. S. H. N. Kim, D.-H- Kang, M. S. Kim, A. Jiao, D.-H. Kim, *Ann Biomed Eng* **2012**, *40*, 1339–1355.
- [75] G. Soldani, P. Losi, M. Bernabei, S. Burchielli, D. Chiappino, S. Kull, E. Briganti, D. Spiller, *Biomaterials* **2010**, *31*, 2592–2605.
- [76] A. P. Khandwekar, D. P. Patil, A. A. Hardikar, Y. S. Shouche, M. Doble, *J. Biomed. Mater. Res. - Part A* **2010**, *95 A*, 413–423.
- [77] T. Abe, K. Kato, T. Fujioka, T. Akizawa, *Int. J. Biomater.* **2011**, *2011*, DOI 10.1155/2011/375390.
- [78] X. Xu, Y. Yang, N. Zhu, *Blood Purif.* **2009**, *27*, 321–329.

- [79] S. Krol, S. Guerra, M. Grupillo, A. Diaspro, A. Gliozzi, P. Marchetti, *Nano Lett.* **2006**, *6*, 1933–1939.
- [80] Y. Teramura, H. Iwata, *Adv. Drug Deliv. Rev.* **2010**, *62*, 827–840.
- [81] H. Iwata, Y. Murakami, Y. Ikada, *Ann. N. Y. Acad. Sci.* **1999**, *875*, 7–23.
- [82] J. E. Babensee, M. V Sefton, *Tissue Eng.* **2000**, *6*, 165–183.
- [83] M. Feng, M. V Sefton, *J. Biomater. Sci. Polym. Ed.* **2000**, *11*, 537–545.
- [84] S. W. S. K. J. L. Burg, *Absorbable and Biodegradable Polymers*, **2015**.
- [85] J. A. Rowley, G. Madlambayan, D. J. Mooney, *Biomaterials* **1999**, *20*, 45–53.
- [86] S. Schneider, P. J. Feilen, F. Brunnenmeier, T. Minnemann, H. Zimmermann, U. Zimmermann, M. M. Weber, *Diabetes* **2005**, *54*, 687–693.
- [87] E. C. Opara, W. F. Kendall, *Expert Opin. Biol. Ther.* **2002**, *2*, 503–511.
- [88] M. V. Risbud, S. Bhargava, R. R. Bhonde, *J. Biomed. Mater. Res. Part A* **2003**, *66*, 86–92.
- [89] A. V. Prochorov, S. I. Tretjak, V. A. Goranov, A. A. Glinnik, M. V. Goltsev, *Adv. Med. Sci.* **2008**, *53*, 240–244.
- [90] L. H. Granicka, A. Weryński, J. Kawiak, in *Sep. Purif. Technol.*, **2005**, pp. 221–230.
- [91] M.-K. Lee, Y. H. Bae, *Adv. Drug Deliv. Rev.* **2000**, *42*, 103–120.
- [92] V. Vaithilingam, B. E. Tuch, *Rev. Diabet. Stud.* **2011**, *8*, 51–67.
- [93] J. L. P. E. Santos, J. Zarate, G. Orive, R. M. Hernandez, *Therapeutic Applications of Cell Microencapsulation*, **2010**.
- [94] P. M. Kharkar, K. L. Kiick, A. M. Kloxin, *Chem. Soc. Rev.* **2013**, *42*, 7335–72.
- [95] E. M. Sletten, C. R. Bertozzi, *Angew. Chemie - Int. Ed.* **2009**, *48*, 6974–6998.
- [96] C. A. DeForest, K. S. Anseth, *Nat. Chem.* **2011**, *3*, 925–931.
- [97] C. P. Ramil, Q. Lin, *Chem. Commun.* **2013**, *49*, 11007–11022.
- [98] C. Lin, K. S. Anseth, *Biomacromolecules* **2009**, *10*, 2460–2467.
- [99] C. C. Lin, A. T. Metters, K. S. Anseth, *Biomaterials* **2009**, *30*, 4907–4914.
- [100] C.-C. Lin, K. S. Anseth, *Proc. Natl. Acad. Sci.* **2011**, *108*, 6380–6385.
- [101] A. C. Farney, D. E. R. Sutherland, E. C. Opara, *Pancreas* **2016**, *45*, 8–20.
- [102] W. Zhang, X. He, *J. Biomech. Eng.* **2009**, *131*, 74515.
- [103] M. Whelehan, I. W. Marison, *J. Microencapsul.* **2011**, *28*, 669–688.
- [104] A. A Tomei, V. Manzoli, C. A Fraker, J. Giraldo, D. Velluto, M. Najjar, A. Pileggi, R. D. Molano, C. Ricordi, C. L. Stabler, J. A. Hubbell, *Proc. Natl. Acad. Sci. U. S. A.* **2014**, *111*, 10514–10519.
- [105] D. Steinhilber, T. Rossow, S. Wedepohl, F. Paulus, S. Seiffert, R. Haag, *Angew.*

- Chemie - Int. Ed.* **2013**, *52*, 13538–13543.
- [106] P. Dey, T. Schneider, L. Chiappisi, M. Gradzielski, G. Schulze-Tanzil, R. Haag, *Macromol. Biosci.* **2016**, *16*, 580–590.
- [107] P. Dey, S. Hemmati-Sadeghi, R. Haag, *Polym. Chem.* **2016**, 375–383.
- [108] B. von Lospichl, S. Hemmati-Sadeghi, P. Dey, T. Dehne, R. Haag, M. Sittinger, J. Ringe, M. Gradzielski, *Colloids Surfaces B Biointerfaces* **2017**, DOI 10.1016/j.colsurfb.2017.07.073.
- [109] E. Tumarkin, E. Kumacheva, *Chem. Soc. Rev.* **2009**, *38*, 2161–2168.
- [110] S. Seiffert, *Angew. Chemie - Int. Ed.* **2013**, *52*, 11462–11468.
- [111] Y. Sun, Y. L. Sun, L. Wang, J. Ma, Y. W. Yang, H. Gao, *Microporous Mesoporous Mater.* **2014**, *185*, 245–253.
- [112] X. Zhou, Q. Zheng, C. Wang, J. Xu, J. P. Wu, T. B. Kirk, D. Ma, W. Xue, *ACS Appl. Mater. Interfaces* **2016**, *8*, 12609–12619.
- [113] M. Calderón, M. A. Quadir, S. K. Sharma, R. Haag, *Adv. Mater.* **2010**, *22*, 190–218.
- [114] A. Thomas, S. S. Müller, H. Frey, *Biomacromolecules* **2014**, *15*, 1935–1954.
- [115] A. O. Fitton, J. Hill, D. E. Jane, R. Millar, *Synthesis (Stuttg.)*. **1987**, *1987*, 1140–1142.
- [116] D. Haamann, H. Keul, D. Klee, M. Möller, *Macromolecules* **2010**, *43*, 6295–6301.
- [117] S. Bräse, C. Gil, K. Knepper, V. Zimmermann, *Angew. Chemie - Int. Ed.* **2005**, *44*, 5188–5240.
- [118] M. Richter, D. Steinhilber, R. Haag, R. Von Klitzing, *Macromol. Rapid Commun.* **2014**, *35*, 2018–2022.
- [119] T. Rossow, J. A. Heyman, A. J. Ehrlicher, A. Langhoff, D. A. Weitz, R. Haag, S. Seiffert, *J. Am. Chem. Soc.* **2012**, *134*, 4983–4989.
- [120] M. Gervais, A. L. Brocas, G. Cendejas, A. Deffieux, S. Carlotti, *Macromolecules* **2010**, *43*, 1778–1784.
- [121] K. Knop, R. Hoogenboom, D. Fischer, U. S. Schubert, *Angew. Chemie - Int. Ed.* **2010**, *49*, 6288–6308.
- [122] A. Sunder, R. Mülhaupt, R. Haag, H. Frey, *Adv. Mater.* **2000**, *12*, 235–239.
- [123] A. L. Sisson, D. Steinhilber, T. Rossow, P. Welker, K. Licha, R. Haag, *Angew. Chemie - Int. Ed.* **2009**, *48*, 7540–7545.
- [124] D. Steinhilber, S. Seiffert, J. A. Heyman, F. Paulus, D. A. Weitz, R. Haag, *Biomaterials* **2011**, *32*, 1311–1316.
- [125] J. Dommerholt, S. Schmidt, R. Temming, L. J. A. Hendriks, F. P. J. T. Rutjes, J. C.

- M. Van Hest, D. J. Lefeber, P. Friedl, F. L. Van Delft, *Angew. Chemie - Int. Ed.* **2010**, *49*, 9422–9425.
- [126] D. Steinhilber, M. Witting, X. Zhang, M. Staegemann, F. Paulus, W. Friess, S. Küchler, R. Haag, *J. Control. Release* **2013**, *169*, 289–295.
- [127] A. K. Ghosh, M. Brindisi, *J. Med. Chem.* **2015**, *58*, 2895–2940.
- [128] F. Vacondio, C. Silva, M. Mor, B. Testa, *Drug Metab. Rev.* **2010**, *42*, 551–589.
- [129] G. W. Ashley, J. Henise, R. Reid, D. V Santi, *Proc. Natl. Acad. Sci. U. S. A.* **2013**, *110*, 2318–2323.
- [130] M. P. Zanin, L. N. Pettingill, A. R. Harvey, D. F. Emerich, C. G. Thanos, R. K. Shepherd, *J. Control. Release* **2012**, *160*, 3–13.
- [131] W. Lee, N.-J. Cho, A. Xiong, J. S. Glenn, C. W. Frank, *Proc. Natl. Acad. Sci. U. S. A.* **2010**, *107*, 20709–20714.
- [132] G. D. Nicodemus, S. J. Bryant, *Tissue Eng. Part B. Rev.* **2008**, *14*, 149–165.
- [133] K. Alessandri, B. R. Sarangi, V. V. Gurchenkov, B. Sinha, T. R. Kießling, L. Fetler, F. Rico, S. Scheuring, C. Lamaze, A. Simon, S. Geraldo, D. Vignjevic, H. Doméjean, L. Rolland, A. Funfac, J. Bibette, N. Bremond, P. Nassoy *Proc. Natl. Acad. Sci. U. S. A.* **2013**, *110*, 14843–14848.
- [134] A. J. Engler, S. Sen, H. L. Sweeney, D. E. Discher, *Cell* **2006**, *126*, 677–689.
- [135] J. S. Park, J. S. Chu, A. D. Tsou, R. Diop, A. Wang, S. Li, *Biomaterials* **2012**, *32*, 3921–3930.
- [136] W. Chen, Y. Hou, Z. Tu, L. Gao, R. Haag, *J. Control. Release* **2017**, *259*, 160–167.
- [137] M. Dimde, D. Steinhilber, F. Neumann, Y. Li, F. Paulus, N. Ma, R. Haag, *Macromol. Biosci.* **2017**, *17*, DOI 10.1002/mabi.201600190.
- [138] Y. Zhong, M. Dimde, D. Stöbener, F. Meng, C. Deng, Z. Zhong, R. Haag, *ACS Appl. Mater. Interfaces* **2016**, *8*, 27530–27538.
- [139] M. Dimde, F. F. Sahle, V. Wycisk, D. Steinhilber, L. C. Camacho, K. Licha, J. Lademann, R. Haag, *Macromol. Biosci.* **2017**, *201600505*, 1–8.
- [140] M. Calderón, S. Reichert, P. Welker, K. Licha, F. Kratz, R. Haag, *J. Biomed. Nanotechnol.* **2014**, *10*, 92–99.
- [141] D. Longnecker, *Pancreapedia Exocrine Pancreas* **2014**, 332–339.
- [142] R. D. Utiger, “No Title,” can be found under <https://www.britannica.com/science/pancreas>, **2017**.
- [143] Boundless, “No Title,” can be found under [www.boundless.com/physiology/textbooks/boundless-anatomy-and-physiology-](http://www.boundless.com/physiology/textbooks/boundless-anatomy-and-physiology-)

- textbook/endocrine-system-16/the-pancreas-159/overview-of-pancreatic-islets-797-1288/.
- [144] L. Orci, *Sci. Am.* **1988**, 259, 85–94.
- [145] J. C. Stendahl, D. B. Kaufman, S. I. Stupp, *Cell Transplant.* **2009**, 18, 1–12.
- [146] C. Ionescu-Tirgoviste, P. A. Gagniuc, E. Gubceac, L. Mardare, I. Popescu, S. Dima, M. Militaru, *Sci. Rep.* **2015**, 5, 14634.
- [147] T. E. of E. Britannica, “No Title,” can be found under <https://www.britannica.com/science/islets-of-Langerhans>.
- [148] J. P. Vu, P. M. Germano, J. R. Pisegna, *Pacap*, Elsevier Inc., **2013**.
- [149] M. R. DiGruccio, A. M. Mawla, C. J. Donaldson, G. M. Noguchi, J. Vaughan, C. Cowing-Zitron, T. van der Meulen, M. O. Huising, *Mol. Metab.* **2016**, 5, 449–458.
- [150] E. Mann, M. D. Bellin, *Pancreapedia* **2016**, DOI 10.3998/panc.2016.3.
- [151] A. G. Jones, A. T. Hattersley, *Diabet. Med.* **2013**, 30, 803–817.
- [152] B. O. Roep, *Nature* **2007**, 450, 799–800.
- [153] J. M. Berg, T. J. L., L. Stryer, *Biochemistry* **1988**, 27, 8509–8515.
- [154] C. Patterson, L. Guariguata, G. Dahlquist, G. Soltész, G. Ogle, M. Silink, *Diabetes Res. Clin. Pract.* **2014**, 103, 161–175.
- [155] A. P. Escher, A. Li, *Type 1 Diabetes*, ISBN: 9789535110170.
- [156] W.-P. You, M. Henneberg, *BMJ open diabetes Res. care* **2016**, 4, e000161.
- [157] R. A. Cobas, M. Bosi Ferraz, A. S. de Mattos Matheus, L. R. Monteiro Tannus, C. Antonio Negrato, L. A. de Araujo, S. Atala Dib, M. Brito Gomes, *Bull. World Health Organ.* **2013**, 91, 434–440.
- [158] B. Zhou, Y. Lu, K. Hajifathalian, J. Benthall, M. Di Cesare, G. Danaei, H. Bixby, M. J. Cowan, M. K. Ali, C. Taddei, et al., *Lancet* **2016**, 387, 1513–1530.
- [159] C. Bommer, E. Heesemann, V. Sagalova, J. Manne-Goehler, R. Atun, T. Bärnighausen, S. Vollmer, *Lancet Diabetes Endocrinol.* **2017**, 5, 423–430.
- [160] D. Nathan, et al., *N. Engl. J. Med.* **2005**, 353, 2643–2653.
- [161] G. A. Nichols, S. Vupputuri, H. Lau, *Diabetes Care* **2011**, 34, 2374–2378.
- [162] A. Dietrich, A. W. Herling, H. Hammes, **2017**, 1–17.
- [163] M. Jaiswal, J. Divers, D. Dabelea, S. Isom, R. A. Bell, C. L. Martin, D. J. Pettitt, S. Saydah, C. Pihoker, D. A. Standiford, L. M. Dolan, S. Marcovina, B. Linder, A. D. Liese, R. Pop-Busui, E. L. Feldman, *Diabetes Care* **2017**, 1–7.
- [164] G. P. Leese, J. Wang, J. Broomhall, P. Kelly, A. Marsden, W. Morrison, B. M. Frier, A. D. Morris, *Diabetes Care* **2003**, 26, 1176–1180.

- [165] G. Shafiee, M. Mohajeri-Tehrani, M. Pajouhi, B. Larijani, *J. Diabetes Metab. Disord.* **2012**, *11*, 17.
- [166] R. Unnikrishnan, V. N. Shah, V. Mohan, *Clin. Diabetes Endocrinol.* **2016**, *2*, 18.
- [167] C. H. Wasserfall, M. A. Atkinson, *Autoimmun. Rev.* **2006**, *5*, 424–428.
- [168] S. Cernea, M. Dobreanu, *Biochem. Medica* **2013**, *23*, 266–280.
- [169] K. Decochez, B. Keymeulen, G. Somers, H. Dorchy, I. H. De Leeuw, C. Mathieu, R. Rottiers, F. Winnock, K. ver Elst, I. Weets, et al., *Diabetes Care* **2000**, *23*, 1072–1078.
- [170] L. M. Duca, B. Wang, M. Rewers, A. Rewers, *Diabetes Care* **2017**, *40*, 1249–1255.
- [171] R. Calafiore, G. Basta, *Adv. Drug Deliv. Rev.* **2014**, *67–68*, 84–92.
- [172] W. M. Kuhlreiber, S. L. L. Washer, E. Hsu, M. Zhao, P. Reinhold, D. Burger, H. Zheng, D. L. Faustman, *Diabet. Med.* **2015**, *32*, 1346–1353.
- [173] A. Haidar, L. Legault, V. Messier, T. M. Mitre, C. Leroux, R. Rabasa-Lhoret, *Lancet Diabetes Endocrinol.* **2015**, *3*, 17–26.
- [174] M. A. Naftanel, D. M. Harlan, *PLoS Med.* **2004**, *1*, 198–201.
- [175] E. J. Sharples, S. M. Mittal, P. J. Friend, *Acta Diabetol.* **2016**, *53*, 871–878.
- [176] S. Mittal, S. C. L. Gough, *Diabet. Med.* **2014**, *31*, 512–521.
- [177] A. Zinger, G. Leibowitz, *Diabetes. Metab. Res. Rev.* **2014**, *30*, 83–87.
- [178] A. J. Vegas, O. Veiseh, J. C. Doloff, M. Ma, H. H. Tam, K. M. Bratlie, J. Li, A. R. Bader, E. Langan, K. Olejnik, et al., *Nat. Biotechnol.* **2016**, *34*, 345–352.
- [179] O. Veiseh, J. C. Doloff, M. Ma, A. J. Vegas, H. H. Tam, A. R. Bader, J. Li, E. Langan, J. Wyckoff, W. S. Loo, et al., *Nat. Mater.* **2015**, *14*, 643–651.
- [180] P. O. Carlsson, F. Palm, A. Andersson, P. Liss, *Diabetes* **2001**, *50*, 489–495.
- [181] P. De Vos, A. F. Hamel, K. Tatarkiewicz, *Diabetologia*, **2002**, *45*, 159–173.
- [182] D. M. Berman, J. J. O’Neil, L. C. K. Coffey, P. C. J. Chaffanjon, N. M. Kenyon, P. Ruiz, A. Pileggi, C. Ricordi, N. S. Kenyon, *Am. J. Transplant.* **2009**, *9*, 91–104.
- [183] A. J. Vegas, O. Veiseh, M. Gürtler, J. R. Millman, F. W. Pagliuca, A. R. Bader, J. C. Doloff, J. Li, M. Chen, K. Olejnik, et al., *Nat. Med.* **2016**, *22*, 306–311.
- [184] R. M. Olabisi, *J. Biomed. Mater. Res. - Part A* **2015**, *103*, 846–859.
- [185] C. C. Lin, K. S. Anseth, *Biomacromolecules* **2009**, *10*, 2460–2467.
- [186] Y. Teramura, Y. Kaneda, H. Iwata, *Biomaterials* **2007**, *28*, 4818–4825.
- [187] G. Yoshimatsu, N. Sakata, H. Tsuchiya, M. Ishida, F. Motoi, S. Egawa, S. Sumi, M. Goto, M. Unno, in *Transplant. Proc.*, **2013**, *45*, 1875–1880.
- [188] M. Skelin, M. Rupnik, A. Cencic, *ALTEX* **2010**, *27*, 105–113.

- [189] S. Efrat, *Ann. N. Y. Acad. Sci.* **2004**, *1014*, 88–96.
- [190] V. Poitout, L. K. Olson, R. P. Robertson, *Diabetes Metab.* **1996**, *22*, 7–14.
- [191] P. D. Yurchenco, *Cold Spring Harb. Perspect. Biol.* **2011**, *3*, 1–27.
- [192] J. Y. C. C. Cheng, M. Raghunath, J. Whitelock, L. Poole-Warren, *Tissue Eng. Part B. Rev.* **2011**, *17*, 235–247.
- [193] T. Schneider, P. Welker, R. Haag, J. Dernedde, T. Hug, K. Licha, B. Kohl, S. Arens, W. Ertel, G. Schulze-Tanzil, *Inflamm. Res.* **2015**, *64*, 917–928.
- [194] C. Holtze, A. C. Rowat, J. J. Agresti, J. B. Hutchison, F. E. Angile, C. H. J. Schmitz, S. Koster, H. Duan, K. J. Humphry, R. A. Scanga, et al., *Lab Chip* **2008**, *8*, 1632–1639.
- [195] J. C. McDonald, D. C. Duffy, J. R. Anderson, D. T. Chiu, H. Wu, O. J. Schueller, G. M. Whitesides, *Electrophoresis* **2000**, *21*, 27–40.